29810 DUP.

UNLIMITED
UNCLASSIFIED

ILLIMITÉE
NON CLASSIFIÉE

Technical Report

Rapport technique

1986 / 10

TR-GD-013
NRC NO. 29810

THE CALCULATION OF THEORETICAL COHERENT ANTI-STOKES RAMAN SPECTRA

Thangam Parameswaran
D.R. Snelling

Division of
Mechanical Engineering

Division de
génie mécanique

National Research Council Canada
Conseil national de recherches Canada

Canada

89-03257/

VISION OF MECHANICAL ENGINEERING PUBLICATIONS

DM	**(Division of Mechanical Engineering Report)** Scientific and technical information considered important, complete and a lasting contribution to existing knowledge.
TR	**(Technical Report)** Information less broad in scope but a substantial contribution to existing knowledge.
CTR	**(Controlled/Classified Technical Report)** A Technical Report with controlled distribution for national security, proprietary or other reasons.
LM	**(Laboratory Memorandum)** Preliminary or exploratory information with controlled distribution.
CAT	**(Calibration Analysis and Test Report)** Information on minor laboratory projects or services.

PUBLICATIONS DE LA DIVISION DE GÉNIE MÉCANIQUE

DM	**(Rapport de la Division de génie mécanique)** Informations scientifiques et techniques jugées importantes, complètes et susceptibles de contribuer de façon durable à l'avancement des connaissances courantes.
TR	**(Rapport technique)** Informations de moindre importance, mais pouvant contribuer substantiellement à l'avancement des connaissances actuelles.
CTR	**(Rapport technique à diffusion contrôlé/classifié)** Rapport technique à diffusion contrôlée pour des raisons de sécurité nationale, de propriété intellectuelle et autres.
LM	**(Mémoire de laboratoire)** Informations préliminaires ou de nature exploratoire à diffusion contrôlée.
CAT	**(Rapport d'étalonnage d'analyse et d'essai)** Informations sur de petits projets ou des services de laboratoire.

UNLIMITED
UNCLASSIFIED

ILLIMITÉÉ
NON CLASSIFIÉÉ

THE CALCULATION OF THEORETICAL COHERENT ANTI-STOKES RAMAN SPECTRA

LE CALCULE DU PROFILE DES SPECTRAS THÉORIQUES DE LA DIFFUSION RAMAN ANTI-STOKES COHÉRENTE

Thangam Parameswaran and D.R. Snelling

Technical Report
1988/10

Rapport technique
TR-GD-013
NRC NO 29810

R.G. Williamson, Head/Chef
Gas Dynamics Laboratory/
Laboratoire de dynamique des gaz

J. Ploeg
Director/
Directeur

ACKNOWLEDGEMENTS

The authors gratefully acknowledge the collaboration and unswerving support of P.M.J. Hughes of the CANMET Laboratories of Energy Mines and Resources. For the last few years, the common costs of data acquisition, data analysis, and theoretical spectra generation software, essential for setting up a CARS system, have been shared by NRC and EMR.

The theoretical modelling of CARS spectra presented here was done under contracts funded mostly by DND and CANMET/EMR. Dr. Thangam Parameswaran would like to thank the above sources for their financial support.

The authors would also like to thank Dr. R. Palmer of the Sandia National Laboratories, Livermore, California, U.S.A. for providing a copy of the Sandia CARS computer program and for several helpful discussions.

ABSTRACT

This report briefly summarizes the theoretical principles underlying coherent anti-Stokes Raman spectroscopy (CARS). The role of collisional narrowing due to overlap of Raman lines, and appropriate convolution with the pump laser profile are discussed in some detail. The implementation of a computer code to calculate broadband nitrogen CARS spectra is described and the effect of the various assumptions and models on the resultant CARS spectrum is examined. The theoretical CARS spectra are compared with those calculated from a code developed at the Sandia National Laboratories, Livermore, California. Computer programs to fit experimental CARS spectra using a precalculated library of theoretical CARS spectra are described and examples are presented.

RÉSUMÉ

Le présent rapport résume les principes théoriques de la spectrométrie Raman anti-Stokes cohérente (CARS). On y discute en détail du rôle du rétrécissement collisionnel attribuable au chevauchement des raises Raman ainsi que de la convolution appropriée avec le profil laser à pompage. Aussi, décrit la mise en oeuvre d'un code informatique de calcul des spectres CARS en bande large de l'azote et examine les effets des diverses hypothèses et divers modèles sur les spectres CARS résultants. Les spectres CARS théoriques sont comparés aux spectres calculés au moyen d'un code élaboré aux Sandia National Laboratories de Livermore, en Californie. Enfin, on décrit, avec exemples, des programmes informatiques d'adjustement des spectres CARS expérimentaux au moyen d'une bibliothèque précalculée de spectres CARS théoriques.

CONTENTS

Page

ACKNOWLEDGEMENTS (ii)

ABSTRACT/RÉSUMÉ (iii)

LIST OF APPENDICES (v)

LIST OF ILLUSTRATIONS (vi)

1.0 INTRODUCTION TO CARS 1

2.0 CARS SPECTRAL SYNTHESIS 3

- 2.1 Theoretical Principles and Generating Equations 3
- 2.2 Collisional Narrowing in CARS Spectra 4
- 2.3 Cross Coherence Effects (K-T Convolution) 6
- 2.4 Yuratich Convolution 6
- 2.5 Convolution of χ and $|\chi|^2$ 7
- 2.6 Closed Form Solutions of Cross Coherence Term 7
- 2.7 Analytic (Closed Form) Solution of All CARS Integrals 8

3.0 THIRD ORDER SUSCEPTIBILITY $\chi^{(3)}$ 10

- 3.1 Energy Levels and Line Positions 10
- 3.2 Population Factor $\Delta\rho$ 11
- 3.3 The Transition Amplitudes 11
- 3.4 Corrections to the Transition Amplitudes 12
- 3.5 Number Density 13
- 3.6 The G-Matrix and the Weight Factors 13
- 3.7 The Nonresonant Susceptibility 13
- 3.8 The Pump Convolved CARS Spectrum 14

4.0 THEORETICAL NITROGEN CARS SPECTRA 14

- 4.1 Molecular Parameters for Nitrogen 15
- 4.2 Sampling Scheme for χ^2 Spectrum 16
- 4.3 Addition of O and S Branches 17
- 4.4 Determination of Line Positions 17
- 4.5 Collisional Narrowing Effects 18
- 4.6 Effect of Cross Coherence Terms 18
- 4.7 Room Temperature N_2 Spectra 19
- 4.8 Comparison of Numeric and Analytic Models 19
- 4.9 Comparison of Spectra from the Old Program with that from the Current Updated Version 19

5.0 FITTING OF EXPERIMENTAL N_2 CARS SPECTRA 20

- 5.1 CARS Spectrometer and Data Acquisition System 20

CONTENTS (Cont'd)

Page

5.2 Least Mean Square Fitting Algorithm 21
5.2.1 Stretch parameter in CARS spectral fits 23
5.3 CARS Spectral Library 24
5.4 Voigt Slit Function 24
5.4.1 Voigt parameters from N_2 CARS spectra 25
5.5 Slit Convolved Theoretical CARS Spectra 29
5.6 Temperatures from N_2 CARS Spectra 29
5.6.1 Results from the FITFLAME Program 29

6.0 REFERENCES 33

LIST OF APPENDICES

APPENDIX

A DESCRIPTION OF THE CARS SPECTRA GENERATING PROGRAM

B TYPICAL INPUT DATA FILE FOR N_2 CARS SPECTRUM

C COMPARISON OF CARS SPECTRA CALCULATED WITH NRC AND SANDIA CARS GENERATING PROGRAMS

D TYPICAL RUN OF THE THEORETICAL CARS SPECTRUM GENERATING PROGRAM

E DESCRIPTION OF THE FIT PROGRAMS

LIST OF ILLUSTRATIONS

Figure **Page**

1 Coherent anti-Stokes Raman spectroscopy (CARS) 39

2 Real and imaginary part of CARS susceptibility 40

3 Effect of insufficient sampling ($\Gamma_j = 0.0004\ \mathrm{cm}^{-1}$ and sampling grid of $0.0025\ \mathrm{cm}^{-1}$) 41

4 Effect of increased sampling ($\Gamma_j = 0.004\ \mathrm{cm}^{-1}$ and sampling grid of $0.001\ \mathrm{cm}^{-1}$) 42

5 Effect of sampling grid size on 2000 K CARS spectrum 43

6a N_2 Q branch spectrum with and without O and S branches from 2260 to 2300 cm^{-1} 44

6b N_2 Q branch spectrum with and without O and S branches from 2300 to 2340 cm^{-1}. 45

7a N_2 CARS spectra with single (curve B) and separate (curve A) matrix diagonalization from 2260 to 2300 cm^{-1} 46

7b N_2 CARS spectrum with single (curve B) and separate (curve A) matrix diagonalization from 2300 to 2340 cm^{-1} 47

8a Effect of collisional narrowing on 1000 K CARS spectrum from 2260 to 2300 cm^{-1} 48

8b Effect of collisional narrowing on 1000 K CARS spectrum from 2300 to 2340 cm^{-1} 49

9a Effect of collisional narrowing on 1550 K CARS spectrum from 2260 to 2300 cm^{-1} 50

9b Effect of collisional narrowing on 1550 K CARS spectrum from 2300 to 2340 cm^{-1} 51

10a Effect of collisional narrowing on 2000 K CARS spectrum from 2260 to 2300 cm^{-1} 52

10b Effect of collisional narrowing on 2000 K CARS spectrum from 2300 to 2340 cm^{-1} 53

LIST OF ILLUSTRATIONS (Cont'd)

11 1550 K N_2 CARS spectra at 12 atm. (curve A) and 10 atm. (curve B) 54

12 1500 K N_2 CARS spectra at 10, 20, 30 and 50 atm. 55

13a Effect of cross coherence on 1000 K CARS spectrum from 2260 to 2300 cm^{-1} 56

13b Effect of cross coherence on 1000 K CARS spectrum from 2300 to 2341 cm^{-1} 57

14a Effect of cross coherence on 1550 K CARS spectrum from 2260 to 2300 cm^{-1} 58

14b Effect of cross coherence on 1550 K CARS spectrum from 2300 to 2340 cm^{-1} 59

15a Effect of cross coherence on 2000 K CARS spectrum from 2260 to 2300 cm^{-1} 60

15b Effect of cross coherence on 2000 K CARS spectrum: 2300 to 2340 cm^{-1} 61

16 Comparison of isolated line (curve B) and collisional narrowing and cross coherence (curve A) models of 300 K N_2 CARS spectra 62

17a Comparison of analytic (GTAN) and numeric (GT) 2000 K CARS spectra from 2260 to 2300 cm^{-1} 63

17b Comparison of analytic (GTAN) and numeric (GT) 2000 K CARS spectra from 2300 to 2340 cm^{-1} 64

18 Voigt parameters from room temperature N_2 CARS spectra 65

19 Voigt parameters and temperature from N_2 CARS flame spectra 66

THE CALCULATION OF THEORETICAL COHERENT ANTI-STOKES RAMAN SPECTRA

1.0 INTRODUCTION TO CARS

Coherent anti-Stokes Raman spectroscopy (CARS) has received much attention in recent years because of its capability for providing remote, in situ measurements of major species concentration and temperature with good spatial and temporal resolution in practical combustion environments (e.g., Druet and Taran 1981; Ecbreth et al., 1984). In CARS, a three-wave optical mixing process occurs in which laser beams at frequencies ω_p (pump) and ω_s (Stokes) interact via a third-order nonlinear susceptibility to produce the CARS signal at frequency $\omega_{as} = 2\omega_p - \omega_s$. The signal is greatly enhanced when the frequency difference $\omega_p - \omega_s$ corresponds to that of a Raman-active molecular transition of the medium, thus allowing different molecular constituents to be measured by varying ω_s. Single pulse CARS measurements are possible if a broadband dye laser is used to generate the Stokes laser frequencies at ω_s. The broadband CARS signal is then dispersed and recorded with a multichannel optical detector. The CARS generation process is summarized in Fig. 1. The geometry of the laser beam mixing must satisfy the phase matching condition to allow efficient buildup of the coherent CARS signal. A method of achieving this condition where the Stokes laser is coaxial with the annular pump beam is shown in Fig. 1. Temperature measurements can be derived from the spectral shape of CARS signals (e.g., nitrogen spectra) by fitting them to calculated theoretical spectra whose temperatures are systematically varied to obtain a best fit.

The CARS output is a coherent signal, which is many orders of magnitude larger than the corresponding spontaneous Raman signal. This increased signal strength, and the ability to use geometric filtering to pass the laser-like CARS signal while discriminating against flame radiation, allows the technique to be used in practical combustion environments. In recent years, CARS temperature measurements have been demonstrated in reciprocating engines, simulated gas turbine combustors (Switzer et al. 1980; Taran and Pealat 1982; Greenhalgh et al. 1983; Eckbreth 1980), and afterburning jet engines (Eckbreth et al. 1984).

A CARS system has been built in the Gas Dynamics Laboratory at NRC, where the technique of nitrogen thermometry has been demonstrated in simple flames (Snelling and Fischer 1985; Snelling et al. 1987) and is currently being extended to more practical combustion devices. These measurements will be used, in part, to validate the predictions of numerical fluid dynamic combustion codes, which are also being developed in this laboratory.

A major part of the effort to set up and apply the CARS technique for nitrogen thermometry has been the development of the computer programs to calculate the theoretical CARS spectra. The amplitude of the CARS signal is proportional to the product of three electric fields (two from the pump photons and one from the Stokes) and is thus a third-order nonlinear effect. The theoretical CARS spectrum for specified input conditions can be obtained by computing the third-order nonlinear electric susceptibility. This susceptibility is a function of the molecular properties such as the position, width, and overlap of the Raman transitions; medium conditions such as the temperature, pressure and species concentration; and experimental parameters such as the instrumental function and laser band widths. The algorithms required to simulate a CARS spectrum are more complicated than those for the conventional Raman spectra, because of the coherent sums of contributions from various transitions.

The original version of our code was based on the theory of Yuratich (1979), but recent advances in CARS theory modified the original approach, which was based on isolated spectral lines and a convolution integral that neglected cross coherence terms in the pump laser convolution (Kataoka et al. 1982; Teets 1984). At higher pressures it is necessary to account for collisional effects that result in the initial broadening and overlapping of individual lines and eventually to line mixing and collisional narrowing. Under these conditions a knowledge of the state-to-state relaxation rates and the inversion of the G-matrix is required (Hall et al. 1980). We have now included the cross coherence effect due to a finite Gaussian pump laser spectral band width and collisional narrowing (Koszykowski et al. 1985) in our code.

In this report we provide a summary of the relevant CARS theory and a detailed description of the implementation of the calculation procedures and the computer program to generate theoretical CARS spectra with emphasis on the spectrum of nitrogen. (Compared with other combustion species, nitrogen has a relatively simple Raman spectrum, and since it is the major species in air-fed combustion, it is widely used for performing temperature measurements.)

Examples of typical CARS spectra of nitrogen are provided for a range of input pressures and temperatures. The effect of collisional narrowing and cross coherence is examined by comparing theoretical CARS spectra calculated with and without these effects.

The NRC CARS spectra are also compared with those calculated from a computer program that was kindly supplied by Dr. R. Palmer of the Sandia National Laboratories, Livermore, California. The Sandia computer program is very complete and is designed to provide CARS spectra for a wide range of experimental conditions, such as scanning CARS with and without nonresonant referencing and polarization control of the various laser beams. By contrast the NRC computer program was designed to efficiently compute libraries of theoretical broadband CARS spectra. The comparison of CARS spectra calculated from the Sandia and NRC programs demonstrated small differences in the calculation procedures. Finding the sources of these small differences and implementing the necessary changes in the computer programs has been an unexpectedly time-consuming task. However, it has resulted in a computer program for calculating theoretical CARS spectra that has been carefully validated and for which the effect of various assumptions concerning CARS amplitudes, etc., has been examined with some care.

Finally, the use of a precalculated library of theoretical CARS spectra to fit experimental CARS spectra is demonstrated. The library approach was implemented so that single shot experimental CARS spectra could be fitted rapidly ($\sim$1-3 s of cpu time using a DEC VAX-11/730 computer). Such a capability is necessary to fit the large number of spectra required to obtain temperature histograms in turbulent combustion.

2.0 CARS SPECTRAL SYNTHESIS

2.1 Theoretical Principles and Generating Equations

The theory of CARS has been dealt with extensively in the literature (see for example, Druet and Taran 1981; Hall and Eckbreth 1984; Harvey 1981; Nibler and Knighten 1979). In brief, CARS is a nonlinear optical phenomenon involving three wave mixing. When two laser beams of frequencies ω_p and ω_s interact in a medium, three wave mixing produces a resultant coherent CARS beam of frequency $\omega_{as} = 2\omega_p - \omega_s$. The mixing occurs for all samples, but the CARS signal is greatly enhanced when $\omega_p - \omega_s$ approaches a Raman frequency of the sample medium.

The interaction of the laser radiation with the medium occurs through the third order nonlinear electric susceptibility denoted by $\chi^{(3)}$. This gives rise to an induced polarization field, which acts as the source term in Maxwell's wave equation. On solving the wave equation one gets, for monochromatic input waves, the intensity of the CARS signal as

$$I(\omega_{as}) \sim I_p^2 I_s \left|\chi^{(3)}\right|^2 \qquad (1)$$

where I_p, I_s, and $I(\omega_{as})$ represent the pump, Stokes, and CARS intensities respectively. $\chi^{(3)}$ has resonant (χ_R) and nonresonant (χ_{NR}) contributions.

The nonresonant susceptibility χ_{NR} is real and proportional to the total number density. χ_{NR} arises owing to small contributions from distant off-resonant electronic transitions and has only a weak frequency dependence. Raman active modes involved in the CARS spectra of combustion processes are strongly polarized vibration rotation transitions. That is, the isotropic part of the polarizability dominates over the anisotropic part (see Section 3.3). Therefore the O and S branch contributions are small and usually it is considered sufficiently accurate to restrict calculations to the Q branch. The widths of these Raman lines are functions of pressure, temperature, and rotational quantum number (Printer 1964). When pressure increases, the lines broaden and may overlap; at higher pressures, when there is sufficient interference between adjacent transitions, collisional narrowing occurs (May et al., 1970; Bonamy et al. 1977) and the system relaxes according to the density matrix equation. The resonant susceptibility χ_R for overlapping Raman lines may then be expressed in terms of the G matrix given by (Hall 1983)

$$G_{jk} = i(\omega_p - \omega_s - \omega_j)\,\delta_{jk} + \frac{\Gamma_j}{2}\cdot\delta_{jk} + \gamma_{jk}(1 - \delta_{jk}) \qquad (2)$$

where ω_p, ω_s, and ω_j denote the pump, Stokes, and Raman frequencies, respectively, Γ_j is the isolated line width (FWHM), δ_{jk} is the Kronecker delta symbol, and γ_{jk} are the off-diagonal elements of the relaxation rate matrix. Koszykowski et al. (1985) have shown that, by using an eigenvalue eigenvector approach, χ_R may be calculated from

$$\chi_R(\delta) = \sum_j \frac{a_j}{\lambda_j' - \delta + i\lambda_j''} \qquad (3)$$

where $\lambda_j = \lambda_j' + i\lambda_j''$ is a complex eigenvalue of the G-matrix, δ is the detuning, $\omega_j - (\omega_p - \omega_s)$ and a_j is in general a complex weight factor whose calculation is described in Section 2.2. At low pressures one may neglect the overlap between lines and set $\gamma_{jk}$to 0; then λ_j' approaches the Raman frequency ω_j, λ_j'' approaches $-\Gamma_j$, (the Raman line width), and χ_R reduces to

$$\chi_R(\delta) = \frac{4\Pi Nc^4}{h\,\omega_s^4} \sum_j \frac{\Delta\rho_{jj}(d\sigma/d\Omega)_j}{2\delta - i\Gamma_j} \qquad (4)$$

This is the isolated line approximation. The Raman cross section $d\sigma/d\Omega$ can be obtained from Placzek-Teller coefficients and the polarizability parameters for the molecule. $\Delta\rho_{jj}$ refers to the fractional population in the j^{th} state, h is the Planck constant and N is the number density.

Knowing χ_R and χ_{NR}, eq. 1 can be directly used to get the CARS spectrum for monochromatic laser beams. The effect of laser band widths on theoretical CARS spectra is treated extensively by Yuratich (1979). In a method widely used in CARS theory, the final CARS intensities are obtained by a simple convolution of $|\chi|^2$ with the pump and Stokes spectral profiles (Hall 1979; Farrow et al. 1982; Lasser 1980). This approach ignores the cross terms that arise from the coherence between the polarization components in which the roles of the driving and scattered pump photons are exchanged. In this approximation and when the pump width is much smaller than the Stokes width, the CARS intensity may be expressed as

$$I(\omega_{as}) \sim I_p \int I_s(\omega_p^{(0)} - \delta) I_p(\omega_{as} - \delta) \left|\chi^{(3)}(\delta)\right|^2 d\delta \qquad (5)$$

where $\omega_p^{(0)}$ is the centre frequency of the pump. In actual calculations the convolution with the dye profile is eliminated by "ratioing" experimental CARS spectra with a nonresonant reference spectrum.

At first, a computer program (Parameswaran and Snelling 1982) based on eq. 5 and the isolated line approximation was used to calculate theoretical spectra. A Gaussian spectral shape was assumed for the pump.

2.2 Collisional Narrowing in CARS Spectra

It is now established (Koszykowski et al. 1985) that, while collisional narrowing of overlapping Raman lines cannot be neglected at high pressures, it can become significant even at atmospheric pressure. To include this effect in the generation of theoretical CARS spectra, matrix elements of the scattering matrix that describe the transition rate between the rotational states are needed. The diagonal elements of the above relaxation rate matrix are related to the width and shift of isolated lines. If shifts are neglected a diagonal element predicts the rate at which collisions transfer intensity from a given line to all other lines in the spectrum. The off-diagonal elements correspond to the negative of the rate at which collisions transfer intensity from line to line (Hall 1983). This interference between overlapping lines causes the collisional narrowing effect. In general, the corresponding vibrational dephasing contributions to the Raman line width are small so that shifts can be neglected and the off-diagonal elements γ_{ij} are assumed to be real. The elements γ_{ij} can be parametrized by means of empirical gap laws such as the inverse power law (Pritchard et al. 1979) or the exponential gap law (Polanyi and Woodall 1971). The various scaling laws available for modelling γ_{ij} and the Raman line widths Γ_j are discussed in detail by Greenhalgh (1988). Rahn and Palmer (1986) have developed a modified exponential gap scaling law for nitrogen based on their inverse Raman spectra measurements. This scaling law used in the present calculations is described below.

The transition rate between states with rotational quantum number i,j (i < j) is given by

$$\gamma_{ji} = \alpha p(T_0/T)^{0.5}\left(\frac{1 - e^{-m}}{1 - e^{-mT/T_0}}\right)\left(\frac{1 + 1.5E_i/kT\delta}{1 + 1.5E_i/kT}\right) \exp\left(-\beta\Delta E_{ij}/kT\right) \tag{6}$$

where p is the pressure, T_0 is a reference temperature (usually 273 K); E_i is the rotational term energy for state i; E_{ij} is the difference in energy between the ith and jth states; and α, β, δ, and m are fitting parameters. From microscopic reversibility the downward transition rate from j to i is determined as

$$\gamma_{ij} = \gamma_{ji}\,\frac{2i + 1}{2j + 1}\exp\left(\Delta E_{ij}/kT\right) \tag{7}$$

The collisional broadening or the width (FWHM) of the jth line of the Q branch can be obtained from the total rate of state perturbing collisions as follows:

$$\Gamma_j/2 = -\sum_{i\neq j} \gamma_{ij} \tag{8}$$

Once the rate matrix elements are evaluated, the G-matrix in eq. 2 can be set up and its eigenvalues and eigenvectors can be used in eq. 3 to calculate the CARS susceptibility. The complex weight factors a_i are related to the matrix of eigen vectors A and its inverse as shown below:

$$a_i = (d \cdot A)_i (A^{-1} \cdot \Delta\rho \cdot d)_i \qquad (9)$$

where d is a vector of transition amplitudes and Δρ is a diagonal matrix of population differences.

2.3 Cross Coherence Effects (K-T Convolution)

Teets and Kataoka (Teets 1984; Kataoka et al. 1982) have observed that neglecting the cross-coherence terms that arise in the laser convolution of CARS intensities can lead to temperature errors, especially when the pump band width is comparable to the Raman line width and the nonresonant contribution competes with the resonant signal. Including this effect, the CARS intensity may be written (not including dye convolution) as

$$\begin{aligned} I_{as}(\omega_{as}) = {} & \chi_{NR}^2 \langle 1 \rangle + 2\chi_{NR} \langle \mathrm{Re}\chi_R(\omega_{as} - \omega') \rangle \\ & + \tfrac{1}{2} \langle \left| \chi_R(\omega_{as} - \omega') \right|^2 \rangle + \tfrac{1}{2} \langle \chi_R(\omega_{as} - \omega') \chi_R^*(\omega_{as} - \omega'') \rangle \qquad (10) \end{aligned}$$

where

$$\langle F \rangle = \int I_p(\omega')d\omega' \int I_p(\omega'')F(\omega',\omega'')d\omega'' \qquad (11)$$

and ω',ω'' refer to the two pump photons and * indicates a complex conjugate.

Equation 10 expresses the CARS intensity as a sum of four terms. The first term clearly is the purely nonresonant contribution (I^{nr}). The second term (I^{int}) arises from the interference between resonant and nonresonant susceptibilities. The third term (I^{rr}) is the conventional, purely resonant component and the last term (I^{cc}) results from cross coherence between the two frequency degenerate pump photons. Note that the third and fourth terms have coefficients of 0.5. While the first three terms above can be calculated with one integration with the pump profile, the fourth term involves a double integration, which can be very time consuming.

2.4 Yuratich Convolution

Let χ' and χ'' be the real and imaginary part of χ_R. Then

$$\left|\chi^{(3)}\right|^2 = \left|\chi_{NR}\right|^2 + 2\left|\chi_{NR}\right|\left|\chi'\right| + \left|\chi'\right|^2 + \left|\chi''\right|^2 \qquad (12)$$

Using < > to represent pump convolution

$$\langle\left|\chi^{(3)}\right|^2\rangle = \langle\left|\chi_{NR}\right|^2\rangle + 2\langle\left|\chi_{NR}\right|\left|\chi'\right|\rangle + \langle\left|\chi'\right|^2\rangle + \langle\left|\chi''\right|^2\rangle \qquad (13)$$

Assuming χ_{NR} to be frequency independent

$$\langle\left|\chi_{NR}\right|^2\rangle = \left|\langle\chi_{NR}\rangle\right|^2 = \chi_{NR}^2 \quad \text{and}$$

$$2\langle\left|\chi_{NR}\right|\left|\chi'\right|\rangle = 2\chi_{NR}\langle\chi'\rangle \qquad (14)$$

Equation 13 is the same as that which would be obtained if, to a first approximation, one assumes that the third and fourth terms in eq. 10 are equal. This is the Yuratich method, which ignores cross coherence.

2.5 Convolution of χ and $|\chi|^2$

Consider the result that would follow if we convolve $\chi^{(3)}$ and then find the absolute square.

$$|\langle\chi^{(3)}\rangle|^2 = |\langle\chi_{NR}\rangle|^2 + 2\langle\chi_{NR}\rangle\langle\chi'\rangle + (|\langle\chi'\rangle|^2+|\langle\chi''\rangle|^2) \qquad (15)$$

The first two terms in eq. 13 and 15 are equal. Therefore, if one takes the mean of the above two equations, the result is equivalent to eq. 10, which properly takes care of cross coherence. Since $\chi^{(3)}$ and $|\chi^{(3)}|^2$ have to be convolved in this method, it is a slow procedure (Farrow and Rahn 1985).

2.6 Closed Form Solution of Cross Coherence Term

A second method of including cross coherence is to evaluate the first three terms in eq. 10 with a single integration numerically, and compute the last term using an analytic closed form expression. Such expressions have been published for Lorentzian pumps (Teets 1984) and for Gaussian pumps (Greenhalgh and Hall 1986). The Gaussian pump approach implemented in the NRC CARS program may be outlined as follows.

The pump laser with a Gaussian spectral profile may be represented as

$$I_p = \left[\frac{1}{\sqrt{\pi}\Delta\omega_p}\right] \exp\left[-(\omega - \omega_p^{(0)})^2/(\Delta\omega_p)^2\right] \qquad (16)$$

where $\omega_p^{(0)}$ is the pump centre frequency and $\Delta\omega_p$ is 0.60056 × pump width (FWHM).

Let

$$D_j(\omega) = \lambda_j' - (\omega_{as} - \omega) + i\lambda_j'' \qquad (17)$$

be the denominator of the Lorentzian line shape of the Raman transitions that contribute to the resonant susceptibility. In terms of $I_p(\omega)$ and $D_j(\omega)$, the cross coherence term $I^{cc}(\omega_{as})$ may be written as

$$I^{cc}(\omega_{as}) = \frac{1}{2} \int I_p(\omega'')d\omega'' \int I_p(\omega')\left[\sum_{jk}\frac{a_j a_k^*}{D_j(\omega')D_k^*(\omega'')}\right]d\omega' \qquad (18)$$

By using the variables $t = \dfrac{\omega' - \omega_p^{(0)}}{\Delta\omega_p}$

$$t' = \frac{\omega'' - \omega_p^{(0)}}{\Delta\omega_p}$$

$$z = \frac{-[\lambda_j' - (\omega_{as} - \omega_p^{(0)})] - i\lambda_j''}{\Delta\omega_p} \qquad (19)$$

eq. (18) can be written as

$$I^{cc}(\omega_{as}) = \frac{1}{2\pi(\Delta\omega_p)^2} \sum_{jk} a_j a_k^* \int \frac{e^{-t^2}}{z_j - t}\, dt \int \frac{e^{-t'^2}}{z_k^* - t'}\, dt' \tag{20}$$

Equation 20 can be further simplified by using the integral representation of the complex error function defined as

$$W(z) = \frac{i}{\pi} \int_{-\infty}^{\infty} \frac{e^{-t^2}}{z-t}\, dt \qquad (I_m(z) > 0) \tag{21}$$

The cross coherence term then becomes

$$\begin{aligned} I^{cc}(\omega_{as}) &= \frac{\pi}{2(\Delta\omega_p)^2} \sum_j a_j a_k^* W_j(z_j) W_k^*(z_k) \\ &= \frac{\pi}{2(\Delta\omega_p)^2} \left| \sum_{j,k} a_j W_j(z_j) \right|^2 \end{aligned} \tag{22}$$

The evaluation of the cross coherence term is speeded up by generating the complex error functions using an efficient algorithm (Hui et al. 1978).

2.7 Analytic (Closed Form) Solution of All CARS Integrals

The use of a complex error function approach to CARS analysis is a familiar one. Within the isolated line model closed form analytic solutions to CARS integrals have been widely used in literature (Yuratich 1979; Lasser 1980; Kataoka et al. 1982; Luthe et al. 1986). Greenhalgh and Hall (1986) have extended the use of these closed form expressions for all the CARS integrals in the presence of overlap and collisional narrowing of Raman lines. From the definitions of $D_j(\omega)$, z, t, and the error function W(z), the CARS interference term I^{int} in eq. 10 may be written as

$$I^{int}(\omega_{as}) = \frac{2\chi_{NR}\sqrt{\pi}}{\Delta\omega_p} \mathrm{Re}[i \sum_j a_j W(z_j)]$$

which may be simplified as

$$I^{int}(\omega_{as}) = -\frac{2\chi_{NR}\sqrt{\pi}}{\Delta\omega_p} \mathrm{Im}[\sum_j a_j W(z_j)] \tag{23}$$

The conventional resonant term I^{rr} is a little more complicated. Once again using the definitions of t, z, W(z), and $D_j(\omega)$.

$$I^{rr}(\omega_{as}) = \frac{1}{2\sqrt{\pi}\, \Delta\omega_p} \sum_{jk} a_j a_k^* \int \frac{e^{-t^2}}{(z_j - t)(z_k^* - t)}\, dt \tag{24}$$

Noting that

$$W(z_j) + W^*(z_k) = \frac{i}{\pi} \int \left[\frac{(z_k^* - z_j) e^{-t^2}}{(z_j - t)(z_k^* - t)} \right] dt \tag{25}$$

and

$$z_k^* - z_j = -[(\lambda_k' - \lambda_j') - i(\lambda_k'' + \lambda_j'')]$$

$$I^{rr}(\omega_{as}) = \frac{i\sqrt{\pi}}{2\Delta\omega_p} \sum_j \sum_k \frac{a_j a_k^*[W(z_k) + W^*(z_k)]}{(\lambda_k' - \lambda_j') - i(\lambda_k'' + {}_j\lambda'')} \qquad (26)$$

Let

$$U_j = \sum_k a_k^*/[\lambda_k' - \lambda_j' - i(\lambda_k'' + \lambda_j'')] \qquad (27)$$

Then I^{rr} becomes

$$I^{rr}(\omega_{as}) = \frac{i}{2\pi} \frac{\sqrt{\pi}}{\Delta\omega_p} \sum_j U_j a_j W(z_j) + \text{complex conjugate} \qquad (28)$$

The analytic form of the total CARS intensity can then be written as follows:

$$I(\omega_{as}) = \chi_{NR}^2 - \frac{2\sqrt{\pi}}{\Delta\omega_p} \chi_{NR} \sum_j \mathrm{Im}[a_j W(z_j)]$$

$$+ \frac{i\sqrt{\pi}}{2\Delta\omega_p} \sum_j U_j a_j W(z_j) + \text{c.c.} + \frac{\pi}{2(\Delta\omega_p)^2} \left| \sum_j a_j W(z_j) \right|^2 \qquad (29)$$

The analytic method outlined above requires less computer cpu time than the partially numeric approach with I^{cc} done analytically and only a small fraction of the time used by the totally numeric method with $\chi^{(3)}$ and $|\chi^{(3)}|^2$ convolution. Typical cpu times required to generate a CARS spectrum at 1550 K, at atmospheric pressure, for a typical 0.67 cm^{-1} pump width using the above three methods are summarized in Table I. The CARS theory program developed at NRC provides a choice of partially analytic or completely analytic forms of the CARS intensity expression.

Table 1. Comparison of cpu times taken by various pump convolution methods in CARS for a typical spectrum at 1 atm and 1550 K, with a pump band width of 0.67 cm^{-1}. The χ grid size was 0.00125 cm^{-1} and the grid for pump convolved spectrum was 0.04 cm^{-1}. These calculations were done in a DEC VAX-11/730 computer

Method	Cpu time
1. Convolve χ and $\lvert\chi\rvert^2$ and take the average	7 h, 50 min (Sandia)
2. Evaluate I^{cc} with analytic closed form expression and other CARS integrals from numerical convolution of $\lvert\chi\rvert^2$	4 h, 10 min (NRC)
3. Evaluate all CARS integrals with analytic closed form expressions	1 h, 10 min (NRC)

3.0 THIRD ORDER SUSCEPTIBILITY $\chi^{(3)}$

It was shown in the previous section that the CARS intensity is proportional to the square of the third-order susceptibility $\chi^{(3)}$. The resonant part χ_R of the susceptibility is proportional to the number density N of the probed molecule and contains information about the temperature and species concentration in the weight factors a_j in eq. 9. Equation 3 contains the line shape function in terms of the detuning frequency and Raman line width. The real part χ' of χ_R has a dispersive behaviour while the imaginary part χ'' has line shape or absorptive behaviour [Fig. 2]. The nonresonant part χ_{NR} of $\chi^{(3)}$ provides only a featureless spectrum that interferes with the resonant spectrum. In the following sections the various molecular parameters and environmental variables that go into calculating χ_R will be discussed.

3.1 Energy Levels and Line Positions

To calculate the eigenvalues λ_j' and λ_j'' that form the denominator of χ_R, one needs to know the rovibrational transition frequencies and the corresponding Raman line widths of the molecule in question. For diatomic molecules such as nitrogen, the vibration rotation energy levels (term energies) can be generated from Dunham expansion (Herzberg 1963) and known spectroscopic constants ω_e, $x\omega_e$, $y\omega_e$, and $z\omega_e$.

If v,J represent the vibration and rotation quantum numbers respectively, the term energies T(v,J) for an anharmonic vibrating rotor are given by

$$T(v,J) = G(v) + Fv(J) \qquad (30)$$

where

$$G(v) = \omega_e(v + \tfrac{1}{2}) - \omega_e x_e(v + \tfrac{1}{2})^2 + \omega_e y_e(v + \tfrac{1}{2})^3 + \omega_e z_e(v + \tfrac{1}{2})^4 \qquad (31)$$

is the vibrational contribution and

$$Fv(J) = B_v J(J + 1) - D_v J^2(J + 1)^2 + H_v J^3(J + 1)^3 \qquad (32)$$

is the rotational contribution.

D_v and B_v are found from the relations

$$B_v = B_e - \alpha_e(v + \tfrac{1}{2}) + \gamma_e(v + \tfrac{1}{2})^2 \qquad (33)$$

$$D_v = D_e + B_e(v + \tfrac{1}{2}) \qquad (34)$$

$$H_v = H_o + H_e(v + \tfrac{1}{2}) \qquad (35)$$

where B_e, α_e, D_e, B_e, H_o, and H_e are also molecular constants. From the term energies, the Raman line positions or transition frequencies $\nu_{v,J,v',J'}$ are determined according to the equation

$$\nu_{v,J,v',J'} = T(v',J') - T(v,J) \tag{36}$$

where v',J' correspond to the final and v,J to the initial levels. The Q branch transitions with $v' = v + 1$ and $J' = J$ essentially provide all the Raman intensity, but small contributions from relatively weak lines also originate from the O branch ($v' = v + 1$, $J' = J - 2$) and S branch ($v' = v + 1$, $J' = J + 2$) transitions. Knowing ν, the corresponding circular frequencies $\omega = 2\pi c\nu$ and the detuning factors $\delta = \omega - \omega_{as}$ can be obtained.

3.2 Population Factor $\Delta\rho$

The strong temperature dependence of the CARS spectrum is due to the population factor $\Delta\rho$, which is the fractional population difference between the higher and lower levels. The population factor enters χ_R through the weight factors a_j in eq. (9) and is defined as

$$\Delta\rho(v,J,v',J') = f(v,J) - f(v',J') \tag{37}$$

where the fraction of molecules f(v,J) in a vibrational rotational level in thermal equilibrium are given by the Boltzmann distribution. For a rigid rotator, these levels have a rotational degeneracy of (2J + 1) and an additional degeneracy G_J arising from nuclear spin. The net nuclear angular momentum for nitrogen has values 2, 1, and 0. The symmetry of the nuclear functions is such that the even J levels have $G_J = 6$ and the odd J levels have $G_J = 3$. Thus

$$f(v,J) = \frac{1}{Q_{rot}Q_{vib}} G_J(2J + 1)e^{-\frac{hc}{kT}G_v} e^{-\frac{hc}{kT}F_v(J)} \tag{38}$$

where Q_{rot} and Q_{vib} are rotational and vibrational partition functions respectively, that define the corresponding state sums.

$$Q_{vib} = \sum_v \exp\left(-\frac{hc}{kT} G_v\right) \tag{39}$$

$$Q_{rot} = \sum_J (2J + 1)\, G_J \exp\left(-\frac{hc}{kT} F_v(J)\right) \tag{40}$$

3.3 The Transition Amplitudes

The vector of transition amplitudes d or polarizability matrix elements can be related to the Raman differential scattering cross-section $\frac{d\sigma}{d\Omega}$ (Farrow et al. 1982; Hall 1979).

$$d^2(v,J) = \frac{2\pi c^4 N}{h\omega_s^4} \frac{d\sigma}{d\Omega}\bigg|_{v,J} \tag{41}$$

where c is the velocity of light, h is the Planck constant, and ω_s is the

Stokes laser frequency. The scattering cross section $d\sigma/d\Omega$, in turn, can be expressed as a function of the derivatives, with internuclear distance, of the mean and anisotropic components (α',γ') of the molecular polarizability, the Placzek Teller factors $B_{JJ'}$ (Stoicheff 1959; Luthe et al. 1986), the harmonic oscillator frequency ω_o, and the reduced mass μ of the molecule,

$$\left.\frac{d\sigma}{d\Omega}\right|_{O,S} = \frac{\omega_s^4}{c^4} \frac{\frac{h}{2\pi}}{2\mu\omega_o} \left(\frac{4}{45} B_{JJ'}\gamma'^2\right)(v + 1) \tag{42}$$

$$\left.\frac{d\sigma}{d\Omega}\right|_{Q} = \frac{\omega_s^4}{c^4} \frac{\frac{h}{2\pi}}{2\mu\omega_o} \left(\alpha'^2 + \frac{4}{45} B_{JJ'}\gamma'^2\right)(v + 1) \tag{43}$$

The factors $B_{JJ'}$ for the Q, O and S branches are:

$$B_{J,J-2} = \frac{3}{2} \frac{J(J - 1)}{(2J + 1)(2J - 1)} \quad \text{... O branch} \tag{44a}$$

$$B_{J,J} = \frac{J(J+1)}{(2J - 1)(2J + 3)} \quad \text{... Q branch} \tag{44b}$$

$$B_{J,J+2} = \frac{3}{2} \frac{(J + 1)(J + 2)}{(2J + 1)(2J + 3)} \quad \text{... S branch} \tag{44c}$$

3.4 Corrections to the Transition Amplitudes

The transition amplitudes $d(v,J)$ or polarizability matrix elements may be subject to corrections owing to centrifugal distortion caused by vibration rotation interaction. These corrections based on Raman intensity calculations by James and Klemperer (James and Klemperer 1959) and Buckingham and Szabo (1978) are as follows:

$$\mathrm{cdcorr}(Q) = 6 \frac{B_e}{\omega_e^{\,2}} \tag{45a}$$

$$\mathrm{cdcorr}(O) = \left[1 + \frac{4B_e}{\omega_e} \kappa \,(2J - 1)\right]^2 \tag{45b}$$

$$\mathrm{cdcorr}(S) = \left[1 - \frac{4B_e}{\omega_e} \kappa \,(2J + 3)\right]^2 \tag{45c}$$

where $\kappa = \gamma/\gamma' r_e$, γ is the mean molecular polarizability, and r_e is the internuclear distance. In the CARS calculations d^2 is multiplied by the above correction factors. The product of d^2 and the population factor $\Delta\rho$ is also referred to as the line strength factor.

3.5 Number Density

The number density, N is related to the mole fraction xmole, pressure P, and temperature T.

$$N = \frac{\text{xmole} \times P \times 1.013 \times 10^6}{kT} \tag{46}$$

where P is in atmospheres, T is in K, the Boltzmann constant k is given by 1.3805×10^{-16} erg/K and N is in molecules/cm^3.

3.6 The G-Matrix and the Weight Factors

The line positions determined as shown above can be combined with the diagonal elements (Raman line widths) and off-diagonal elements of the rate matrix, as described in section 2.1 to generate the G-matrix whose eigenvalues λ_j' and λ_j'' are used to define the denominator of χ_R. The transformation matrix A formed from the corresponding eigenvectors, together with the transition amplitudes d(v,J), the population factors $\Delta\rho$, and the number density, yield the complex weight factors a_j. Then the resonant CARS susceptibility can be calculated from eq. 3.

3.7 Nonresonant Susceptibility

The nonresonant susceptiility has a weak frequency dependence and is essentially featureless over the frequency range under consideration. However it modulates the resonant spectrum noticeably when the probed species concentration xmole is low (see Fig. 2 for weak lines). Consider the expression for the CARS intensity in eq. 10. When the probed species forms more than 70% of the medium, it is clear that the resonant terms are much greater than χ_{NR} and the latter plays little role in defining the spectrum. When xmole is small the resonant terms compete with that from χ_{NR} through the interference term $2\chi_{NR}\langle\chi_R\rangle$. This interference depends on the strength and overlap of Raman resonances in a given frequency region. When the probed species is present in too small amounts, the resonant spectrum disappears into the dispersionless non resonant background.

One useful outcome of χ_{NR} modulation is a technique to determine the concentration xmole of the species from the shape of the CARS spectrum as shown by Hall and Boedker (1984). By defining $\bar{\chi}_R$ and $\bar{\chi}_{NR}$ as the per molecule contributions and dividing by χ_{NR}, the CARS intensity may be expressed as

$$\begin{aligned} I(\omega_{as}) \sim\ & \langle 1\rangle + 2C\,\langle \mathrm{Re}\,\bar{\chi}_R(\omega_{as} - \omega')\rangle \\ & + \frac{C^2}{2}\langle|\bar{\chi}_R(\omega_{as} - \omega')|^2\rangle + \frac{C^2}{2}\langle\bar{\chi}_R(\omega_{as} - \omega')\bar{\chi}_R^*(\omega_{as} - \omega'')\rangle \end{aligned} \tag{47}$$

where C is the ratio xmole/$\bar{\chi}_{NR}$. If temperature and χ_{NR} are known it is clear that the above equation can be used to find the concentration xmole. When uncertainties are present in the values of χ_{NR} only the ratio C can be obtained. Using eq. 47 the NRC CARS program can be easily modified to estimate the ratio C, and thus the species concentration xmole.

3.8 The Pump Convolved CARS Spectrum

Once χ_R and χ_{NR} are known one of the three methods discussed in Section 2.0 can be employed for generating pump convolved theoretical CARS spectra. The current NRC CARS code has the ability to produce one or more theoretical CARS spectra of diatomic molecules, such as N_2, CO, and O_2, as a function of temperature and store them in a file. As shown in Section 3.5, this program can easily be modified to generate the spectra for any value of C. These spectra can then be used with slit convolution and fitting programs to estimate best fit temperatures from experimental CARS spectra produced from a flame.

4.0 THEORETICAL NITROGEN CARS SPECTRA

As discussed in the previous sections theoretical modelling of a CARS spectrum involves several complex steps. The accuracy of the spectra calculated is a function of the various molecular input parameters and the procedure used to represent the convolution with a multimode pump laser. To simplify matters early CARS calculation around the world (for example, Hall 1979; Switzer et al. 1980) were done with the isolated line approximation, further assuming constant Raman line width and scattering cross section. More recent developments discussed in sections 1 and 2 have shown that overlap of Raman lines (pressure effects) and cross coherence between the two frequency degenerate pump photons can play major roles in defining a CARS spectrum. The current version of the CARS generating program at the Gas Dynamics Laboratory includes these recent advancements, but it can also use the simpler approximate models. The salient features of this FORTRAN code and the important variables therein are described in Appendix A.

The purpose of this section is to present the results of a study, that compares the various models under varied conditions of temperature, pressure, and pump laser band width. Nitrogen is the most abundant species in air fed combustion environments and N_2 CARS are commonly used for flame thermometry. Therefore, all the results presented here are based on nitrogen CARS spectra. Among other comparisons, the sensitivity of the final spectrum to molecular parameters and sampling interval used to calculate the digital spectrum is also discussed.

Some of the refinements in the code such as the including of O and S branches, were made as a result of comparing our program with a similar CARS program made available to us from Sandia Laboratories. A detailed comparison of spectra generated by the two CARS programs was undertaken as a separate task. These investigations, which validate the results, obtained from both the codes, are presented in Appendix B.

4.1 Molecular Parameters for Nitrogen

The molecular constants (we, xwe, ywe, zwe, Be, De, αe, βe), and run time parameters (pressure, temperature range, frequency range, model description), and pump laser parameters are read from an input data file such as the one shown in Appendix C. The Raman line positions are quite sensitive to these constants. Our earlier calculations were done with constants deduced by Gilson et al. (1980). More recently they were replaced by accurate measurements provided by L. Rahn (Sandia National Laboratories, private communication). These values are in the data file shown in Appendix C.

The off-diagonal elements of the relaxation matrix and the Raman line widths were determined by the Sandia scaling law described in Section 2.3. For nitrogen, the scaling law parameters are m = 0.1487, α = 0.023, β = 1.67 and [illegible] (Rahn and Palmer 1986). At present these parameters are used as fixed constants in the source code because these parameters are known only for nitrogen. The program can handle other diatomics, such as O_2 and CO, by making the above parameters part of the input data file.

The polarizability derivatives were obtained from experimental Raman cross sections and polarizability ratios (Farrow and Rahn 1985). Since the anisotropic contribution in eq. 48 is small, α' can be related to room temperture Q branch cross sections (Schrotter and Klockner (1979).

$$\left.\frac{d\sigma}{d\Omega}\right|_{v=0} = \frac{\hbar\omega_s^4}{2\mu\omega_c c^4}(\alpha')^2 \qquad (48)$$

The derivative of the anisotropic component γ' is found from the Q branch depolarization ratio given by

$$\rho_J = \frac{3B_{JJ'}(\gamma')^2}{45(\alpha')^2 + 4B_{JJ}(\gamma')^2} \qquad (49)$$

where B_{JJ} is set equal to its asymptotic value of 0.25 and can be expressed in units of area similar to cross section. In the input data table, α' = ALPHA and γ' = GAMMA.

CONST in the input data file is given by $1/(2\times\pi c)\mu\nu_o$ where c is the velocity of light in cm/s, the oscillator frequency $\nu_o = 2331\ \text{cm}^{-1}$, and the reduced mass μ = 7.0015 atomic mass units (Huber and Herzberg 1979).

The centrifugal distortion corrections need, in addition to γ', the anisotropic component γ of the polarizability. This is usually obtained from known value of γ' and experimentally observed values of the ratio $\gamma'/r_e\gamma$ where r_e is the internuclear distance (James and Klemperer 1959). The present calculations use $\gamma = 4.764$. The internuclear distance r_e (= 2.074 in Bohr radii) and the polarizability γ are used as fixed constants in the present CARS code.

The spectra were calculated for the products of a hydrogen air flame equivalence ratio of 0.575 with assumed composition of 70% N_2, 21.5% H_2O, 7.8% O_2, and 0.8% Ar. There has been some uncertainty in the χ_{NR} values of diatomic molecules. In units of 10^{-18} ergs/cm^3, the values used are 8.31 for N_2, 7.81 for O_2, 18.28 for H_2O, and 9.31 for Ar. The nitrogen value is the average of that quoted by Farrow and Rahn (1985) and Rosasco and Hurst (1985). The χ_{NR} of O_2 and Ar were taken from the latter reference. Such a mixture of gases yields a combined background susceptibility of 10.4 at NTP.

4.2 Sampling Scheme for $\chi^{(3)}$ Spectrum

Before studying the variation of the N_2 CARS spectra with temperature, pressure, and pump laser band width, etc., it is necessary to establish that the sampling schemes and convolution algorithms are satisfactory. The isolated line model with Yuratich convolution was chosen for this purpose because of its simplicity and smaller cpu times. To select this model the variable MODEL was set equal to 'IY'.

The $\chi^{(3)}$ spectrum gets contributions from Raman lines of varying amplitude and width. Care should be taken to include sufficient number of points to properly describe these lines. At atmospheric pressure and the flame temperature of 1550 K, typical widths of Raman lines are about 0.04 cm^{-1} (FWHM). To test the convolution algorithm, a spectrum was computed over a two wave number region with a 0.1 cm^{-1} pump and a grid of 0.0025 cm^{-1} for χ evaluation. The Raman line widths Γ_J were forced to be 0.001 times the actual value. With such narrow lines the grid spacing of 0.0025 is greater than the Raman width and hence inadequate. In Fig. 3 the square root of the intensity is plotted for one peak in the region. The convolved peak has a superimposed fine structure. This structure is probably due to the use of insufficient number of points and Simpson's rule of integration, which employs weighted sums of the function at these points. This structure disappeared when the above calculation was repeated with Γ_J = 0.1 of the actual value and a grid of 0.001 [Fig. 4]. In the latter case $\Gamma_J/0.001 \cong 4$; thus there are about four points used to describe most of the lines. The square root plot of the convolved spectrum in both cases reflects the 0.1 cm^{-1} band width of the pump laser, and hence indicates that the convolution algorithm is good when the sampling grid is narrow enough. Although it was assumed above that typical lines have Γ_J = 0.04 cm^{-1}, there may be Raman lines with high J values and widths as low as 0.02 cm^{-1} (Appendix D). Subsequently, the variation of a 2000 K spectrum (over a 40 cm^{-1} region) with grid size was investigated. The comparison of spectra obtained with grid size of 0.00125 cm^{-1} and a yet finer grid of 0.000625 cm^{-1} is shown in Fig. 5. These spectra show that changes produced by the smaller grid (curve A) are less than 0.05%. Thus, it was deecided that a grid size of 0.00125 cm^{-1} was sufficient to accurately describe even the narrow high J lines at flame temperatures. The smaller grid, of course, resulted in much longer cpu times, as compared with our earlier work (Snelling et al. 1987) done with a coarse grid of 0.01 cm^{-1} for $\chi^{(3)}$ generation.

4.3 Addition of O and S Branches

One of the refinements introduced in the current spectrum generating program is the addition O and S branches. Although usually neglected in most published CARS work, these lines make small contributions to the CARS spectrum. Figures 6a and 6b show the effect of these additions to a 1550 K spectrum calculated with 0.2 cm^{-1} pump band width. In this and most other plots that follow, the 80 cm^{-1} frequency region of the N_2 CARS spectrum is shown in two parts to allow better representation of the finer details. Whenever two spectra are compared the top plot in the figure shows the superimposed spectra, while the bottom one is the difference spectrum (A - B) or the ratio spectrum (A/B). The text above the graphs shows the file name, temperature (T), spectral shift in cm^{-1} (S), xmole/$\overline{\chi}_{NR}$ (C), pump laser band width FWHM in cm^{-1} (PW), model used (M), and a variable defining the Raman line widths used (S). For a 0.2 cm^{-1} pump, the square root plots indicate that the O and S contributions are of the order of a few percent near the 2-3 band, decrease as we move to higher wave number regions, and are practically insignificant for the 0-1 band. This is not surprising because the relatively weak O and S lines can compete with only the weaker Q branch lines near the hot band. The locations of these lines, along with their widths, populations, and peak amplitudes, for a typical flame temperature spectrum are summarized in Appendix D.

4.4 Determination of Line Positions

The Raman shifts or line positions are determined from term energy differences as given by eq. 36. When several closely spaced overlapping lines are present in a region it is important to calculate these numbers as precisely as possible. The Raman shifts for N_2 are of the order of 2000 cm^{-1}. To retain more precision in these numbers without resorting to double precision calculations, the term energies were offset by $\omega_e \times v$, where v is the vibrational quantum number and the shifts were stored as smaller numbers with more significant digits. The frequencies ω_{as} at which the susceptibility was calculated were similarly offset to accurately find the detuning δ. At the end of the susceptibility calculation the Raman shifts were restored by a negative offset.

4.5 Collisional Narrowing Effects

Collisional narrowing, as described earlier, was implemented through the G-matrix approach. In actual calculations, however, only the Q branch transitions are treated in this manner. The O and S branch lines are assumed to be isolated. Throughout this report all G matrix calculations referred to have this restriction implied. Within the G-matrix model, it is interesting to compare the errors introduced by performing a single matrix diagonalization (that can reduce the cpu time) as opposed to separate matrix manipulations for all the vibrational bands. In Fig. 7, 1550 K spectra with one- (curve B) and three matrix inversions (curve A) are compared. The plots of the square root of intensity show that noticeable differences are produced near the hot band as expected. Convolution with a narrow pump of 0.2 cm^{-1} makes the differences appear more pronounced. Based on these spectra, it was decided that individual matrix diagonalization and inversion are required to accurately determine the eigenvalues and eigenvectors.

In the following plots, N_2 CARS spectra generated with the isolated line approximation (IY) (curve B) are compared with that obtained with the G-matrix model (GY) (curve A) which uses the eigenvalue eigenfunction approach. Both IY and GY models perform Yuratich type convolution. Spectra produced with a 0.2 cm^{-1} pump width are displayed in Figs. 8-10. Plots are shown for temperatures of 1000, 1550, and 2000 K. All the spectra are at atmospheric pressure. These spectra show that the difference between the IY and GY models is most significant near the band head for all three temperatures. This is because collisional narrowing becomes important in this region owing to the presence of several closely spaced strong lines.

The true significance of line narrowing becomes clear at higher pressures. Figure 11 a shows a 1 atm. spectrum (curve A) (1 atm = 101.325 kPa) superimposed on a spectrum at 10 atm (curve B). These 1550 K spectra were produced with a larger pump band width of 0.7 cm^{-1}, so that there is less rotational structure displayed. The spectra show that, while the individual lines broaden with increasing pressure, the total spectrum collapses around the strong lines, resulting in a narrowing effect.

Figure 12 compares collisionally narrowed spectra at pressures of 10, 20, 30, and 50 atm. One can infer from these plots that collisional narrowing is dramatic for the initial increase in pressure above 1 atm, but changes in the shape of the spectrum that are caused by a further increase in pressure are less pronounced.

4.6 Effect of Cross Coherence Terms

It is important to see the effect of including the cross coherence effects by means of the K-T convolution. When the pump laser band width $\Delta\omega_p$ is much less than the Raman line width Γ_J (this condition is met with single mode lasers or at high pressures for multimode lasers), the conventional resonant term I^{rr} is equal to the cross coherence term I^{cc}. Then Yuratich convolution can give the same CARS spectrum as K-T convolution. At the other limit, when $\Delta\omega p >> \Gamma_J$, $I^{cc} \rightarrow 0$. In this case the Yuratich convolution can still give correct results provided I^{rr} is halved.

When $\Delta\omega_p$ is slightly greater than Γ_J, the K-T convolution becomes significantly different from the Yuratich approach. This is illustrated in Figs. 13-15, where spectra are shown for 1000, 1550 and 2000 K. At these temperatures, the Raman line widths at 1 atm range between 0.04 and 0.02 $cm^{-1}$for the prominent Q branch lines. With a pump of 0.2 cm^{-1}, the cross coherence term is of the order of $\Gamma_J/\Delta\omega_p$ (Hall 1985). The ratio of $\Delta\omega_p$ and Γ_J is such that cross coherence effects are noticeable. The plots show that the difference between spectra calculated with Yuratich (GY) and K-T (GT) convolution increases with decreasing temperature. The Yuratich method sets the I^{rr} and I^{cc} terms equal and thus overestimates the ratio χ_R/χ_{NR}. As temperature decreases, this ratio increases, and hence, the error caused by ignoring coherence also increases.

4.7 Room Temperature N_2 Spectra

Figure 16 compares 300 K, 1 atm N_2 CARS spectra obtained with the simplest IY model (curve B) and that obtained with the most accurate GT model (curve A). The unnormalized square root spectra reveal the changes produced by properly accounting for collisional narrowing of Raman lines and cross coherence effects.

4.8 Comparison of Numeric and Analytic Models

Finally it is interesting to compare typical flame CARS spectra generated by using the partially analytic GT model with that from the much faster GTAN model, which uses closed form solutions for the CARS integrals. Figure 17 displays this comparison for 2000 K spectrum at 1 atm, generated for a pump band width of $\Delta\omega_p = 0.7$ cm^{-1}. The plots demonstrate that the agreement between the spectra is very good. As shown in Table 1, the GTAN model runs about four times faster and can generate a pump convolved library in a much shorter time.

4.9 Comparison of Spectra from the Old Program with that from the Current Updated Version

It is interesting to examine whether the recent refinements introduced in the current theory program of NRC has resulted in significant changes in the fitted temperature, as compared with the older version used in our earlier work (Snelling et al. 1987). With this objective, a typical theoretical spectrum (1550 K, 1 atm, 0.67 cm^{-1} pump band width) that was generated by the old program was fitted against a slit convolved spectral library from the current version. The fitting was accomplished with the FIT_FLAME program (see Section 5) and the results are summarized in Table 2. The refinements have produced a modest change of 8.5 degrees in the fitted temperature. This shows that the earlier program, which also had collisional narrowing and cross coherence effects, was basically correct. The addition of O and S branches and using a finer grid size for a more accurate calculation of χ has indeed resulted in a small change in the temperature, as expected.

Table 2. Fit of a CARS theoretical spectrum from the "old" program (Snelling et al. 1987) against the current updated version of the theory program

Cycle	Temperature	Frequency shift	%SD
0	1800.0	0.000	23.341
1	1558.8	0.015	3.227
2	1558.7	0.013	3.120
3	1558.8	0.013	3.119

5.0 FITTING OF EXPERIMENTAL N_2 CARS SPECTRA

5.1 CARS Spectrometer and Data Acquisition System

The optical layout of the CARS spectrometer and a detailed description of the operating procedure has been described previously (Snelling et al. 1985, 1987). The pump is a frequency doubled Nd:Yag laser operating at 10 Hz, which also serves to pump the dye laser oscillator and amplifier. The centre wavelength of the dye laser was tuned by varying the dye concentration, which is typically 2.6×10^{-4} M rhodamine 640 or more, conveniently by inserting a band-pass filter in the dye cavity (centered at 620 nm with a width (FWHM) of 9.5 nm). The filter is typically set at 20 degree to obtain a centre wavelength of 606 nm for N_2 CARS. The filter reduces the dye laser bandwidth from 150 to 70 cm^{-1} (FWHM).

Galilean telescopes are installed in the path of the pump and Stokes beams to control beam diameter and focal spot location. The telescopes provide beam magnification of 1.9. The two beams are combined collinearly with a dichroic mirror and focused with a 203 mm focal length lens. Typically 30-40 mJ of pump radiation and 10 mJ of Stokes radiation are used. The three-dimensional phase-matching technique employed [Fig. 1] involves passing the ω_s Stokes beam coaxially through the annular pump beam. The ω_p and ω_s beams and the resulting CARS (ω_{as}) beam are recollimated and low pass filters are used to reflect the now unwanted pump and Stokes radiation. A beam splitter directs part of the CARS signal to a photomultiplier tube connected to an EG&G model 162 boxcar integrator. The boxcar signal gives a measure of the time averaged (time constant of 5 s) undispersed CARS signal. The remaining CARS radiation is focused on the entrance slit of a spectrometer utilizing a single concave holographic diffraction grating (American Holographics). This grating disperses the CARS radiation across the face of a Tracor Northern 1024-element intensified diode array rapid scan detector (IDARSS TN-6132). The 1.6 m spectrometer has a reciprocal linear dispersion of 2.24 Å/mm (1 Å = 0.1 nm), corresponding to 0.25 cm^{-1} per diode. The spectral width of the pump laser was measured with a Fabry-Perot etalon.

Nonresonant CARS spectra were recorded by placing a carbon dioxide filled cell at the focal volume. To provide a CARS signal that needed to overcome the shot noise of the detector, it was sometimes necessary to pressurize the cell to 3 atm.

It was also necessary to correct the CARS signals by subtracting the background that results from detector dark current, detector fixed pattern noise, and a small signal due to scattered 532 nm radiation. This background signal was obtained by acquiring spectra while blocking the Stokes laser. To remove the small residual signals remaining on the detector owing to image lag, it was necessary to perform two "cleansing scans" of the detector between each laser pulse. The cleansing scans were initiated by the external read signal from the timing circuits that triggered the optical multichannel analyzer (OMA) to read but not store the diode intensities. The laser pulse and signal integration began immediately after completion of the cleansing scans. The entire cycle was completed within 100 ms for the 10 Hz operation.

The acquisition and storage of 1024-element spectra at a 10 Hz rate was as follows. As each spectrum was collected by the OMA, a previous one was transferred to the DEC VAX11/730 via the parallel long line drivers, where it was checked for saturation or transmission errors. The data was transmitted and temporarily stored in binary form to increase speed and reduce storage. Upon completion of a collection run, the data was treated by post processing software on the VAX. This included multiplication by 8 (to retain accuracy during later manipulation of the data), subtraction of the background spectrum, division by the nonresonant spectrum (to correct for diode to diode sensitivity variations and the spectral variations owing to the dye laser, spectrometer, etc.), calculation of the average spectrum for the collection, and permanent storage of these treated spectra in binary form (2 k bytes per spectrum).

The flame spectra were recorded in a hydrogen/air flat-flame burner (Snelling et al. 1985, 1987) operating at an equivalence ratio of 0.574 with carbon dioxide as sheath gas.

5.2 Least Mean Square Fitting Algorithm

To extract useful information such as the estimate of temperature from the N_2 CARS spectra, it is necessary to fit the experimental spectra with theoretical spectra generated from equations described in earlier sections. In the present work, this fitting is done by means of a nonlinear Gauss-Newton (Hartley 1961) least mean square scheme, as outlined by Kim (1970). This technique may be explained as follows.

Let Y_i be a set of experimental values that need to be fitted. Let $F(\alpha_1,\alpha_2,\alpha_3,\ldots,\alpha_L,X)$ be the theoretical function that models the data, with X as the independent variable and $\alpha_1,\alpha_2,\ldots,\alpha_L$ as parameters to be estimated. According to the principle of least mean squares the best estimate for the parameters is obtained when the residual sum of the squares given by

$$R = \sum_{i=1}^{M} (Y_i - F(\alpha_1,\alpha_2,\ldots,\alpha_L,X))^2 \qquad (50)$$

of the differences between calculated and observed values is a minimum.

This condition yields the following normal equations

$$\frac{\partial R}{\partial \alpha_1} = \frac{\partial R}{\partial \alpha_2} = \ldots \frac{\partial R}{\partial \alpha_L} = 0 \qquad (51)$$

When the regression function F in eq. 50 is linear in the parameters α, the L normal equations obtained above are linear in α and can be easily solved to yield the parameters. When the regression function is nonlinear in α, the estimation procedure becomes more difficult.

The CARS spectrum is a nonlinear function of temperature. In such cases, the theoretical function F may be expanded in terms of a Taylor series about a set of trial values of the parameters.

$$F_i(\alpha_1,\alpha_2,\ldots\alpha_L,X) = Y_i^o + \frac{\partial F_i}{\partial \alpha_1}(\Delta\alpha_1) + \frac{\partial F_i}{\partial \alpha_2}(\Delta\alpha_2) + \ldots \left[\frac{\partial F_i}{\partial \alpha_L}\right](\Delta\alpha_L)$$

$$+ \text{ higher order terms} \qquad (52)$$

Here $Y_i^o = F(\alpha_1^o,\alpha_2^o,\alpha_3^o,\ldots\alpha_L^o,X_i)$ and $\alpha_1^o,\alpha_2^o,\alpha_3^o,\ldots$ are the initial trial parameters.

If we neglect terms higher than second order in the above equation, it can be shown that eq. 51 and 52 will give a set of linear normal equations that can be solved to yield the parameters, α.

In practice we start with a set of initial guesses for α and form the error vector $\utilde{\epsilon}$ as

$$\utilde{\epsilon} = \utilde{Y} - \utilde{Y}^o \qquad (53)$$

where $\epsilon_i = Y_i - Y_i^o$.

A small increment, $\Delta\alpha_j$, is given to the j^{th} parameter and the function Y^1 at $\alpha_j + \Delta\alpha_j$ is calculated. The differentials form the first column of a

Jacobian matrix. Other columns of the Jacobian matrix are constructed in a similar way, by varying a given parameter while all others are held constant.

Thus the elements of the Jacobian matrix J may be defined as

$$J_{ij} = \frac{\partial F_i}{\partial \alpha_j} = \frac{Y_i^1 - Y_i^o}{\Delta\alpha_j} \qquad (54)$$

Then the matrix $\tilde{\Delta Y} = \tilde{Y}^1 - \tilde{Y}^o$ and the matrix $\tilde{\Delta\alpha} = \tilde{\alpha}^1 - \tilde{\alpha}^o$ are related to $\tilde{J}$ according to the equation

$$\tilde{\Delta Y} = \tilde{J} \cdot \tilde{\Delta\alpha} \qquad (55)$$

The sum of residuals R in eq. 50 may now be expressed in matrix notation as

$$\tilde{R} = [\tilde{Y} - (\tilde{Y}^o + \tilde{\Delta Y})]^*[\tilde{Y} - (\tilde{Y}^o + \tilde{\Delta Y})] \qquad (56)$$

where * indicates the transpose.

Upon differentiation of R and rearranging terms, one can obtain the column matrix which gives the corrections to the parameters for the first cycle.

$$\tilde{\Delta\alpha} = (\tilde{J}^* \cdot J)^{-1} \tilde{J}^* \cdot \tilde{\epsilon} \qquad (57)$$

This correction procedure is repeated iteratively until convergence is achieved.

Equationn (57) assumes equal weights for all the experimental data. If a nonuniform weighting scheme is used, the correction matrix can be calculated as

$$\tilde{\Delta\alpha} = (\tilde{J}^* \cdot \tilde{W} \cdot \tilde{J})^{-1} \cdot (\tilde{J}^* \cdot \tilde{W} \cdot \tilde{\epsilon}) \qquad (58)$$

where W is a column matrix of weights. Using eq. 58 experimental CARS spectra can be fitted with theory to yield best fit values of temperature, frequency shift, and slit function parameters.

5.2.1 Stretch parameter in CARS spectral fits

Experimental data are in arbitrary units so that the absolute values of the theoretical and experimental CARS spectra are scaled differently. In the fitting process, it is therefore necessary to normalize either theory or experiment suitably. This can be achieved by multiplying the theorertical spectrum with a factor K, such that the residual sum of squares is minimized. The stretch factor K is obtained from the equation $\frac{\partial R^1}{\partial K} = 0$, where R^1 is given by

$$R^1 = \sum_{i=1}^{M} [Y_i - KF(\alpha_1,\alpha_2,\ldots,\alpha_L,X_i)]^2 \ . \qquad (59)$$

For equally weighted data

$$K = \frac{\sum_{i=1}^{M} F(\alpha_1,\alpha_2,\ldots,X_i)Y_i}{\sum_{i=1}^{M} F^2(\alpha_1,\alpha_2,\ldots,X_i)} \qquad (60)$$

For a weighted fit the corresponding expression is

$$K_W = \frac{\sum_{i=1}^{M} W_i \ F(\alpha_1,\alpha_2,\ldots,X_i)Y_i}{\sum_{i=1}^{M} W_i \ F^2(\alpha_1,\alpha_2,\ldots,X_i)} \qquad (61)$$

All the fit programs described below have the stretch factor K estimated in every cycle of iteration.

5.3 CARS Spectral Library

In any normal least mean square analysis of experimental data the theoretical modelling equation is calculated at each cycle of iteration. In CARS broadband analysis this is not practical, because a few hours of cpu time may be needed to generate a single theoretical spectrum at flame temperature. Therefore, the concept of generating a set of spectra as a function of temperature and storing them in a library is in wide use in CARS thermometry. The fitting programs retrieve the spectra from this spectral library and use them after suitable interpolation to obtain intermediate temperatures. It was found that a temperature step of 50 K in the library was sufficient for CARS analysis.

5.4 Voigt Slit Function

The CARS integrals in eq. 10 give the theoretical intensity of the CARS signal as it enters the detector elements. The spectrum should, therefore, be convolved with a suitable slit function that describes the frequency response of the detection system to a monochromatic input signal. In the present work an approximate Voigt function was used for this purpose. In this approximation (Whiting 1968), the Voigt width w_V and Lorentz width w_L are related to the Gaussian width w_G as follows:

$$w_V = w_L + [\frac{w_L^2}{4} + w_G^2]^{1/2} \qquad (62)$$

An asymmetric Voigt function with different values of w_V and w_L on the high and low (cm^{-1}) sides, respectively, was found to be suitable.

The parameters w_L and w_V (slit widths FWHM) may be determined by fitting room temperature (293 K) CARS spectra with theory. In this method, theoretical room temperature CARS spectrum is convolved with a Voigt of trial widths and also frequency shift. This slit convolved spectrum is compared with experimental spectra and best fit values of the parameters are obtained by means of the least mean square scheme explained in Section 5.2.

The slit function parameters can also be obtained from hot spectra. In this case, it is necessary to include temperature as an additional parameter in the fitting process. Further a library of pump convolved theoretical CARS spectra (Section 5.3) is also required.

A computer program called FIT was written to estimate the Voigt slit parameters from room or flame temperature CARS spectra. A brief description of this program is given in Appendix E.

5.4.1 Voigt parameters from N_2 CARS spectra

A typical run of the FIT program to obtain Voigt parameters from room temperature N_2 CARS spectrum is shown below.

```
$ FITT
Fitting options:
     1 - fit Voigt and shift
     2 - fit all six parameters
Select fitting option(1 to 2;default = 1):
1
Plotting options:
     0 - none
     1 - after last cycle
     2 - after each cycle
Select plotting option (0 to 2;default = 1):
0
Enter the theoretical filename (default='N2RT'):
DV:N2RT.SPT.2
Reading theoretical spectrum file DUAO:[SANDIA.VERSION2]N2RT.SPT;2
Enter the weighting coefficients CL, CM, and CN
     (default is 1.0,0.0,0.0):
2.,1.03E-3,4.E-6
Enter the shift guess and the Voigt slit parameters:
Lorentz-low, Voigt-low, Lorentz-high, Voigt-high is 0.0,1.0,2.0,1.0,2.0):

Select form of non-linear correction
(0=none,1=file,2=NRC,3=EMR,4=user) (0 to 4;default = 1):
2
Do you want to use the default fitting values (YN,default=Y):
N
Enter the lowest wavenumber to be plotted (in 1/cm)

  (2295.0 to 2360.0;default = 2300.0):
2305.
Enter the highest wavenumber to be plotted (in 1/cm)
  (2305.0 to 2360.0;default = 2355.0):
```

```
2345.
Enter the lowest wavenumber to be fitted (in 1/cm)

  (2305.0 to 2345.0;default = 2305.0):
2305.
enter the highest wavenumber to be fitted (in 1/cm)

  (2305.0 to 2345.0;default = 2345.0):
2345.
Enter the maximum number of spectra per file to process

(>= 0; default = 0):

Enter the minimum number of cycles for fitting (1 to 20;default = 4):

Enter the maximum number of cycles for fitting (4 to 20;default = 10):

Enter the temperature increment (in deg. K) for the jacobian

(>= 0.0;default = 50.0):

Enter the max. temp. change (in deg. K) between cycles

  (>= 0.0; default = 3.0):

Enter the wavenumber increment (in 1/cm) for the jacobian

  (>= 0.0; default = 0.1):

Group how many experimental points (>= 1; default = 2):
1
Enter the experimental filename  (no default):
EAGLE:[TRACOR]S38111003.SPT.1
The input filename is EAGLE:[TRACOR]S38111003.SPT;1.
There are 401 experimental spectra in this file.
Pump ranges from 2295.00 to   2360.00 step  0.10
Slit ranges from 2305.00 to   2345.00 step  0.20

MODEL = GT             SCLNG = SN
GDIAG = ALL            Pump width = 0.67 cm-1

-------------------------------Spectrum 0-------------------------------

            Low cm-1                 High cm-1

Cycle S_FIT  LW    VW    HEQWL  LW    VW    HEQWH B_STD% EQWID STCH_FCTR
  0   0.000 1.000 2.000 1.296 1.000 2.000 1.296 30.551 2.593 0.433E-04
  1   0.538 1.075 2.177 1.408 1.072 1.185 0.897  5.332 2.305 0.498E-04
  2   0.404 1.101 1.886 1.263 1.045 1.361 0.979  3.064 2.241 0.514E-04
  3   0.349 1.132 1.756 1.204 1.008 1.457 1.018  2.800 2.222 0.519E-04
  4   0.343 1.134 1.723 1.188 1.008 1.446 1.012  2.758 2.200 0.524E-04
  5   0.337 1.136 1.713 1.183 1.003 1.458 1.017  2.738 2.200 0.524E-04
  6   0.339 1.135 1.714 1.184 1.005 1.451 1.014  2.730 2.197 0.525E-04
```

The program outputs the best fit values for each cycle of the iteration of the nonlinear least mean squares fit, where S_FIT is the shift and LW, VW are the Lorentz and Voigt slit parameters (FWHM) in cm^{-1}. HEQWL, HEQWH, and EQWID give the equivalent half widths (the equivalent width of a rectangle of area equal to the peak considered) of the low and high cm^{-1} Voigt parameters and their sum. N_STD% is defined as the square root of the variance divided by the average CARS intensity and expressed as a percentage. STCH_FCTR is the stretch factor discussed earlier.

The fit converges smoothly and the best fit plot in Fig. 18 shows excellent agreement between experiment and theory.

The slit function can also be obtained from CARS flame spectra, although with single-shot spectra the six parameter fit will frequently not converge. An average of 100 or more flame spectra is sufficiently noise-free to permit convergence and gives a reproducible fit. A typical run of this program is given below.

```
$ FITT
Fitting options:
     1 - fit voigt and shift
     2 - fit all six parameters
Select fitting option (1 to 2;default  1):
2
Plotting options:
     0 - none
     1 - after last cycle
     2 - after each cycle
Select plotting option (0 to 2;default = 1):
0
Enter the theoretical filename (default='N2PC'):
DV:N_LIB.SPT.6
Reading theoretical spectrum file DUAO:[SANDIA.VERSION2]N_LIB.SPT;6,
Enter the initial temperature guess (1300.0 to 2000.0;default = 1550.0):
1600
Enter the weighting coefficients CL, CM and CN (default is 1.0,0.0,0.0):
2.,1.03E-3,4.E-6
Enter the shift guess and the Voigt slit parameters:
Lorentz-low, Voigt-low, Lorentz-high, Voigt-high(default is
0.0,1.0,2.0,1.0,2.0):

Select form of non linear correction
(0=none,1=file,2=NRC,3=EMR,4=user)(0 to 4;default = 1):
2
Do you want to use the default fitting values (YN,default=Y):
N
Enter the lowest wavenumber to be plotted (in 1/cm)
(2263.0 to 2353.0;default = 2263.0):
2265.

Enter the highest wavenumber to be plotted (in 1/cm)
(2265.0 to 2353.0;default = 2353.0):
2343.
```

```
Enter the lowest wavenumber to be fitted (in 1/cm)
(2265.0 to 2343;default = 2273.0):

Enter the highest wavenumber to be fitted (in 1/cm)
(2273.0 to 2343.0;default = 2343.0):

Enter the maximum number of spectra per file to process(>= 0;default =
0):

Enter the minimum number of cycles for fitting (1 to 20;default = 4):

Enter the maximum number of cycles for fitting (4 to 20;default = 10):

Enter the temperature increment (in deg. K) for the jacobian
(>= 0.0;default = 50.0):

Enter the max. temp. change (in deg. K) between cycles

(>= 0.,0;default = 3.0):

Enter the wavenumber increment (in 1/cm) for the jacobian
(>= 0.0;default = 0.1):

Group how many experimental points (>= 1;default = 2):
1
Enter the experimental filename (no default):

EAGLE:[TRACOR]S48111005.SPT;1
There are 401 experimental spectra in this file.
Pump ranges from 2263.00 to 2353.00 step 0.04
Slit ranges from 2265.00 to 2343.00 step 0.24

MODEL = GT            SCLNG = SH
GDIAG = ALL           Pump width = 0.67 cm-1

--------------------------------Spectrum 0---------------------------------
                Low cm-1                High cm-1

Cyc  T_FIT  S_FIT  LW    VW    HEQWL  LW    VW    HEQWH  N_STD% EQWID STCH_FCTR
  0 1600.00 0.000 1.000 2.000 1.296 1.000 2.000 1.296 17.188 2.593 0.109E-01
  1 1690.11 0.730 0.706 2.232 1.347 1.171 1.446 1.057  5.735 2.403 0.142E-01
  2 1695.76 0.234 0.875 1.126 0.812 0.846 2.267 1.398  4.218 2.211 0.156E-01
  3 1696.01 0.415 0.690 1.417 0.914 1.079 1.631 1.126  3.553 2.040 0.169E-01
  4 1695.36 0.400 0.763 1.407 0.928 1.038 1.753 1.178  3.350 2.106 0.164E-01
```

The output is identical to that of the room temperature fit with the addition of the best-fit temperature. The fit converges rapidly and the plot of the best-fit spectrum is shown in Fig. 19. In general the fit is not as good as the room temperature spectra, and although the total equivalent width is very similar for the two fits, the individual Voigt parameters are often very different.

5.5 Slit Convolved Theoretical CARS Spectra

Once the instrument slit function parameters were determined the library of pump convolved CARS spectra over a range of temperatures were subjected to a slit convolution to produce a slit convolved library. This was done by means of a simple program called CONVOLVE, whose function is to read a set of theoretical CARS spectra at equal temperature intervals and convolve them sequentially with a triangular, Gaussian, or Voigt function, with specified parameters, and save the resulting spectra in a slit convolved spectral library.

5.6 Temperatures from N_2 CARS Spectra

Finally experimental CARS spectra (single shot and average) were fitted with theoretical CARS spectra from the slit convolved library, by means of the least mean square fitting algorithm described in Section 5.2. This part of the analysis was done with an efficient computer program named FITFLAME. Since the slit function was predefined, the only parameters directly included in the least mean square scheme were temperature and frequency shift. The best-fit temperatures and shifts thus obtained were stored in an output file to allow further statistical analysis. The details of the FITFLAME are outlined in Appendix F.

5.6.1 Results from FITFLAME program

A typical analysis performed by FITFLAME on flame CARS spectra is shown in this section.

The FITFLAME program produces more than one output file. One of them is a 'TH' file which contains detailed information about the theoretical file, the experimental file, the fit parameters for each spectrum for each iteration, and the mean temperature and standard deviation for the file analyzed. Frequently this program is used to analyze several data files containing hundreds of spectra. A summary of all files analyzed is saved in a TSUMMARY file. Examples of a 'TH' and TSUMMARY files are presented below. To reduce the size, the 'TH' file shown here was edited and results for only some of the spectra are displayed.

'TH' FILE:

```
This file is fitted temperature file
     SYS$SYSDEVICE:[SNELLING.CARSANALYSIS]TH6170004.LIS;1.
The data source file is
     DUA0:[DATA.DAFILES]DA6170004.DAT;1.
     It is a version 0 file with a NRC wavenumber scale.
The theoretical source file is
     DUA0:[SANDIA.VERSION2]N2SC.SPT;2.
The file was processed by program SPT_FIT_FLAME, version 1-015.
The time of processing is 14-APR-1988 14:48:31.68.
The weighting coefficients are:  2.000000  0.4100000E-02  0.1600000E-03
The fitting routine does 4 to 10 cycles.
It is satisfied when the temperature change is less than 3.0 degrees Kelvin.
The jacobian uses a temperature increment of 50.0 degrees Kelvin

     and a shift increment of 0.1 cm-1.
```

The fitting range (in 1/cm) is
2273.000 to 2343.000 .

The nitrogen ratio χ_{mole}/χ_{NR} in units of 10^{18} erg/cm^3 is 0.067.

A non-linear correction was performed using the slope constant 13.010
and a cutoff point of 25.00 counts.

Miscellaneous Theoretical Documentational Variables:

```
Variable PRESSURE:              1.000000
Variable MOLAR_CONC:           0.7000000
Variable NON_RESN_SUSCEP:      0.1040000E-16
Variable START_TEMP:            1300.000
Variable FINISH_TEMP:           2000.000
Variable TEMP_STEP:             50.00000
Variable WE:                    2358.518
Variable XWE:                   14.29350
Variable YWE:                 -0.5929490E-02
Variable ZWE:                 -0.2400000E-03
Variable BE:                    1.998260
Variable DE:                   0.5774000E-05
Variable B1:                   0.1730350E-01
Variable B2:                  -0.3153610E-04
Variable D1:                   0.1550000E-07
Variable CONST:                0.1958538E+09
Variable ALPHA:                0.1772000E-15
Variable GAMMA:                0.2066000E-15
Variable PUMP_WID:             0.6700000
Variable STNUC:                 6.000000        3.000000
Variable CHISQFRQSTP:          0.1250000E-02
Variable PUMP_CONV_STP:        0.4000000E-01
Variable STRT_FREQ:             2263.000
Variable FIN_FREQ:              2353.000
Variable NUM_PUMP_CONV_PTS:     2251
Variable NUM_CHISQ_PTS:        11825
Variable H2O_BRD_CORR:         0.9000000E-01
Variable WSLIT1:                1.104000
Variable WSLIT2:                1.652000
Variable WSLIT3:               0.9650000
Variable WSLIT4:                1.334000
Variable SLIT_CONV_STP:        0.8000000E-01
Variable NUM_VIBR_LVLS:            2
Variable NUM_ROTNL_LVLS:          52
Variable MODEL:               "GT   "
Variable GDIAG:               "ALL"
Variable SCLNG:               "SH "
Variable SLIT_FUNC:           "VO "
```

```
   Spectrum  0                 Spectrum  1                  Spectrum  2
 TFIT  SFIT  % S.D.          TFIT  SFIT  % S.D.           TFIT  SFIT  % S.D.
1600.0 0.000 23.286         1600.0 0.000 28.279          1600.0 0.000 24.375
1722.4 0.580 14.955         1686.9 0.690 20.167          1736.1 0.324 19.189
1721.0 0.582 14.953         1692.6 0.686 20.164          1738.1 0.297 19.153
1721.0 0.582 14.954         1693.1 0.686 20.164          1738.8 0.293 19.151

   Spectrum  3                 Spectrum  4                  Spectrum  5
 TFIT  SFIT  % S.D.          TFIT  SFIT  % S.D.           TFIT  SFIT  % S.D.
1600.0 0.000 26.902         1600.0 0.000 34.111          1600.0 0.000 24.649
1706.7 0.599 21.276         1812.8 0.582 23.972          1721.8 0.305 20.613
1699.4 0.553 21.204         1814.7 0.546 23.907          1725.7 0.312 20.618
1699.5 0.545 21.199         1814.6 0.532 23.889          1725.8 0.313 20.619

    Spectrum  6                Spectrum  7                  Spectrum  8
 TFIT  SFIT  % S.D.          TFIT  SFIT  % S.D.           TFIT  SFIT  % S.D.
1600.0 0.000 32.250         1600.0 0.000 30.777          1600.0 0.000 23.209
1718.4 0.782 23.328         1753.2 0.770 21.155          1703.3 0.513 17.283
1717.3 0.798 23.333         1753.2 0.774 21.158          1699.2 0.486 17.257
1717.2 0.802 23.335         1753.2 0.775 21.159          1699.5 0.484 17.258

   Spectrum  9                 Spectrum 10                  Spectrum 11
 TFIT  SFIT  % S.D.          TFIT  SFIT  % S.D.           TFIT  SFIT  % S.D.
1600.0 0.000 29.966         1600.0 0.000 25.987          1600.0 0.000 25.924
1725.7 0.704 20.838         1751.7 0.425 18.561          1678.6 0.645 18.491
1728.2 0.773 20.759         1754.1 0.438 18.564          1679.0 0.638 18.486
1728.6 0.796 20.774         1754.1 0.441 18.566          1679.0 0.637 18.486

    ..............................................................

   Spectrum 100
 TFIT  SFIT  % S.D.
1600.0 0.000 25.442
1755.4 0.474 17.587
1755.4 0.444 17.543
1755.9 0.440 17.541

Analysis completed.
     TEMP_MEAN =  1723.085571
     TEMP_ST_DVN =    36.687874

TSUMMARY FILE:

The theoretical source file is
     DUA0:[SANDIA.VERSION2]N2SC.SPT;2.
The file was processed by program SPT_FIT_FLAME, version 1-015.
The time of processing is 14-APR-1988 14:48:26.90.
The weighting coefficients are:   2.000000      0.4100000E-02  0.1600000E-03
The fitting routine does  4 to 10 cycles.
It is satisfied when the temperature change is less than 3.0 degrees Kelvin.
The jacobian uses a temperature increment of 50.0 degrees Kelvin
     and a shift increment of 0.1 cm-1.
The fitting range (in 1/cm) is
          2273.000     to   2343.000     .
The nitrogen concentration is 70%.
A non-linear correction was performed using the slope constant 13.010
     and a cutoff point of 25.00 counts.

                    Spectrum 0            Average      Standard
Filename       Temperature Variance    Temperature    Deviation

DA6170004.DAT      1721.0     14.954    1723.085571    36.687874
DA6170005.DAT      1712.5     15.472    1713.168701    38.164120
DA6170006.DAT      1719.9     13.194    1725.793335    43.448246
DA6170007.DAT      1718.8     13.128    1724.017212    43.520111
DA6170008.DAT      1718.9     15.039    1722.914185    44.036915
DA6170009.DAT      1706.7     14.041    1710.371704    36.800137
DA6171005.DAT      1692.7     12.933    1693.724121    43.522984
DA6171006.DAT      1699.9     11.965    1707.033691    42.889393
DA6171007.DAT      1696.5     11.238    1704.758911    41.898685
DA6171008.DAT      1683.8     12.240    1687.147705    38.932632
DA6171010.DAT      1687.8     12.906    1688.485962    38.623180
DA6171011.DAT      1686.4     12.562    1689.754517    37.013512
DA6171012.DAT      1700.3     12.508    1705.887085    43.448246
DA6171016.DAT      1685.7     12.330    1689.140991    36.817116
DA6171017.DAT      1676.6     11.915    1681.210205    43.500000
DA6171019.DAT      1681.2     12.551    1683.493774    39.290585
DA6171020.DAT      1677.2     12.088    1680.649658    40.317490
DA6171022.DAT      1681.1     10.967    1688.273315    42.793106
DA6176010.DAT      1609.8     13.817    1609.557129    33.737961
DA6176011.DAT      1614.5     13.388    1617.131226    42.438190
DA6176012.DAT      1592.3     12.015    1594.496094    38.694313
DA6176038.DAT      1631.8     11.324    1631.228271    38.173943
DA6176039.DAT      1636.4     11.484    1639.205322    36.534229
DA6176040.DAT      1637.1     10.426    1639.958862    38.768543
DA6176042.DAT      1659.3     10.423    1662.125122    40.911491
DA6176043.DAT      1641.5     13.488    1641.141602    33.904278
DA6176044.DAT      1649.4     11.838    1654.936401    39.708313
DA6176045.DAT      1632.5     12.608    1633.758423    37.453304
DA6176046.DAT      1649.9     10.957    1653.581055    42.198933
DA6176047.DAT      1631.5     12.112    1631.389648    34.799427
```

SUMMARY

A coherent anti-Stokes Raman spectroscopy (CARS) system has been assembled in the Gas Dynamics Laboratory at NRCC for measurements of temperature and major species concentration in flames. These measurements are made by fitting experimental flame CARS spectra with theoretically calculated CARS spectra. In the CARS process a pump laser beam at frequency ω_p and a Stokes laser beam at frequency ω_s interact in a medium to produce a CARS signal at a frequency $2\omega_p - \omega_s$. The intensity of this signal is greatly enhanced when the frequency difference $\omega_p - \omega_s$ approaches that of an active Raman transition. The CARS spectrum originates from the third-order nonlinear susceptibility and it involves constructive and destructive interference between the resonant and nonresonant parts of the susceptibility and between neighbouring Raman transitions.

This report describes a multi-year effort to develop the software to generate the theoretical CARS spectra of nitrogen and to fit them to experimental CARS spectra.

A review of the principles of CARS theory starting with a simple isolated line model, which formed the basis of early work in CARS, is presented. Recent advances in CARS theory have required two major modifications to this simple model: first, the implementation of the G-matrix approach to account for the collisional narrowing caused by line overlap at higher pressures and second, the modification of the method of pump convolution to allow for the cross coherence between the two frequency degenerate pump photons. A partially analytic and a completely analytic method of evaluating the CARS integrals are compared.

A computer program to calculate theoretical nitrogen CARS spectra that incorporates the above recent developments in CARS theory is described in detail. Procedures and various strategies used to speed up the numerical computations of collisional narrowing and cross coherence effects are explained.

The molecular parameters required for calculating a CARS spectrum and the selection of their values for nitrogen from currently available data are detailed. Nitrogen CARS spectra calculated under various assumptions of line overlap and pump convolution models are compared. The sensitivity of the CARS spectrum to the above models under varying conditions of temperature and pressure is examined. The minor changes caused by the addition of the O and S branches to the usual Q branch spectrum nitrogen are shown. The effects of the sampling grid size used in the numerical schemes are discussed. Finally a detailed comparison between nitrogen CARS spectra generated from the NRCC programs with those from a program provided by the Sandia Laboratories is presented.

A set of programs developed for fitting experimental CARS spectra with theoretical spectra, including the nonlinear least mean squares fitting scheme used, is described. The calculation of a typical CARS flame spectrum can take a few hours with a DEC VAX-11/730 computer. Therefore a method of estimating temperatures by fitting experimental CARS spectra to a

precalculated library of theoretical CARS spectra at various temperatures is implemented. The instrument function required to create this library is obtained by fitting room temperature nitrogen CARS spectra. With this approach less than two seconds of DEC VAX-11/730 cpu time are required to fit a single experimental flame spectrum.

In summary, this report describes a computer program incorporating all the recent advances in CARS theory for generating theoretical CARS spectra of nitrogen. The techniques and programs used for fitting experiment with theory are also presented.

6.0 REFERENCES

ANDERSEN, H.C., and B.S. HUDSON. 1978. Coherent Anti-Stokes Raman Scattering. Molecular Spectroscopy (Chemical Society, London), **5**: 142.

BONAMY, J., L. BONAMY, and D. ROBERT. 1977. Overlapping Effects and Motional Narrowing in Molecular Band Shapes: Application to the Q Branch of HD: Journal of Chemical Physics, **67**: 4441.

BOTHA, J.P., and D.B. SPALDING. 1954. The Laminar Flame Speed of Propane/Air Mixtures with Heat Extraction from the Flame. Proceedings of the Royal Society of London, **225A**: 71.

BUCKINGHAM, A.D., and A. SZABO. 1978. Determination of Derivatives of the Polarizability Anisotropy in Diatomic Molecule from Relative Raman Intensities, Journal of Raman Spectroscopy, **7**: 46-48.

DEWITT, R.N., A.B. HARVEY, and W.M. TOLLES. 1976. Theoretical Development of Third-Order Susceptibility as Related to Coherent Anti-Stokes Raman Spectroscopy (CARS). NRL Memorandum Report 3260.

DRUET, S.A.J., and J.P.E. TARAN. 1981. CARS Spectroscopy. Progress in Quantum Electronics, **7**: 1.

ECKBRETH, A.C. 1980. CARS Thermometry in Practical Combustors. 1980. Combustion Flame, **39**: 133.

ECKBRETH, A.C., G.M. DOBBS, J.H. STUFFLEBEAM, and P.A. TELLEX. 1984. CARS Temperature and Species Measurements in Augmented Jet Engine Exhausts. Applied Optics, **23**: 1328.

FARROW, R.L., and L.A. RAHN. 1985. Interpreting Coherent Anti-Stokes Raman Spectra Measured with Multimode Nd:Yag Pump Lasers. Journal of the Optical Society of America, **2**: 903-906.

FARROW, R.L., P.L. MATTERN, and L.A. RAHN. 1982. Comparison Between CARS and Corrected Thermocouple Temperature Measurements in a Diffusion Flame. Applied Optics, **21**: 3119-3125.

GILSON, T.R., T.R. BEATTIE, I.R. BLACK, D.A. GREENHALGH, and S.N. JENNY. 1980. Redetermination of Some of the Spectroscopic Constants of the Electronic Ground State of di-Nitrogen Using Coherent Anti-Stokes Raman Spectroscopy. Journal of Raman Spectroscopy, **9**: 361.

GOSS, L.P., D.D. TRUMP, B.G. MACDONALD, and G.L. SWITZER. 1983. 10 Hz Coherent Anti-Stokes Raman Spectroscopy Apparatus for Turbulent Combustion Studies. Review of Scientific Instruments, **54**: 563.

GREENHALGH D.A. 1988. Quantitative CARS Spectroscopy. Advances in Non-Linear Spectroscopy. Chapter 5. John Wiley, New York. pp. 193-251.

GREENHALGH, D.A., and R.J. HALL. 1986. A Closed Form Solution for the CARS Intensity Convolution. Optics Communications, 57: 125.

GREENHALGH, D.A. F.M. PORTER, and W.A. ENGLAND. 1983. The Application of Coherent Anti-Stokes Raman Scattering to Turbulent Combustion Thermometry. Combustion and Flame, 49: 171.

HALL, R.J. 1979. CARS Spectra of Combustion Gases. Combustion and Flame, 35: 77.

HALL, R.J. 1983. Coherent Anti-Stokes Raman Spectroscopic Modelling for Combustion Diagnostics. Optical Engineering, 22: 322-329.

HALL, R.J. 1985. Intensity Convulutions of CARS Spectra. Optics Communications, 52: 360.

HALL, R.J., and L.R. BOEDKER. 1984. CARS Thermometry in Fuel Rich Flames. Applied Optics, 23: 1340-1346.

HALL, R.J., and A.C. ECKBRETH. 1984. Coherent Anti-Stokes Raman Spectroscopy (CARS): Application to Combustion Diagnostics. In Laser Applications. Vol. 5. Edited by J.F. Ready and R.K. Erf. Academic Press, New York. pp. 213-309.

HALL, R.J., J.F. VERDIECK, and A.C. ECKBRETH. 1980. Pressure-Induced Narrowing of the CARS Spectrum of N_2. Optics Communications, 35: 69.

HARTLEY, H.O. 1961. The Modified Gauss-Newton Method for the Fitting of Non-Linear Regression Functions by Least Squares. Technometrics, 3: 269-280.

HARVEY, A.B. (Editor). 1981. Chemical Applications of Nonlinear Raman Spectroscopy. Acadamic Press, New York.

HERZBERG, G. 1963. Molecular Spectra and Molecular Structure. I. Spectra of Diatomic Molecules. Van Nostrand Reinhold, New York.

HUBER, K.P., and G.E. HERZBERG. 1979. Molecular Spectra and Molecular Structure. IV. CONSTANTS of Diatomic Molecules. Van Nostrand Reinhold, New York.

HUI, A.K., B.H. ARMSTRONG, and A.A. WRAY. 1978. Rapid Computation of Voigt and Complex Error Functions. Journal of Quantitative Spectroscopy Radiative Transfer, 19: 509-516.

JAMES, T.C., and W. KLEMPERER. 1959. Line Intensities in the Raman Effect of $^1\Sigma$ Diatomic Molecules. Journal of Chemical Physics. 31: 130-134.

KATAOKA, H., S. MAEDA, and C. HIROSE. 1982. Effects of Laser Line Width on the Coherent Anti-Stokes Raman Spectroscopy Spectral Profile. Applied Spectroscopy. 36: 565.

KIM, H. 1970. Computer Programming in Physical Chemistry Laboratory. Journal of Chemical Education, 47: 120-122.

KOSZYKOWSKI, M.L., R.L. FARROW, and R.E. PALMER. 1985. Calculation of Collisionally Narrowed Coherent Anti-Stokes Raman Spectroscopy Spectra. Optics Letters, 10: 478.

LASSER, T.H. 1980. An Alternative Method of CARS Spectra Calculation. Optics Communications, 35: 447.

LUTHE, J.C., E.J. BEITING, and F.Y. YUEH. 1986. Algorithms for Calculating Coherent Anti-Stokes Raman Spectra: Application to Several Small Molecules, Computer Physics Communications, 42: 73-92.

MARKO, K.A., and L. RIMAI. 1979. Space- and Time-Resolved Coherent Anti-Stokes Raman Spectroscopy for Combustion Diagnostics. Optics Letters, 4: 211.

MAY, A.D., J.C. STRYLAND, and G. VARGHESE. 1970. Collisional Narrowing of the Vibrational Raman Band of Nitrogen and Carbon Monoxide. Canadian Journal of Physics, 48: 2331.

NIBLER, J.W., and G.V. KNIGHTEN. 1979. Coherent Anti-Stokes Raman Spectroscopy. In Raman Spectroscopy of Gases and Liquids. Edited by A. Weber. Springer, Berlin. pp. 253-299.

PARAMESWARAN, T., and D.R. SNELLING. 1982. A computer Program to Generate Coherent Anti-Stokes Raman Spectra. Technical Note 81-18. Defence Research Establishment, Dept. of National Defence, Ottawa. Ont.

PENNEY, C.M., R.L. ST-PETERS, and M. LAPP. 1979. Absolute Rotational Raman Cross Sections in Gases and Liquids. Topics in Current Phyics, 11: 712.

POLANYI, J.C., and K.B. WOODALL. 1971. Mechanism of Rotational Relaxation. Journal of Chemical Physics, 56: 1563.

PRICHARD, D.E., N. SMITH, R.C. DRIVER, and T.A. BRUNNER 1979. Power Law Scaling of Rotational Energy Transfer. Journal of Chemical Physics, 70: 2115.

PRINTER, F. 1964. Dependence of the Width of the Rotational Raman Lines of N_2 and CO on the Quantum Number. J. Optics and Spectrroscopy (English Translation), 17: 428.

RAHN, L.A., and R.E. PALMER. 1986. Studies of Nitrogen Self Broadening at High Temperature with Inverse Raman Spectroscopy. Journal of the Optics Society of America, 3: 1164.

ROH, W.B., P.W. SCHREIBER, and J.P.E. TARAN. 1976. Single-Pulse Coherent Anti-Stokes Raman Scattering. Applied Physics Letters, 29: 174.

ROSASCO, G.J., and W.S. HURST. 1985. Measurement of Resonant and Nonresonant Susceptibilities by Coherent Anti-Stokes Raman Spectroscopy. Physical Review A: General Physics, 32: 281.

SCHROTTER, H.W., and H.W. KLOCKNER. 1979. Raman Spectroscopy of Gases and Liquids. Edited by A. Weber. Springer, New York. p. 123.

SNELLING, D.R., and M., FISCHER. 1985. Design and Calibration of a Flat-Flame Burner Using Line-Reversal Techniques. Defence Research Establishment, Department of National Defence, Ottawa, Ont. Technical Note 85-4.

SNELLING, D.R., R.A. SAWCHUK, and G.J. SMALLWOOD. 1984. Multichannel Light Detectors and Their Use for CARS Spectroscopy. Applied Optics., **23**: 4083.

SNELLING, D.R., R.A. SAWCHUK, and R.E. MUELLER. 1985. Single Pulse CARS Noise: A Comparison Between Singlemode and Multimode Pump Lasers. Applied Optics, **24**: 2771.

SNELLING, D.R., G.J. SMALLWOOD, R.A. SAWCHUK, and T. PARAMESWARAN. 1987. Precision of Multiplex CARS Temperatures Using Both Single-Mode and Multimode Pump Lasers. Applied Optics, **26**: 99.

STOICHEFF, B.P. 1959. Advances in Spectroscopy. Edited by H.W. Thompson, Interscience, New York.

SWITZER, G.L., L.P. GOSS, W.M. ROQUEMORE, R.P. BRADLEY, P.W. SCHREIBER, and W.B. ROB. 1980. Application of CARS to Simulated Practical Combustion Systems. Journal of Energy, **4**: 209.

TARAN, J.P., and M. PEALAT. 1982. Practical CARS Temperature Measurements, Temperature Its Measurement and Control in Science and Industry. American Institute of Physics, **5**: 575.

TEETS, R.E. 1984. Accurate Convolutions of Coherent Anti-Stokes Raman Spectra. Optics Letters, **9**: 226.

WHITING, E.E. 1968. An Empirical Approximation to the Voigt Function. Journal of Quantum Spectroscopy and Radiative Transfer, **8**: 1379.

YUEH, F.Y., and E.J BEITING. 1986. Analytical Expressions for Coherent Anti-Stokes Raman Spectral (CARS) Profiles, Computer Physics Communications. **42**: 65-71.

YURATICH, M.A. 1979. Effect of Laser Linewidth on Coherent Anti-Stokes Raman Spectroscopy. Molecular Physics, **38**: 625.

Fig. 1. Coherent anti-Stokes Raman spectroscopy (CARS)

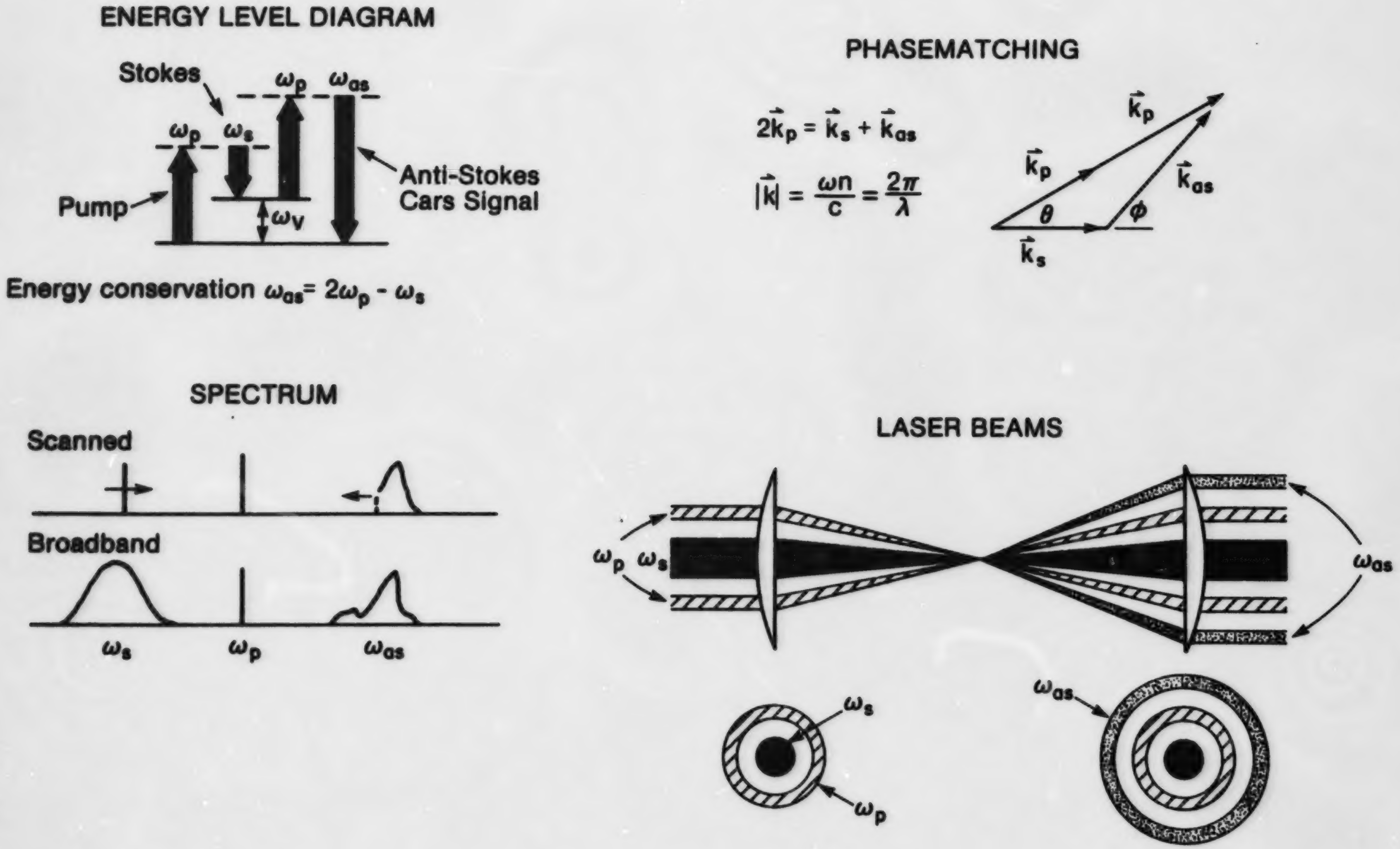
ENERGY LEVEL DIAGRAM
Stokes
Pump
ω_p
ω_s
ω_p
ω_{as}
ω_v
Anti-Stokes Cars Signal
Energy conservation $\omega_{as} = 2\omega_p - \omega_s$
PHASEMATCHING
$2\vec{k}_p = \vec{k}_s + \vec{k}_{as}$
$|\vec{k}| = \frac{\omega n}{c} = \frac{2\pi}{\lambda}$
$\vec{k}_p$
$\vec{k}_p$
$\vec{k}_{as}$
θ
ϕ
$\vec{k}_s$
SPECTRUM
Scanned
Broadband
ω_s
ω_p
ω_{as}
LASER BEAMS
ω_p
ω_s
ω_{as}
ω_s
ω_p
ω_{as}

Fig. 2. Real and imaginary part of CARS susceptibility

STRONG LINE

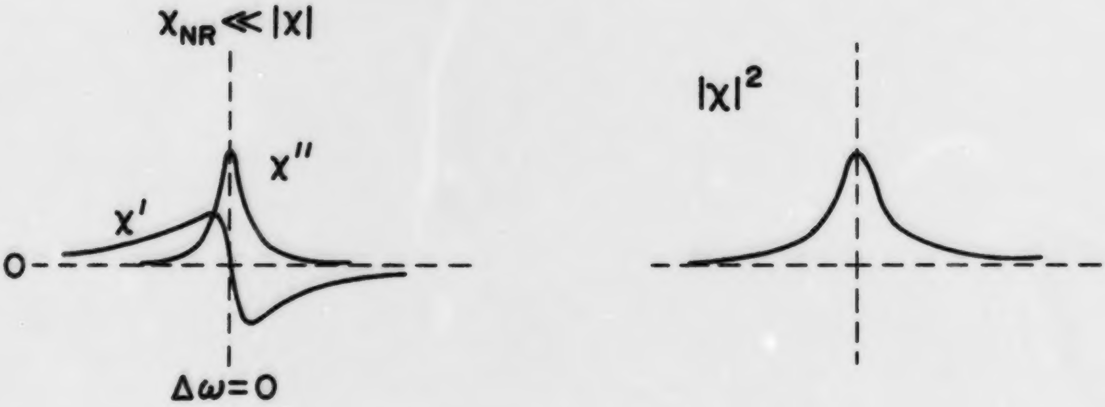
$\chi_{NR} \ll |\chi|$
χ''
χ'
0
$\Delta\omega = 0$
$|\chi|^2$

WEAK LINE

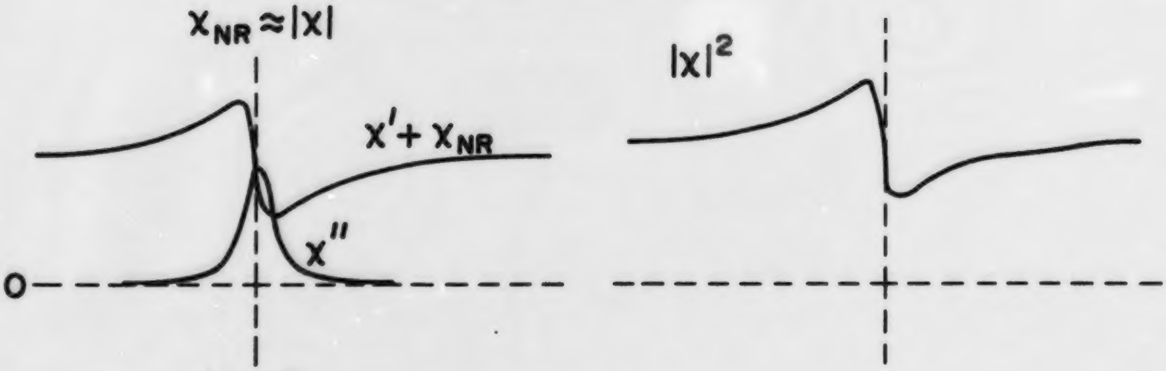
$\chi_{NR} \approx |\chi|$
$\chi' + \chi_{NR}$
χ''
0
$\Delta\omega = 0$
$|\chi|^2$

Fig. 3. Effect of insufficient sampling ($\Gamma_j = 0.0004\ \mathrm{cm}^{-1}$ and sampling grid of $.0025\ \mathrm{cm}^{-1}$)

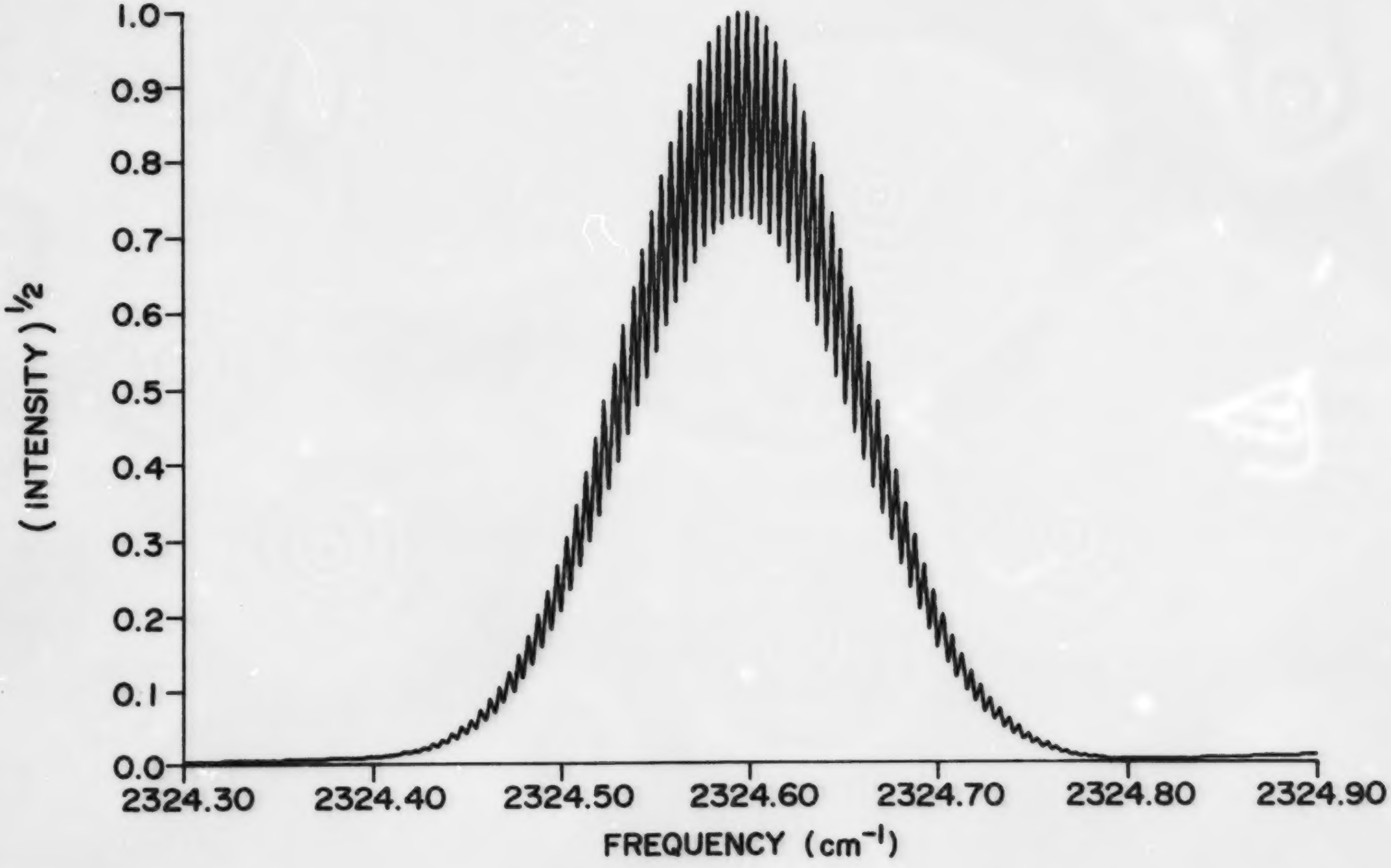

Fig. 4. Effect of increased sampling ($\Gamma_j = 0.004\ cm^{-1}$ and sampling grid of $0.001\ cm^{-1}$)

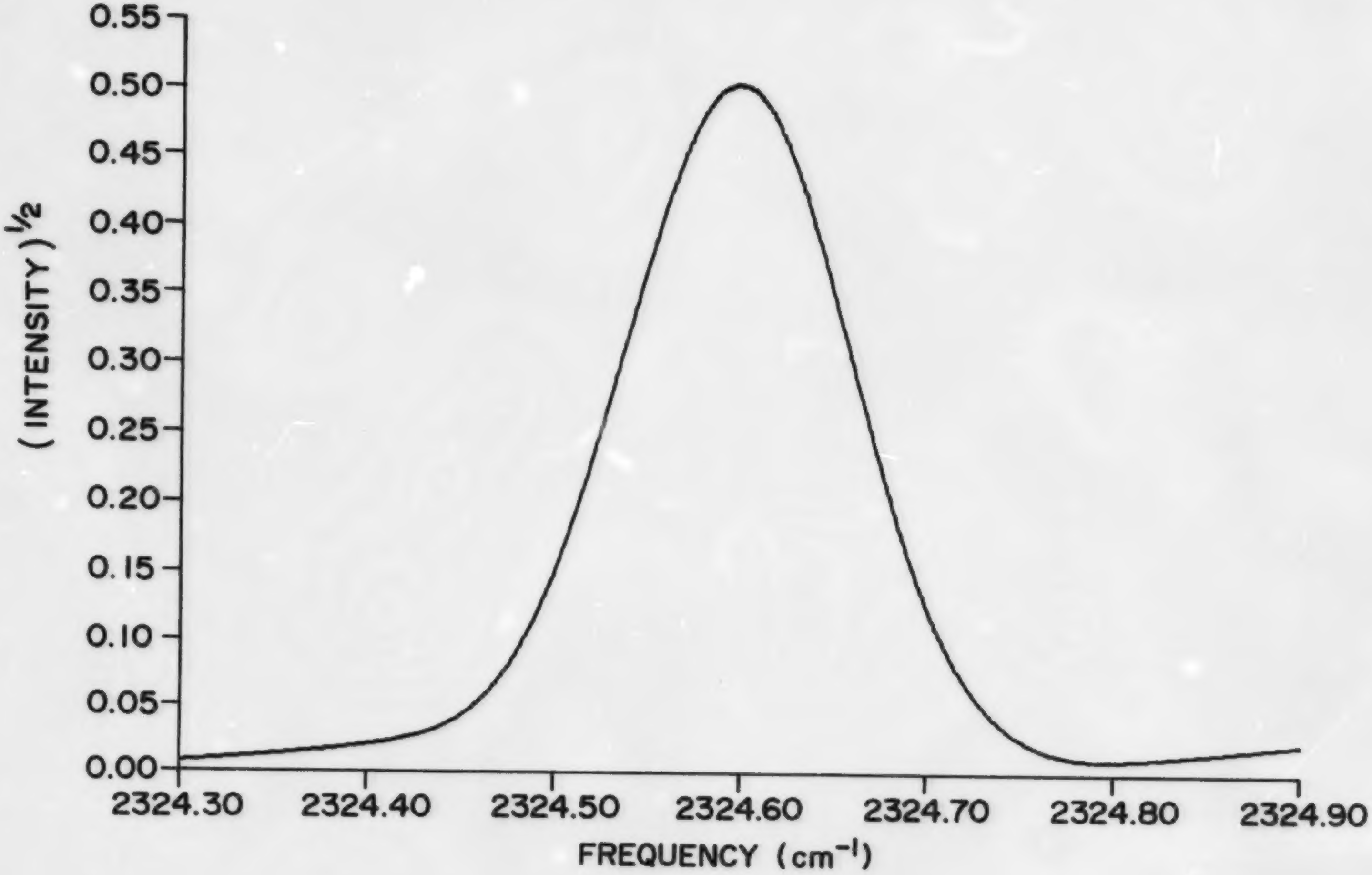

Fig. 5. Effect of sampling grid size on 2000 K CARS spectrum

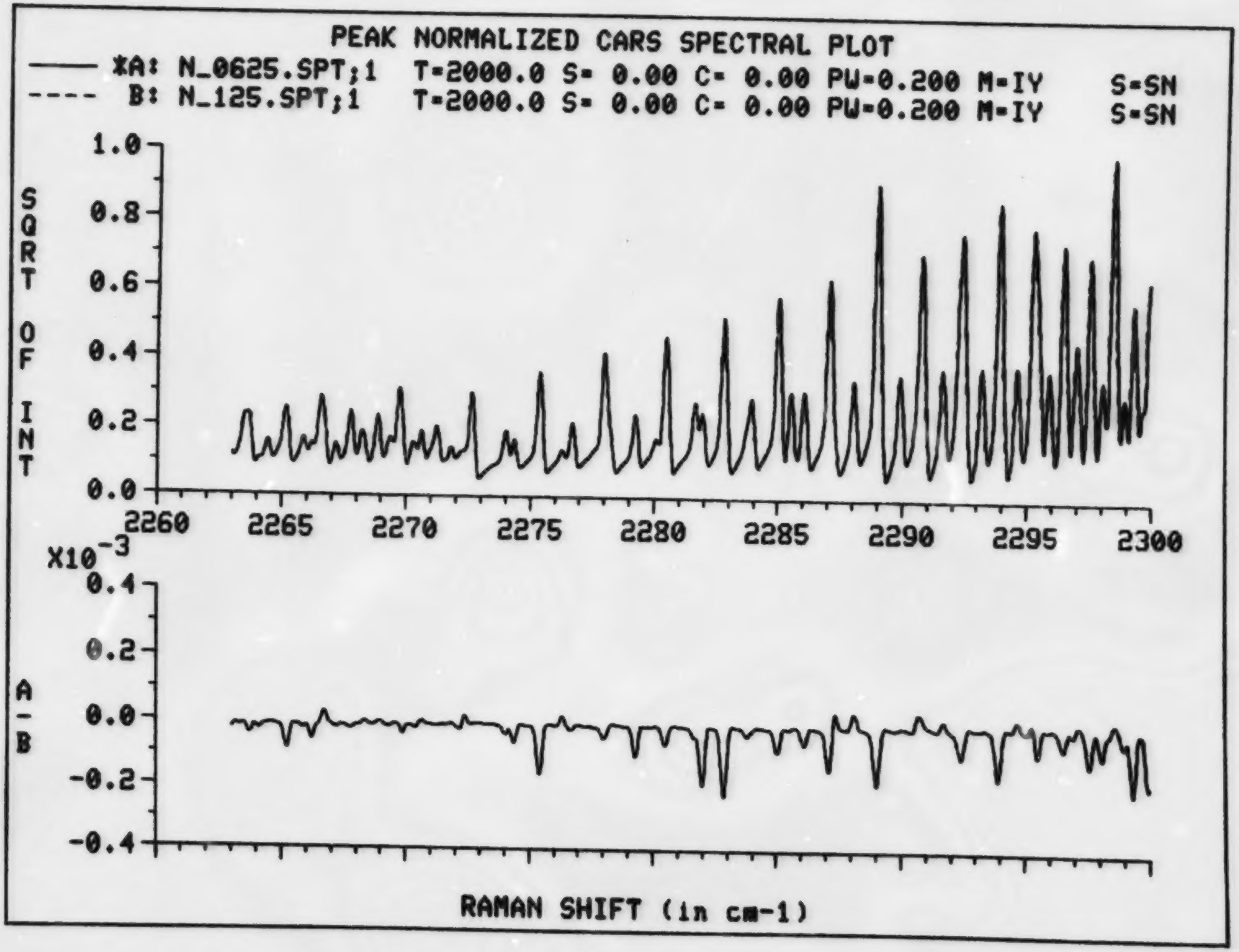

Fig. 6a. N_2 Q branch spectrum with and without O and S branches from 2260 to 2300 cm^{-1}

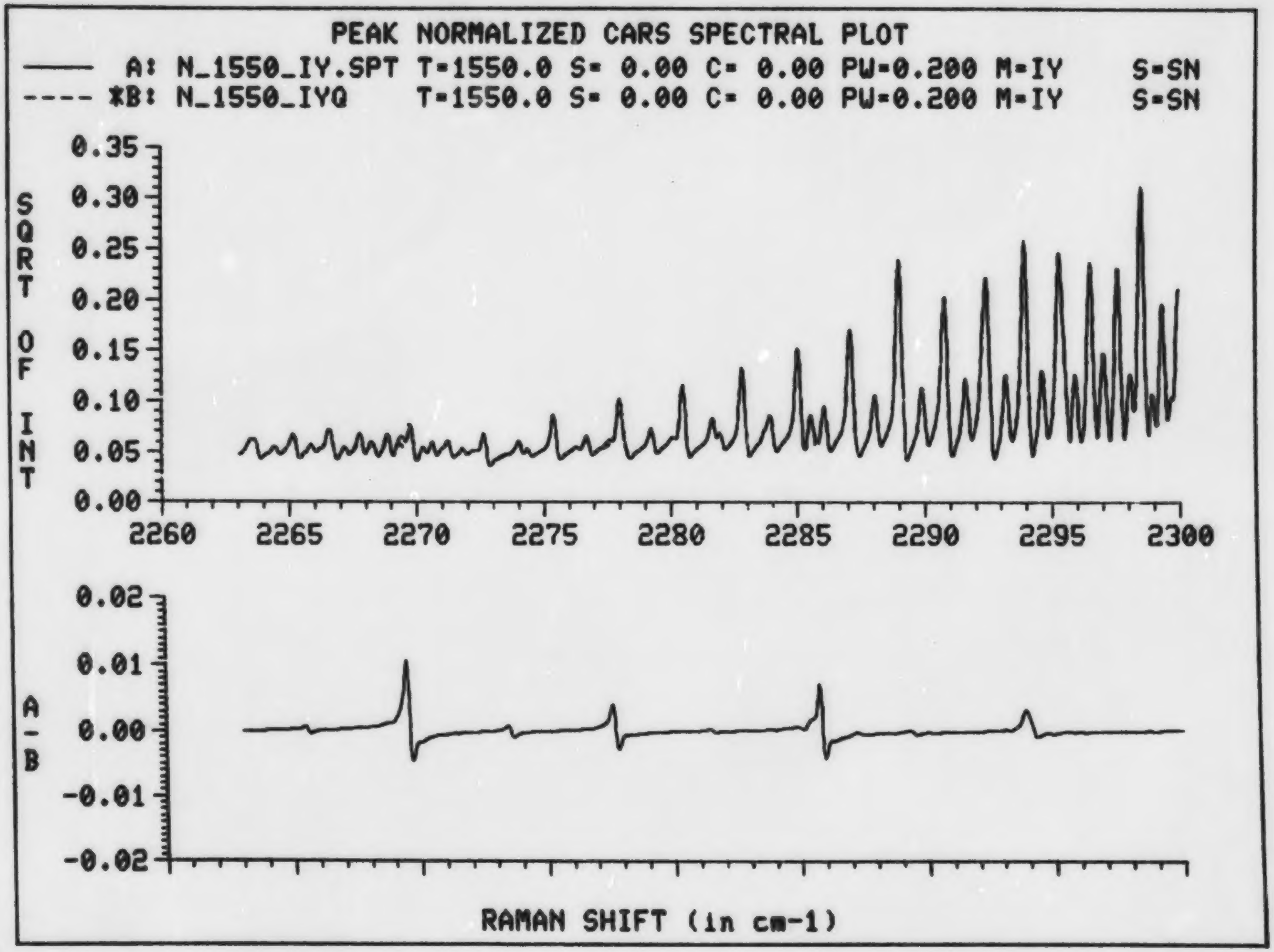

Fig. 6b. N_2 Q branch spectrum with and without O and S branches from 2300 to 2340 cm^{-1}

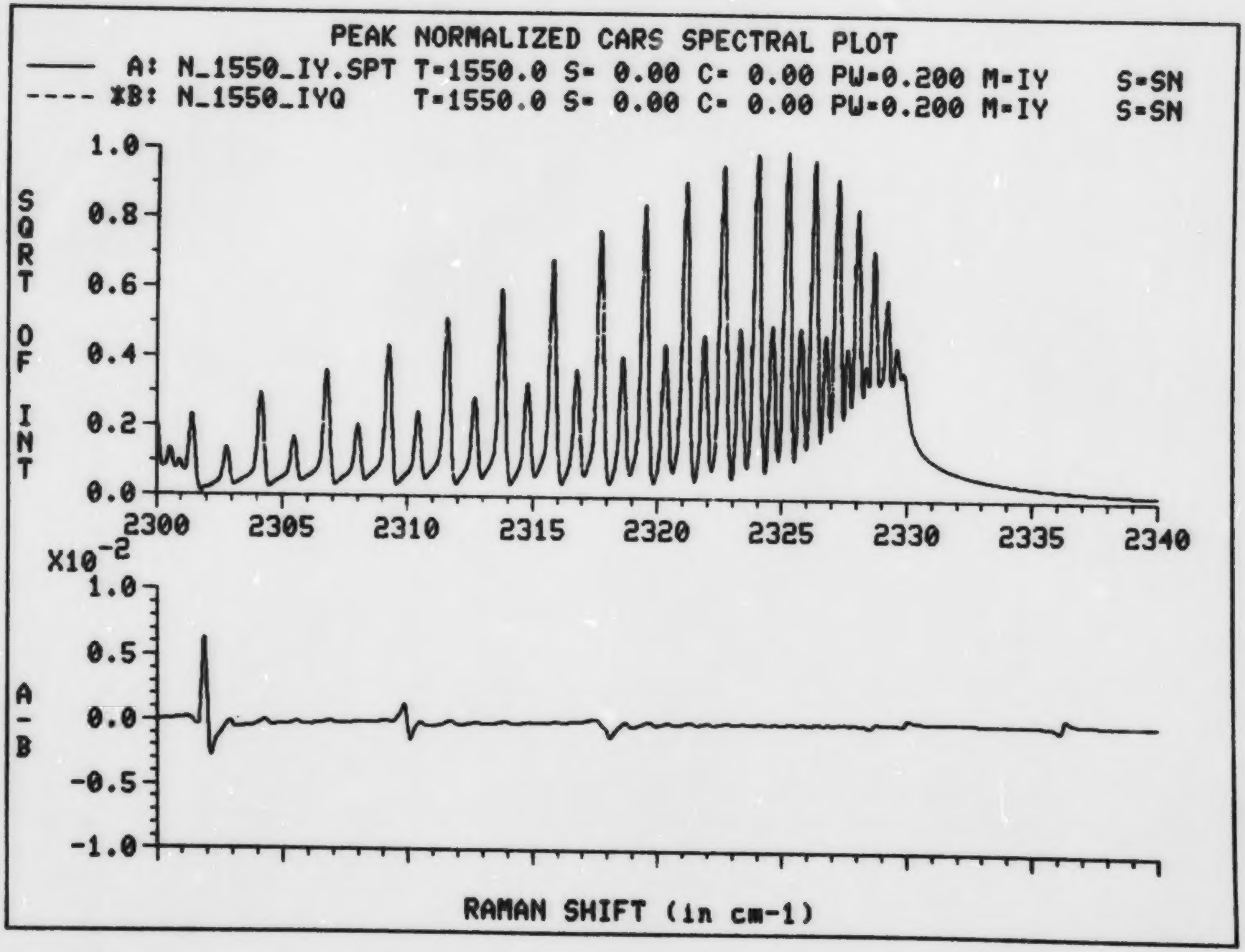

Fig. 7a. N_2 CARS spectra with single (curve B) and separate (curve A) matrix diagonalization: from 2260 to 2300 cm^{-1}

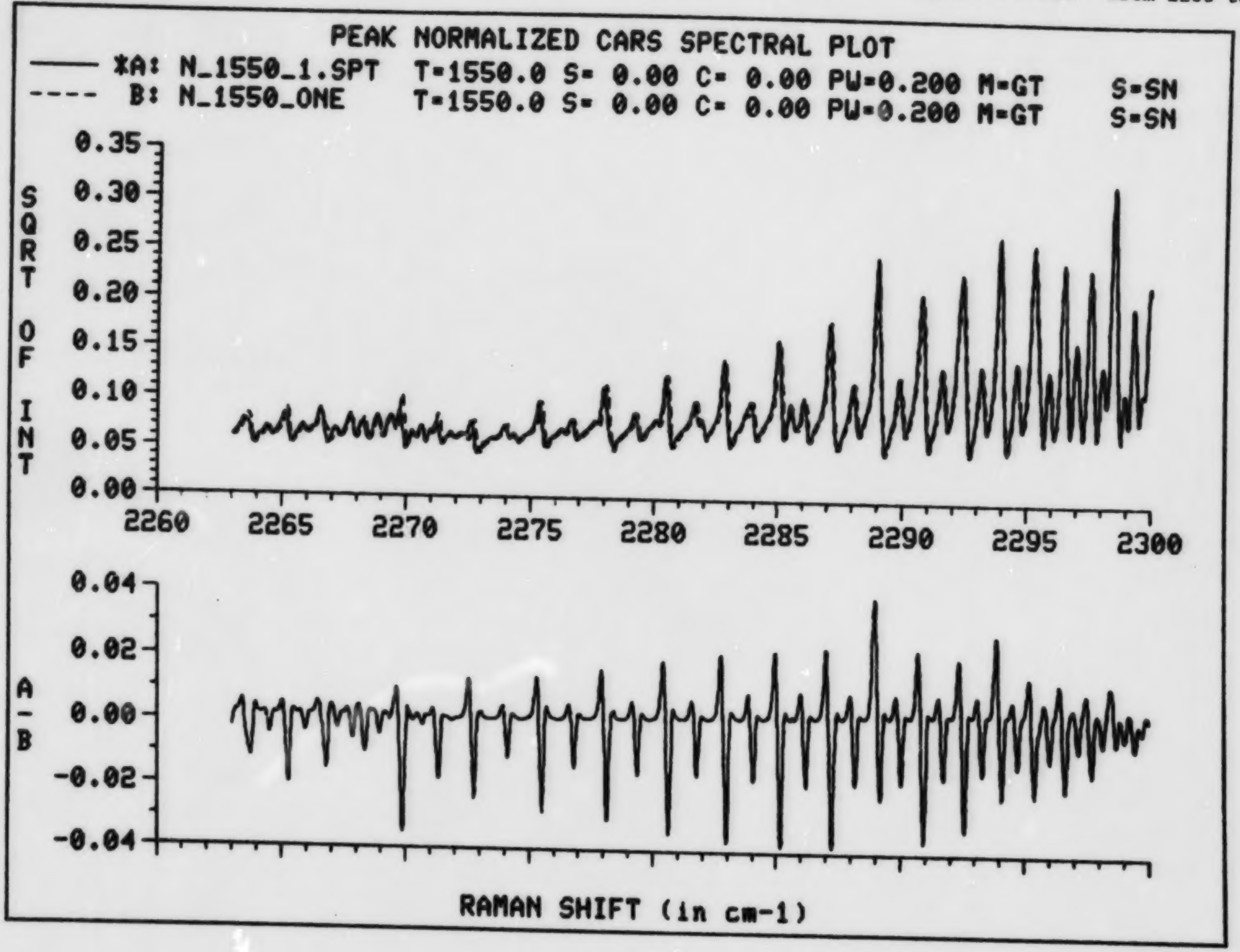

Fig. 7b. N_2 CARS spectra with single (curve B) and separate (curve A) matrix diagonalization from 2300 to 2340 cm^{-1}

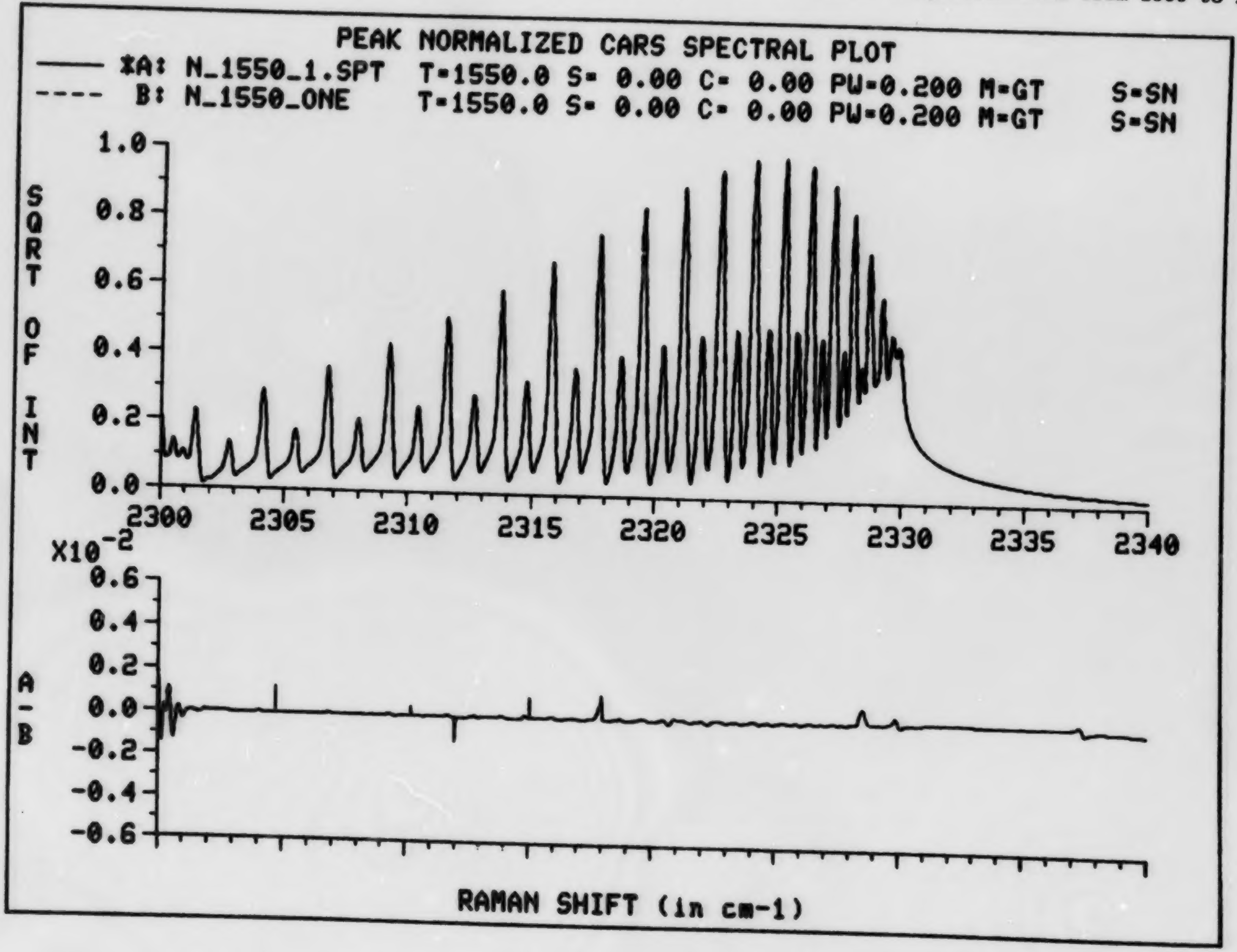

Fig. 8a. Effect of collisional narrowing on 1000 K CARS spectrum from 2260 to 2300 cm^{-1}

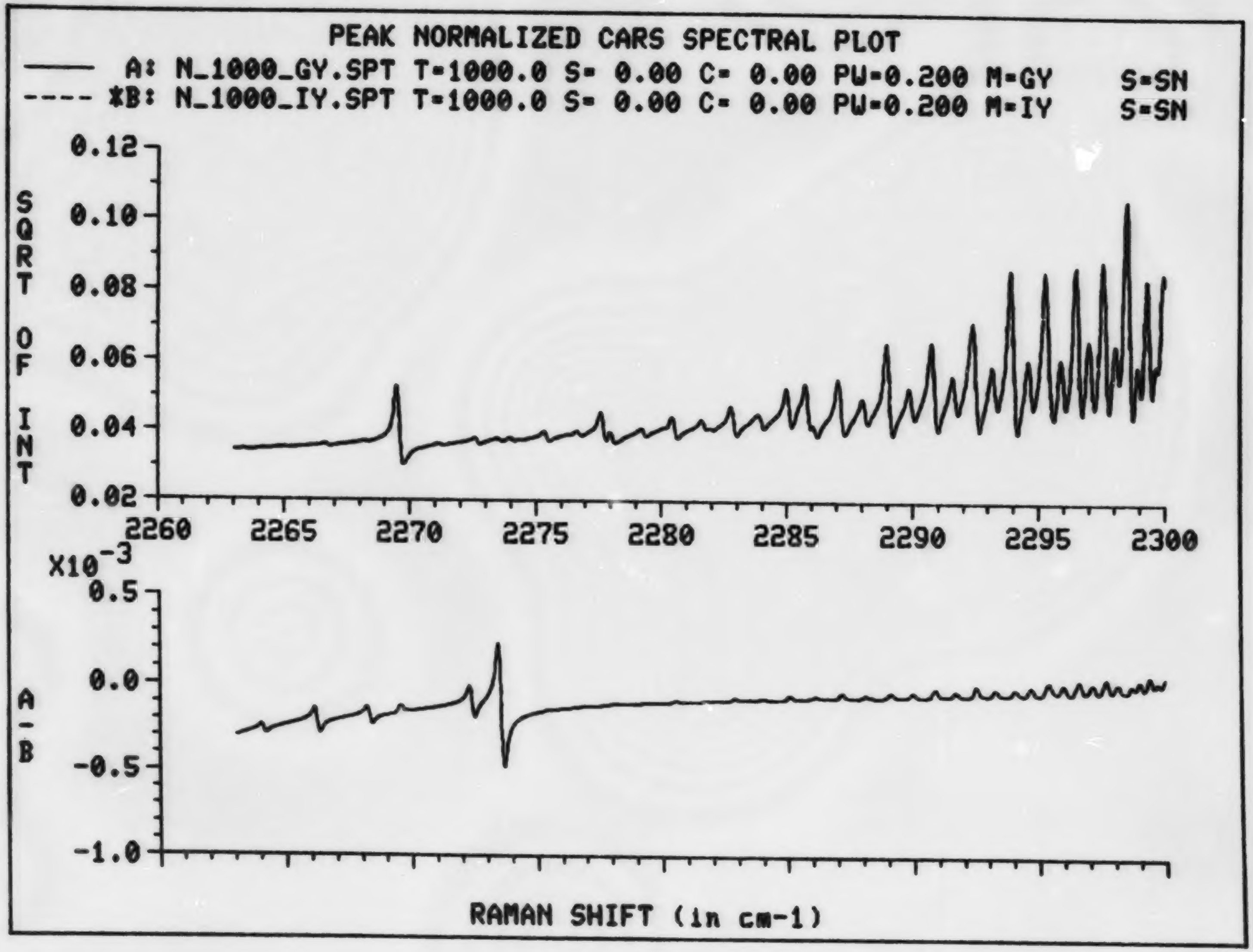

Fig. 8b. Effect of collisional narrowing on 1000 K CARS spectrum from 2300 to 2340 cm^{-1}

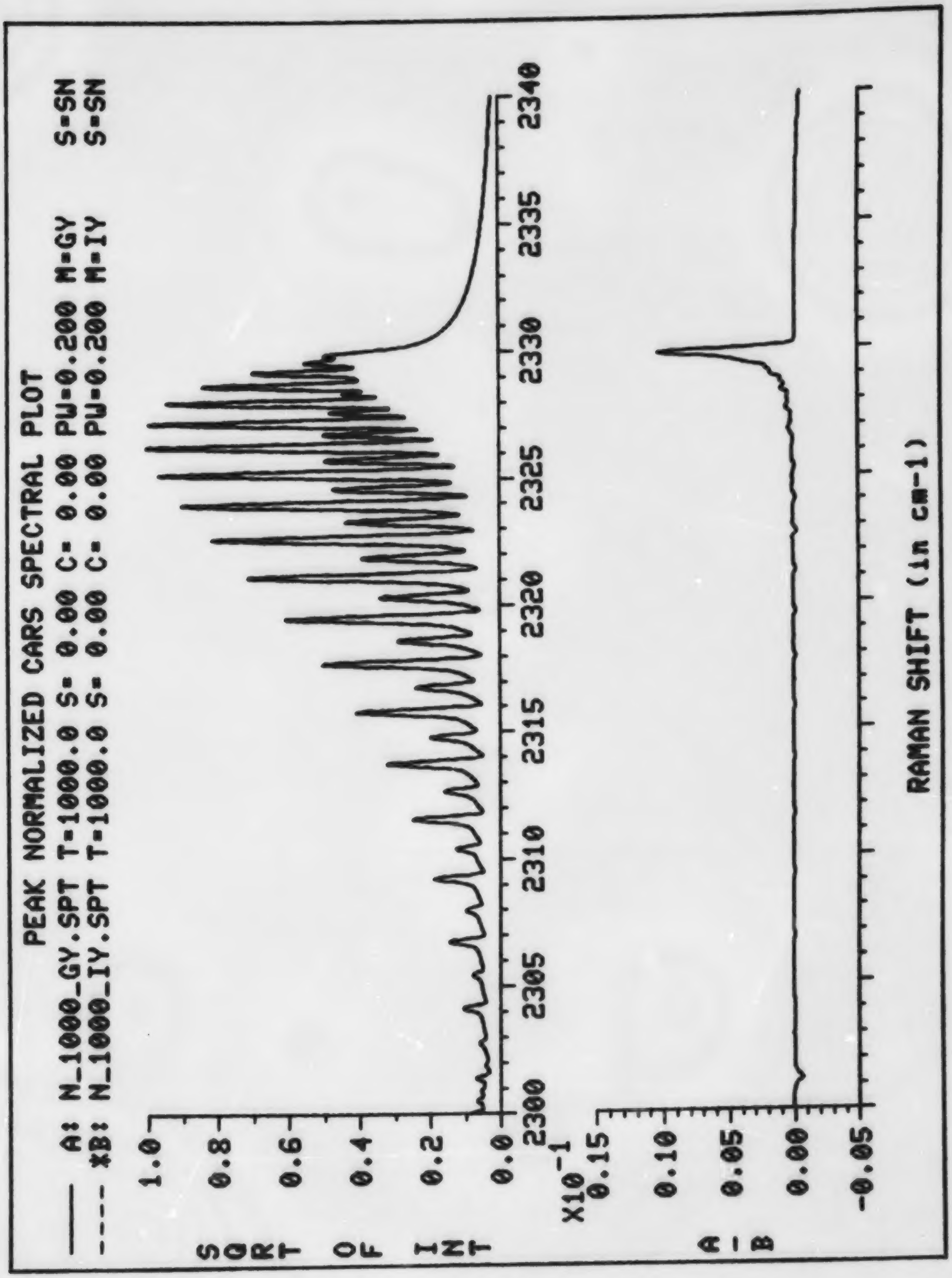

Fig. 9a. Effect of collisional narrowing on 1550 K CARS spectrum from 2260 to 2300 cm^{-1}

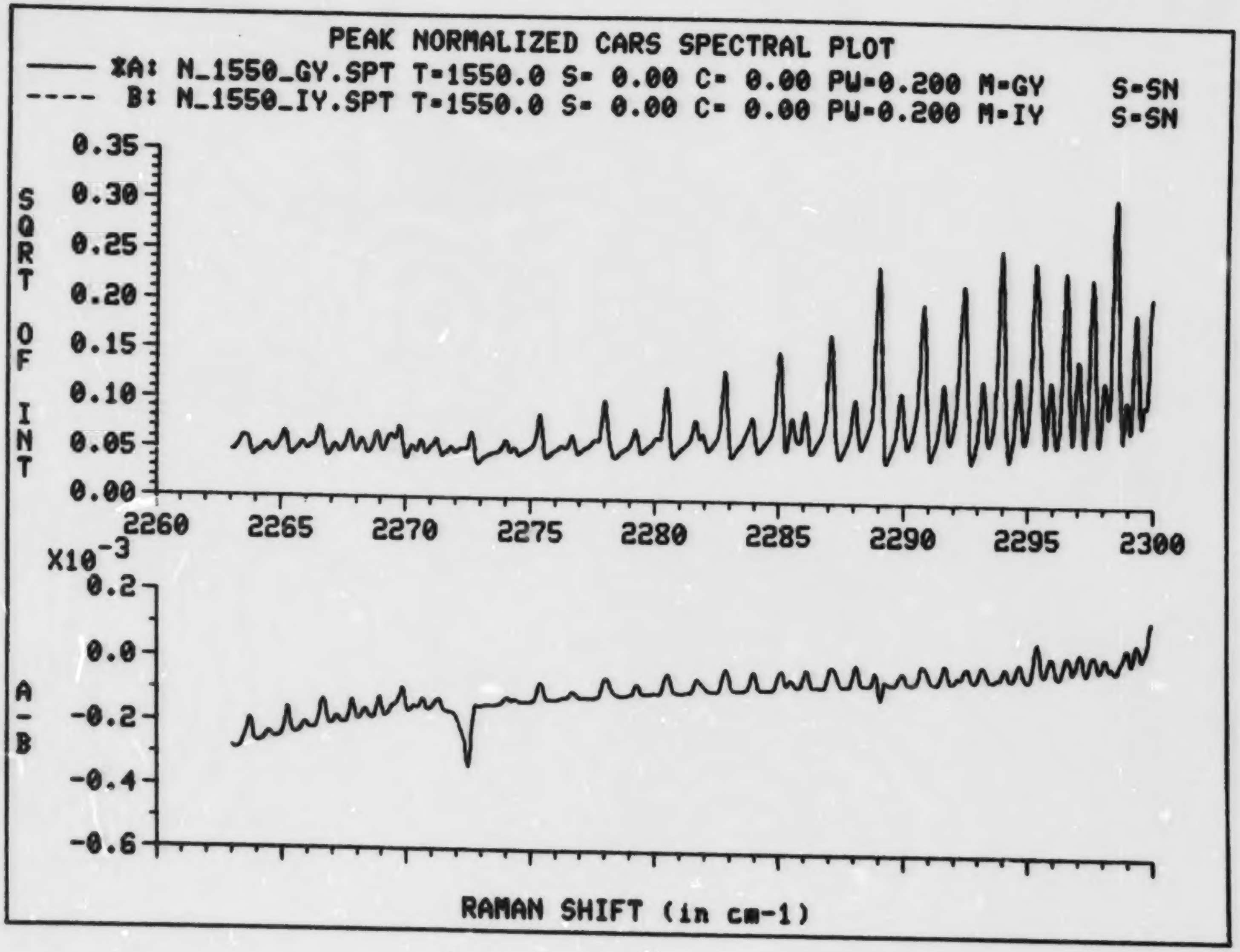

Fig. 9b. Effect of collisional narrowing on 1550 K CARS spectrum from 2300 to 2340 cm^{-1}

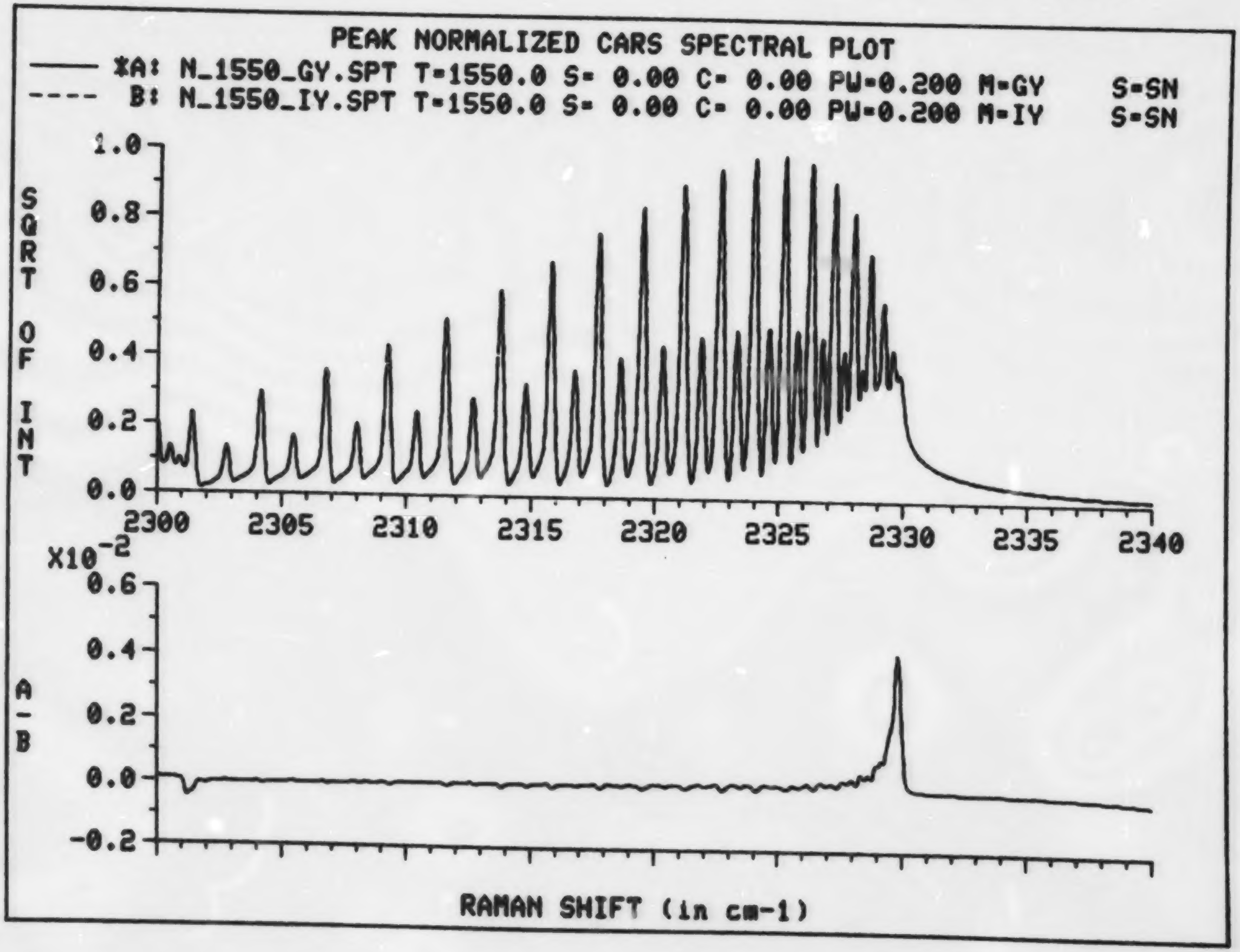

Fig. 10a. Effect of collisional narrowing on 2000 K CARS spectrum from 2260 to 2300 cm^{-1}

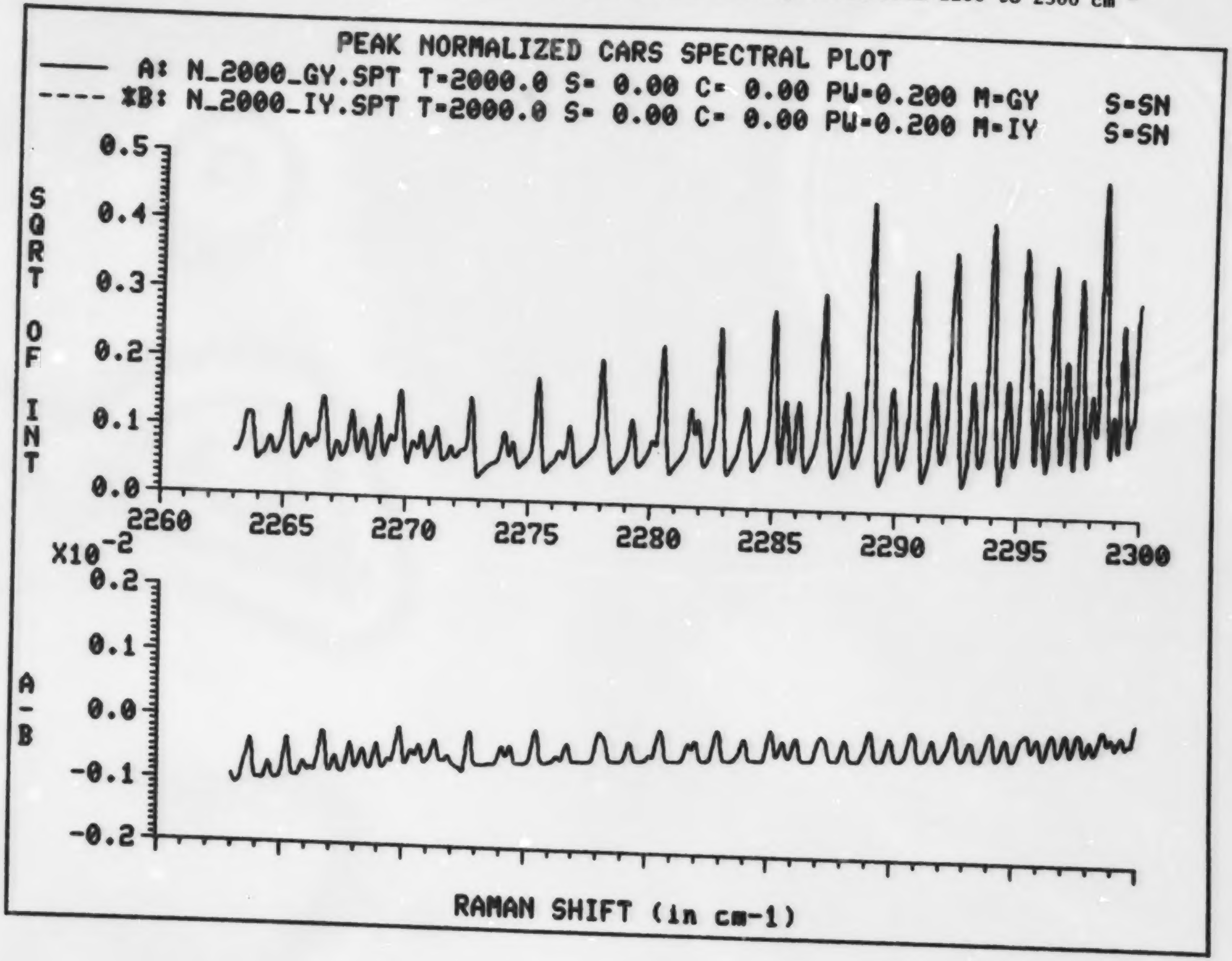

Fig. 10b. Effect of collisional narrowing on 2000 K CARS spectrum from 2300 to 2340 cm^{-1}

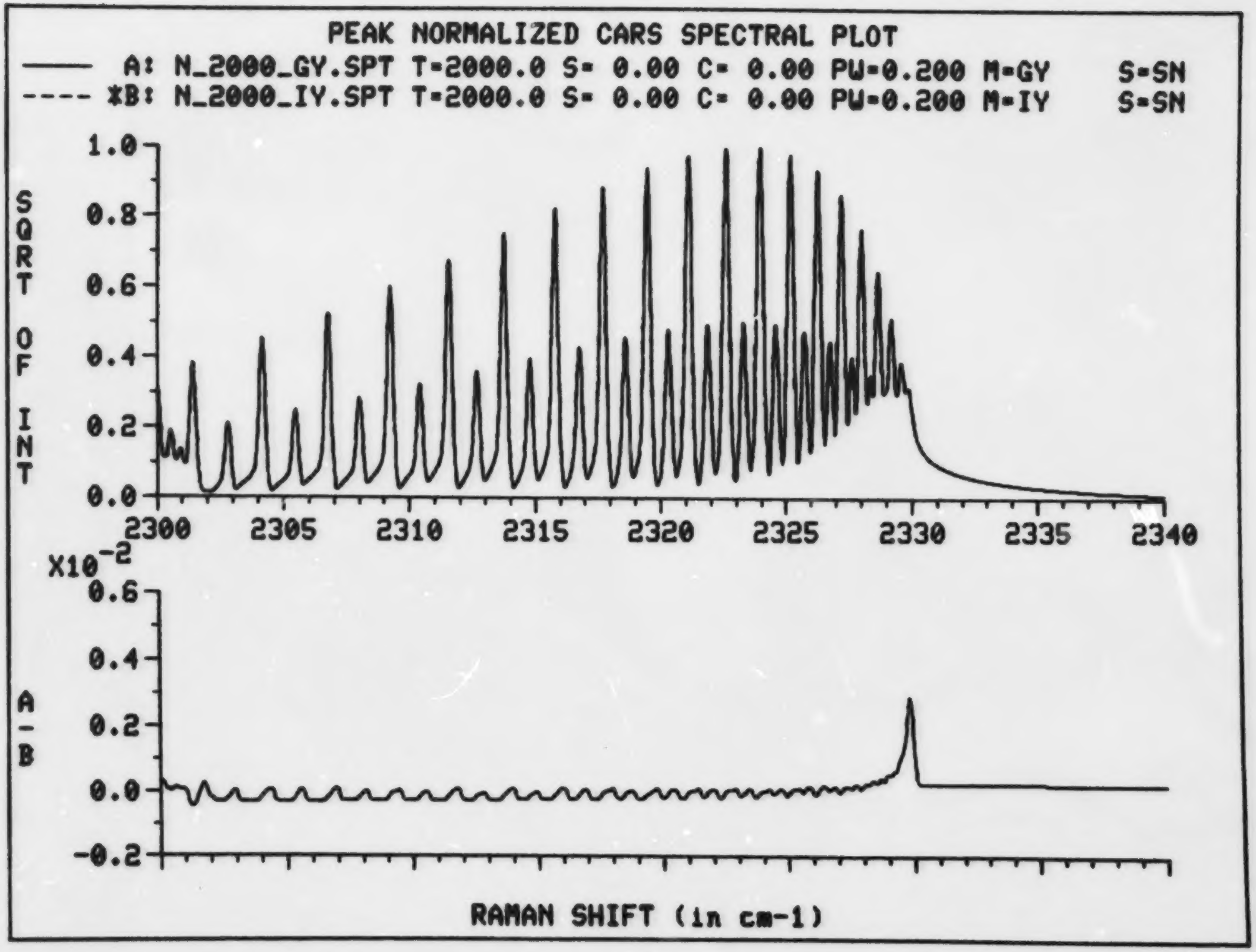

Fig. 11. 1550 K N_2 CARS spectra at 1 atm (curve A) and 10 atm (curve B)

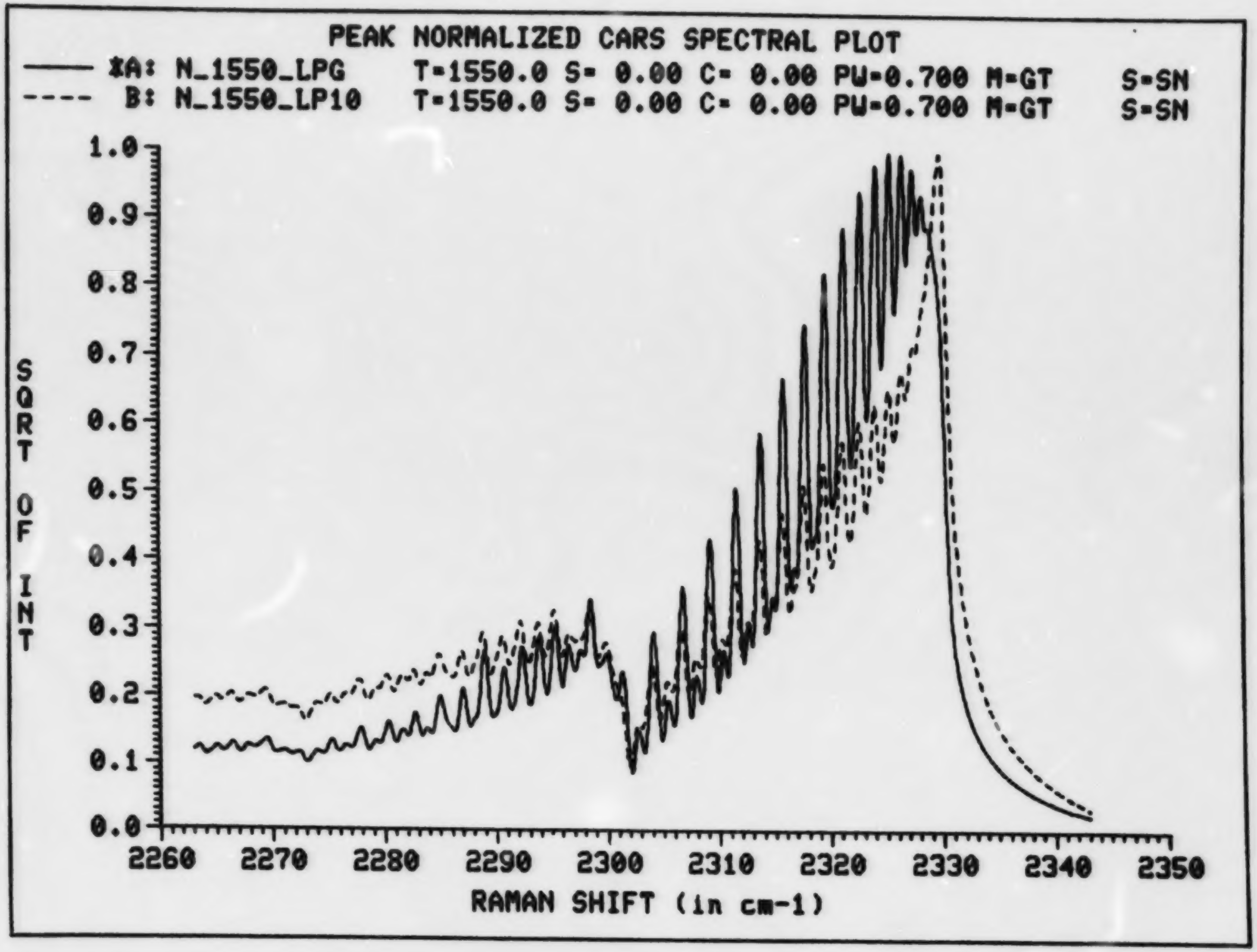

Fig. 12. 1500 K N_2 CARS spectra at 10, 20, 30 and 50 atm

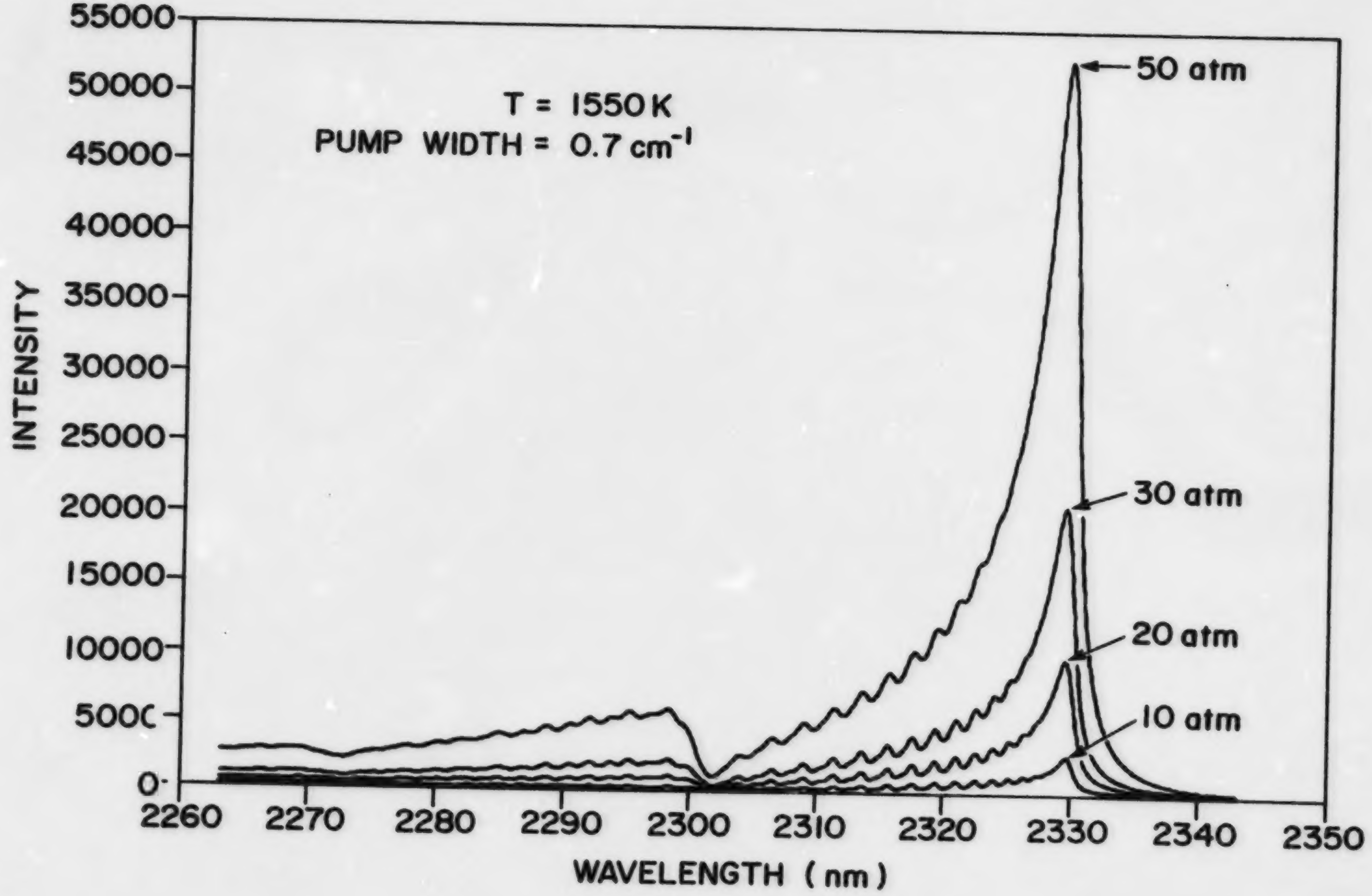

Fig. 13a. Effect of cross coherence on 1000 K CARS spectrum from 2260 to 2300 cm^{-1}

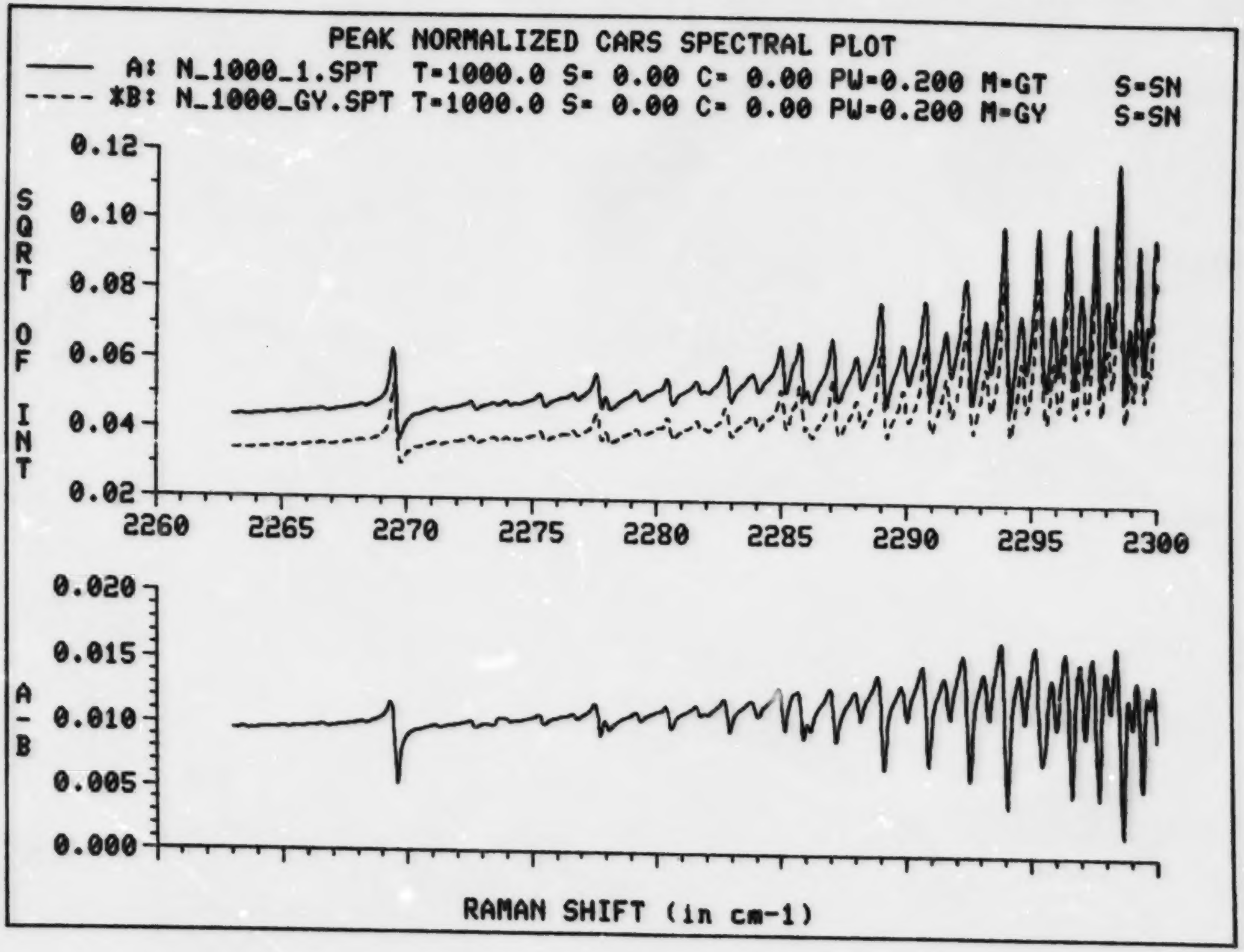

Fig. 13b. Effect of cross coherence on 1000 K CARS spectrum from 2300 to 2340 cm^{-1}

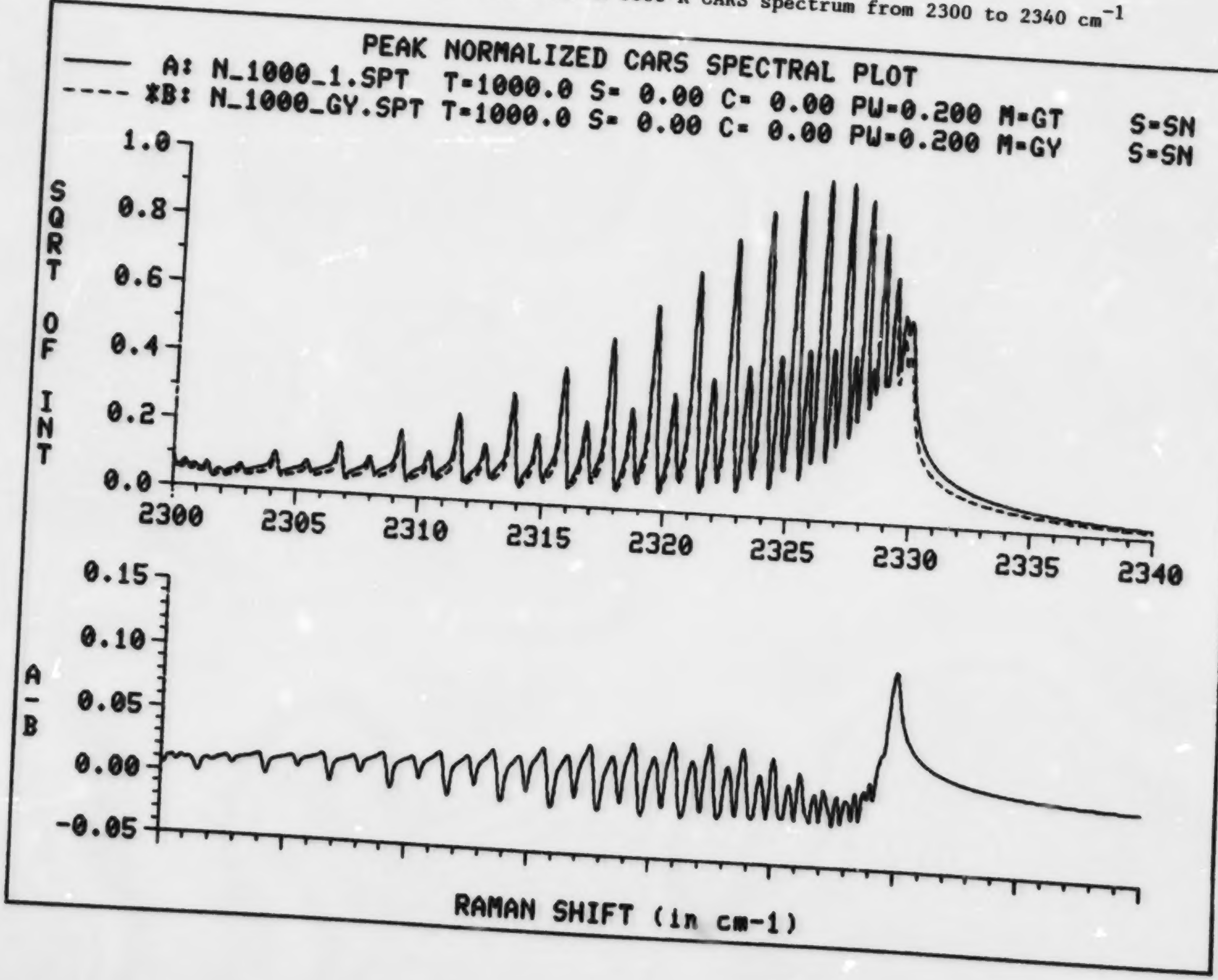

Fig. 14a. Effect of cross coherence on 1550 K CARS spectrum from 2260 to 2300 cm^{-1}

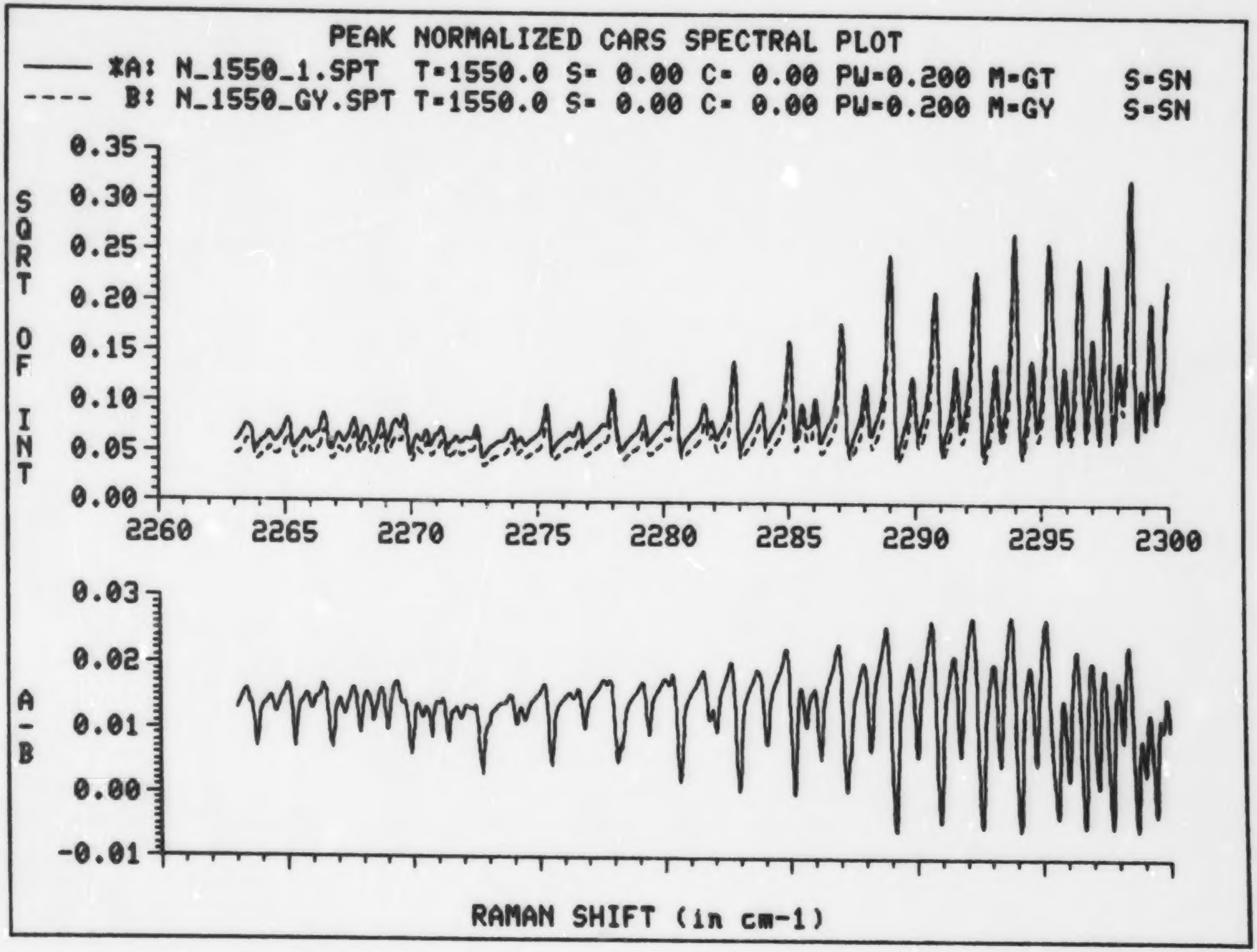

Fig. 14b. Effect of cross coherence on 1550 K CARS spectrum from 2300 to 2340 cm^{-1}

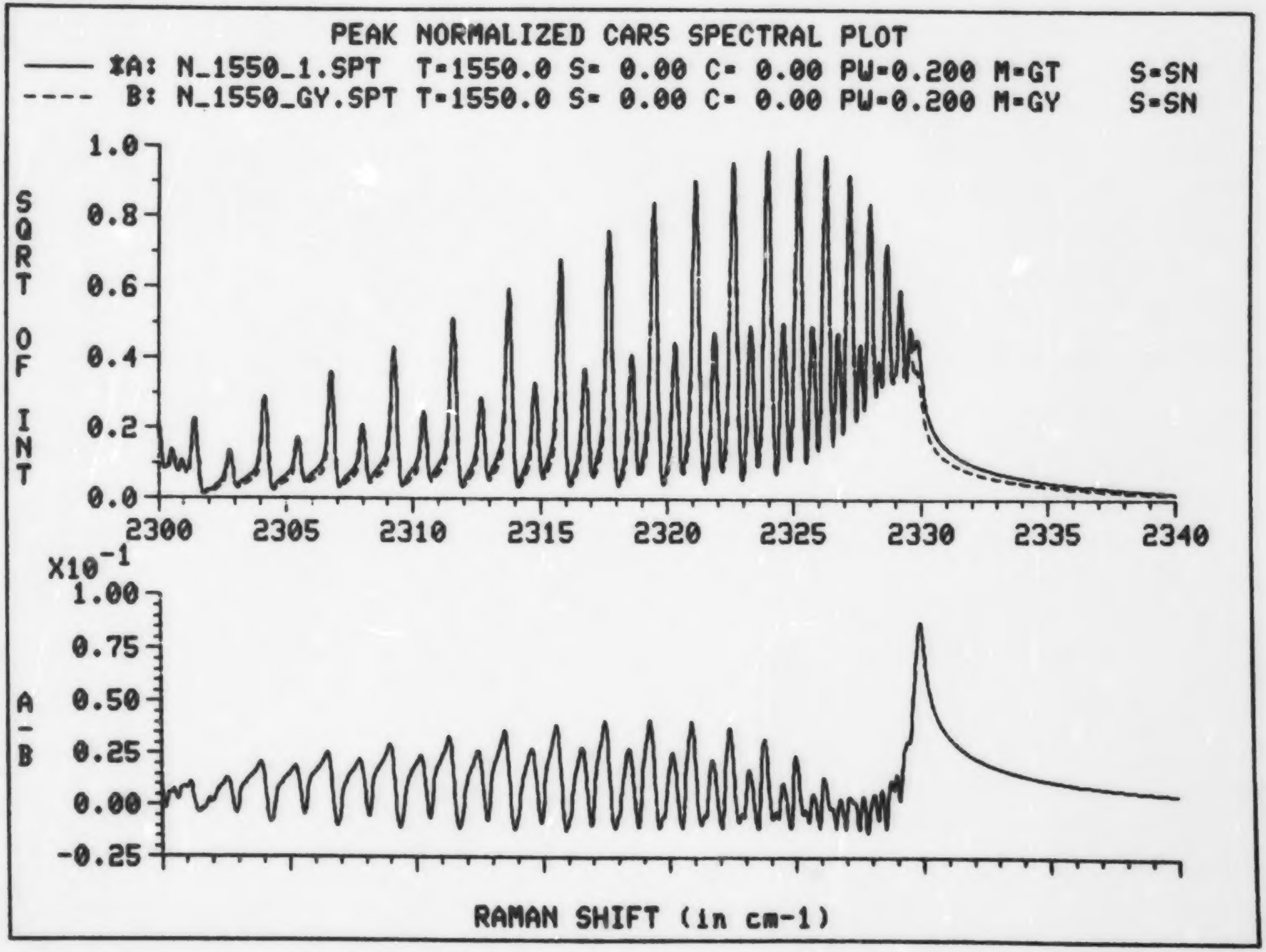

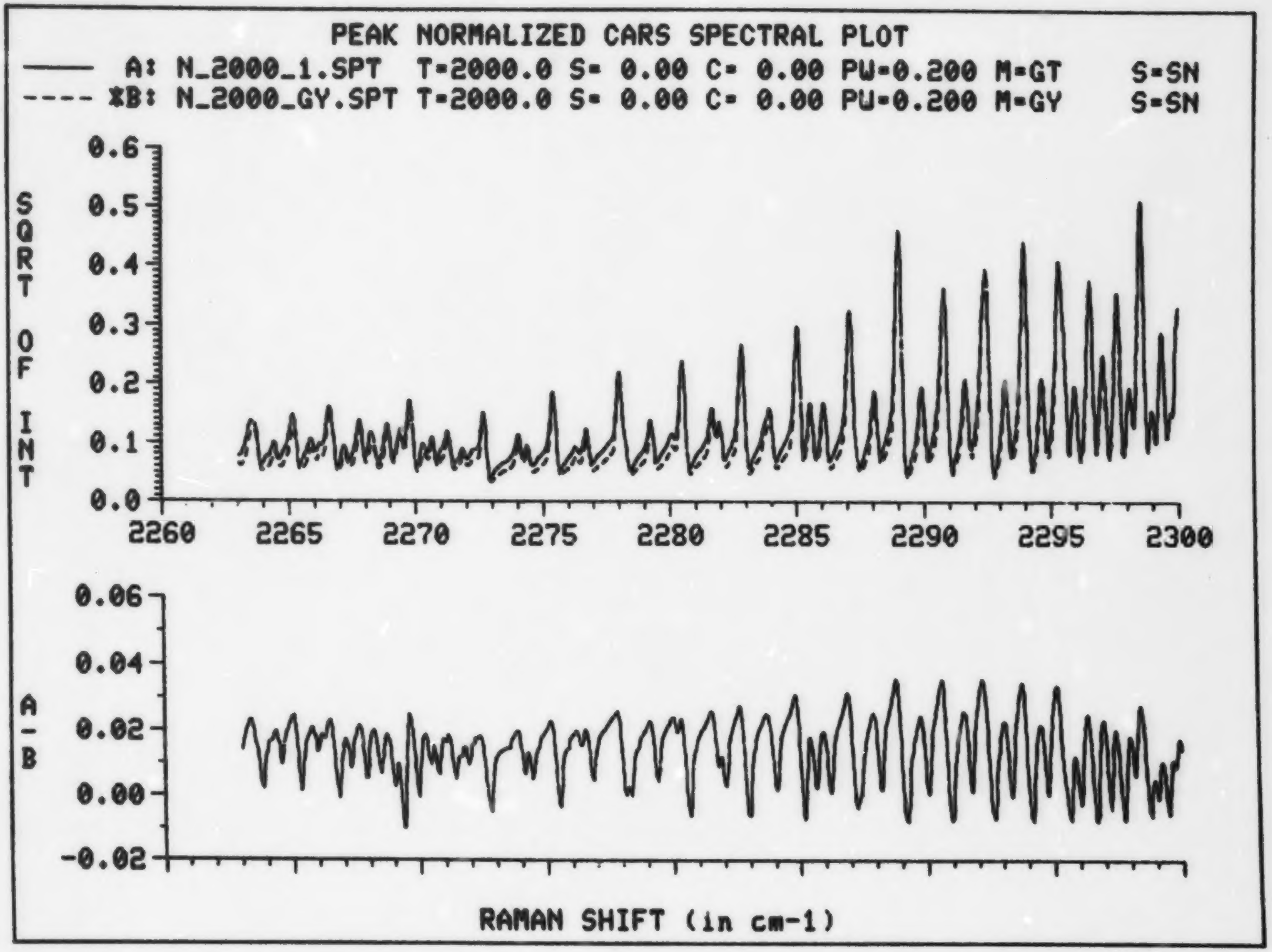

Fig. 15a. Effect of cross coherence on 2000 K CARS spectrum from 2260 to 2300 cm^{-1}

Fig. 15b. Effect of cross coherence on 2000 K CARS spectrum from 2300 to 2340 cm^{-1}

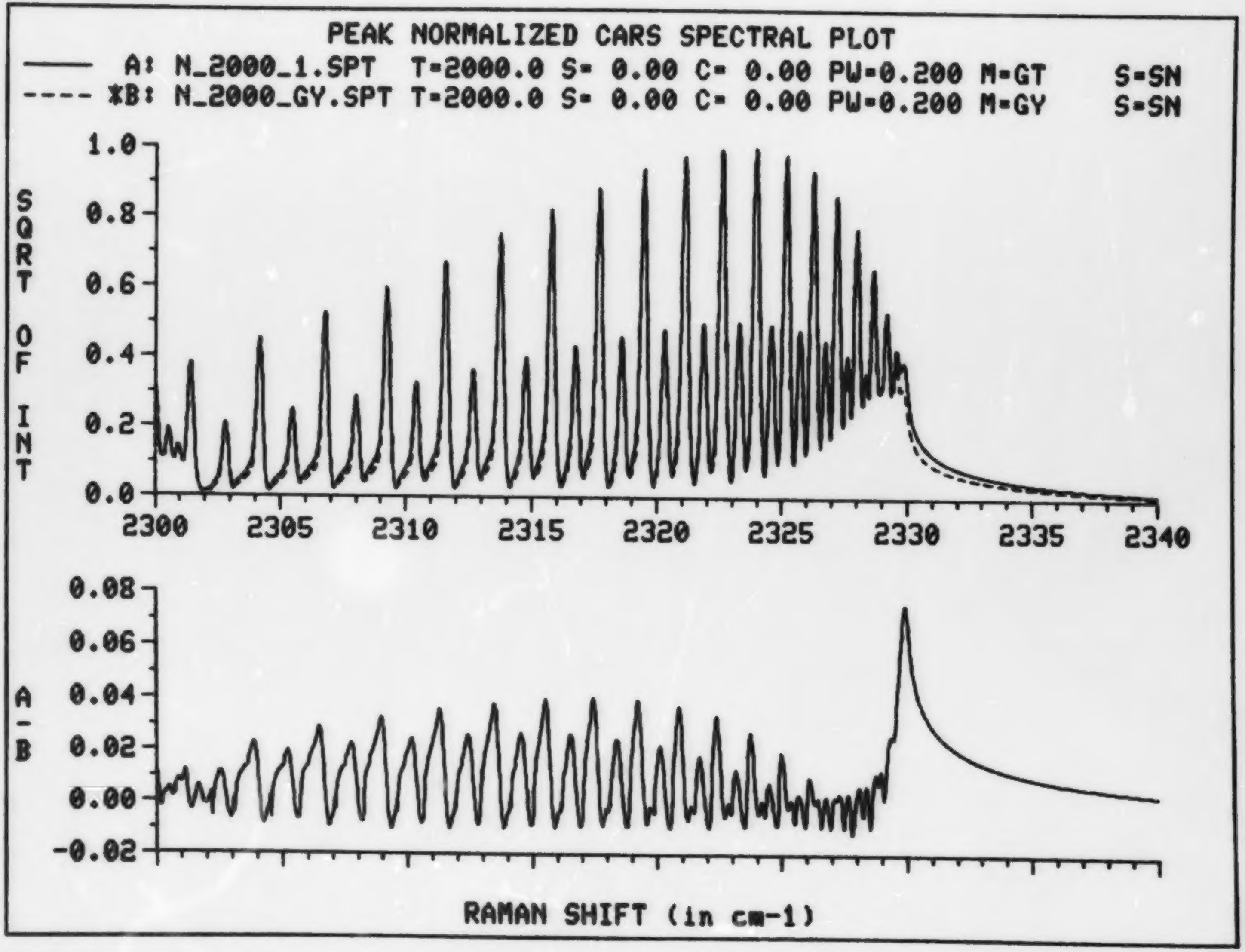

Fig. 16. Comparison of isolated line (curve B) and collisional narrowing and cross coherence (curve A) models of 300 K N_2 CARS spectra

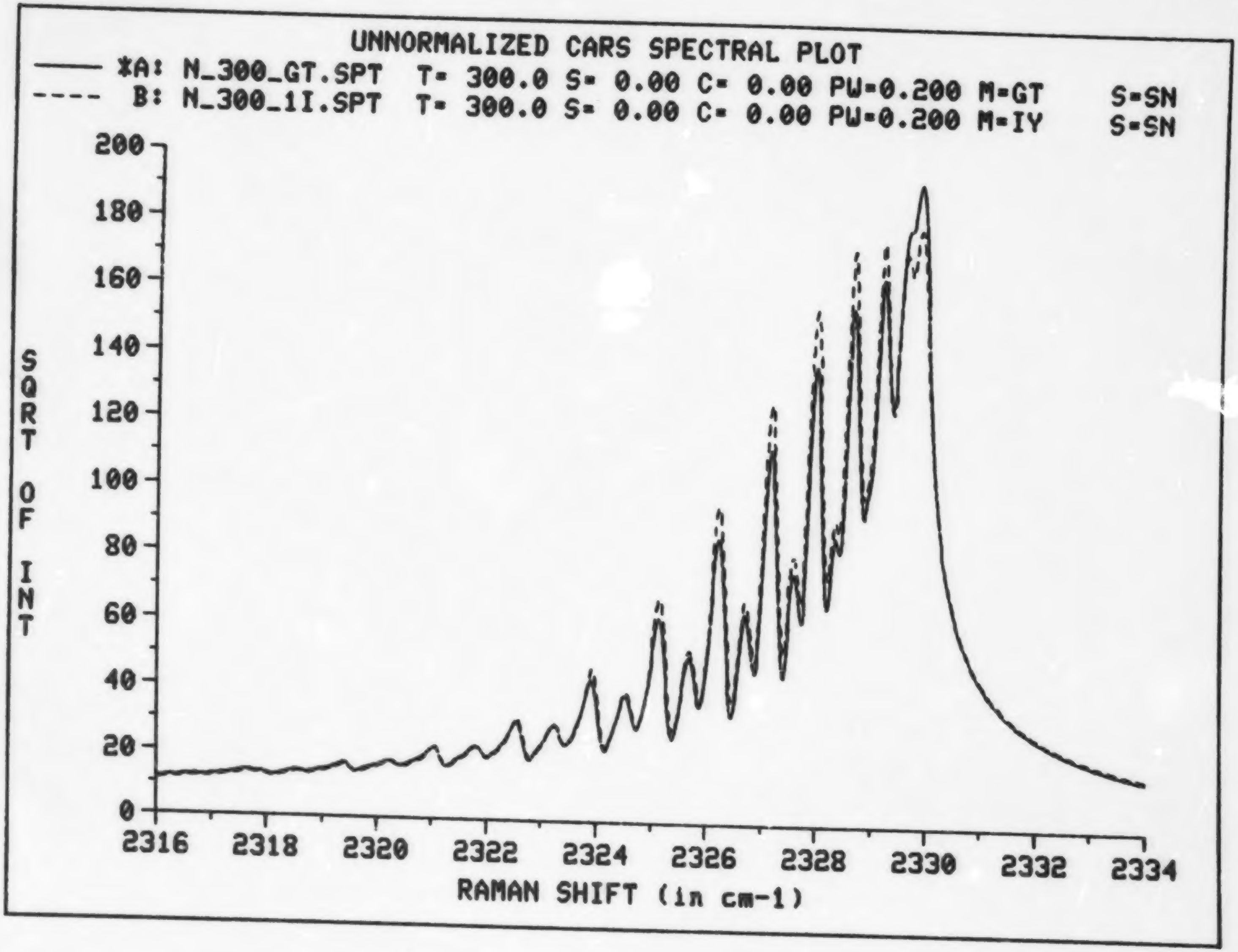

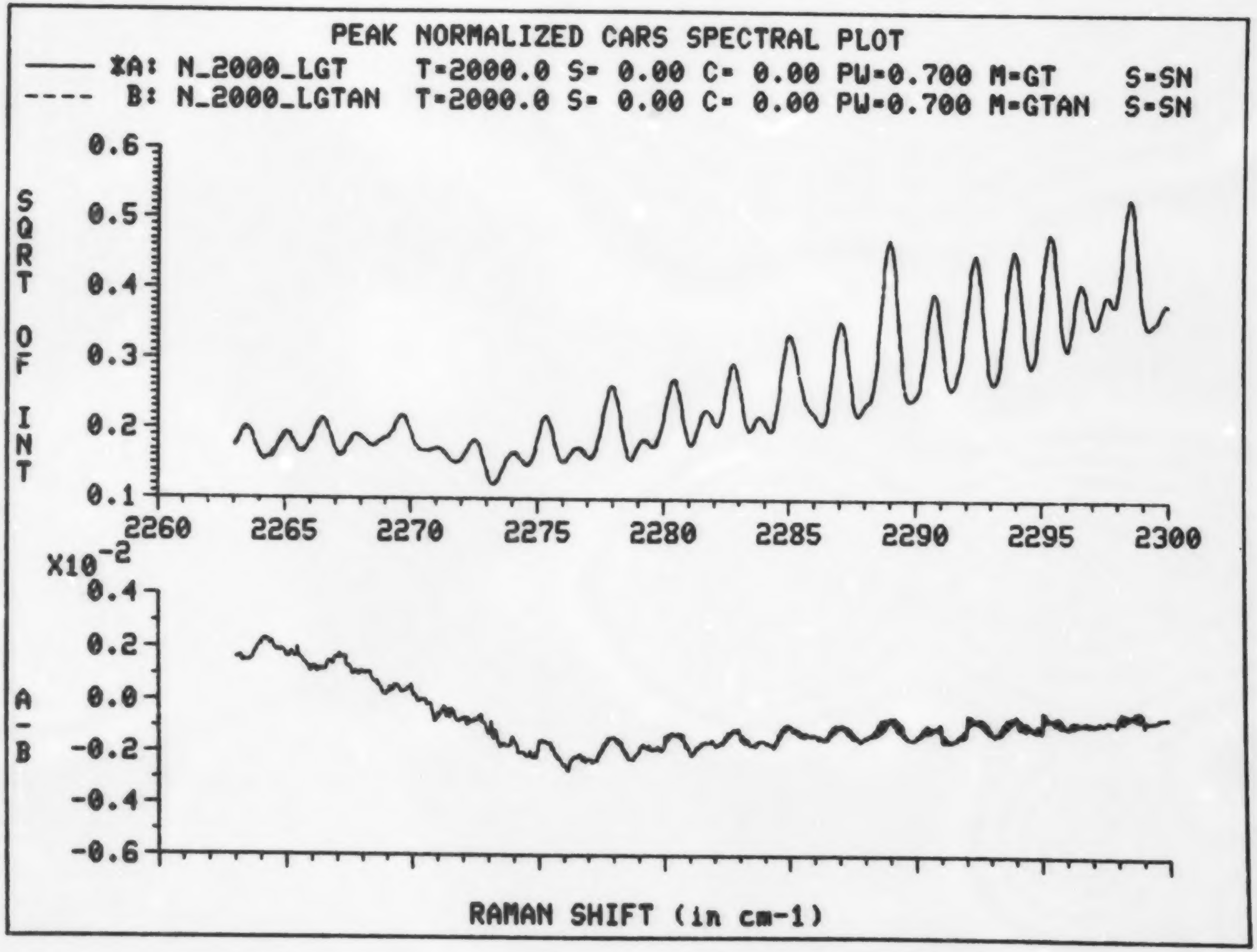

Fig. 17a. Comparison of analytic (GTAN) and numeric (GT) 2000 K CARS spectra from 2260 to 2300 cm^{-1}

Fig. 17b. Comparison of analytic (GTAN) and numeric (GT) 2000 K CARS spectra from 2300 to 2340 cm^{-1}

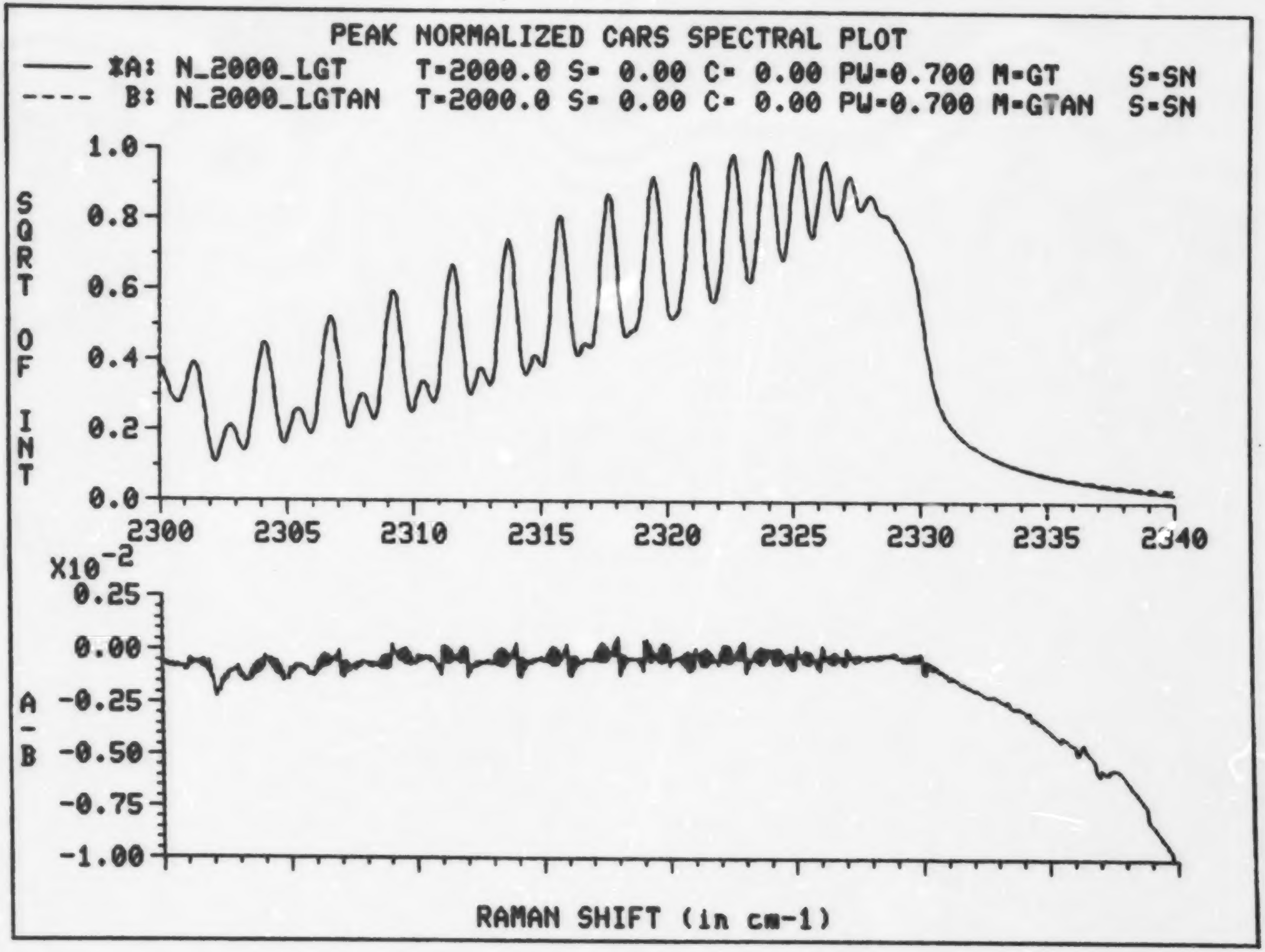

Fig. 18. Voigt parameters from room temperature N_2 CARS spectra

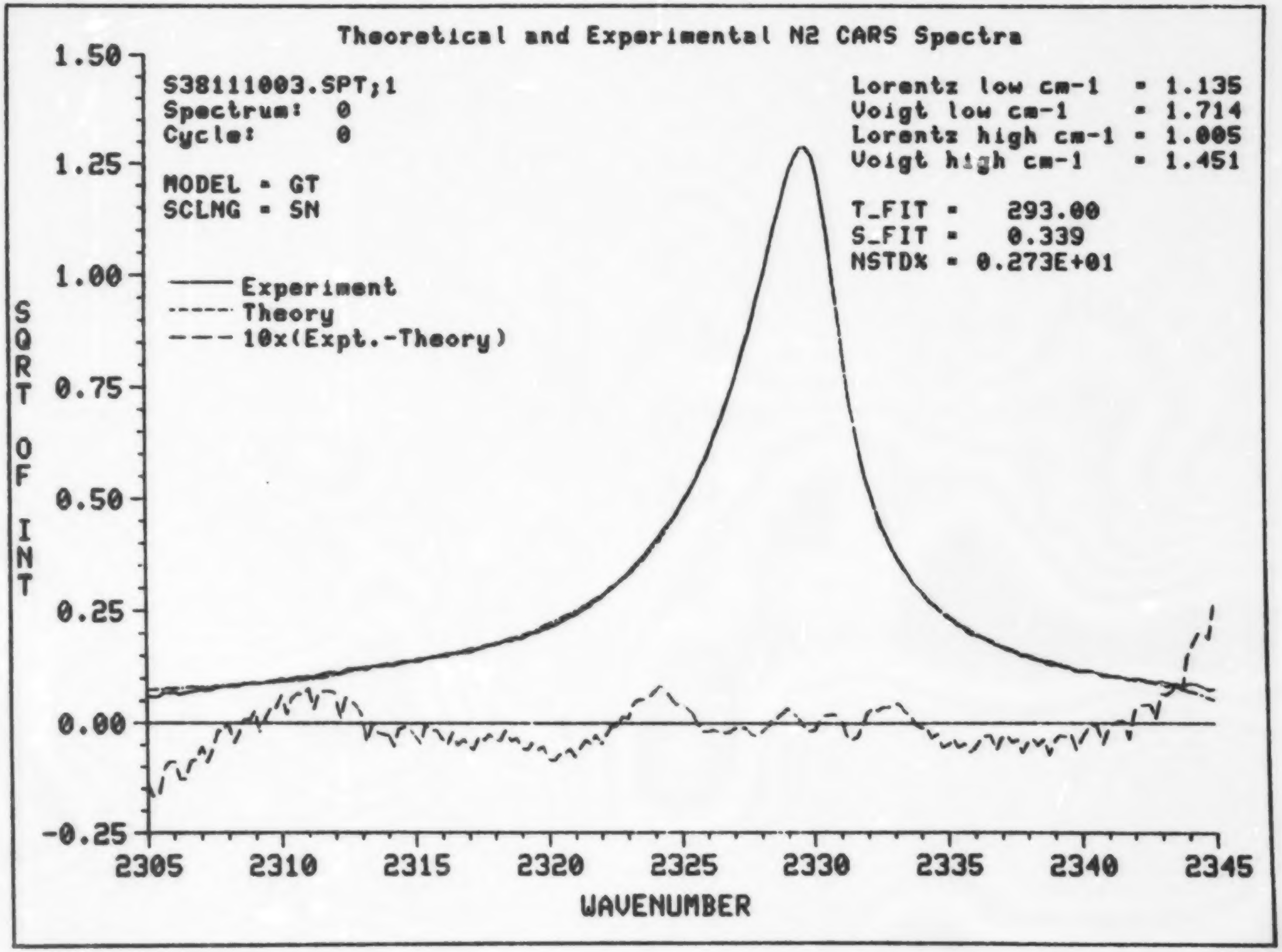

Fig. 19. Voigt parameters and temperature from N_2 CARS flame spectra

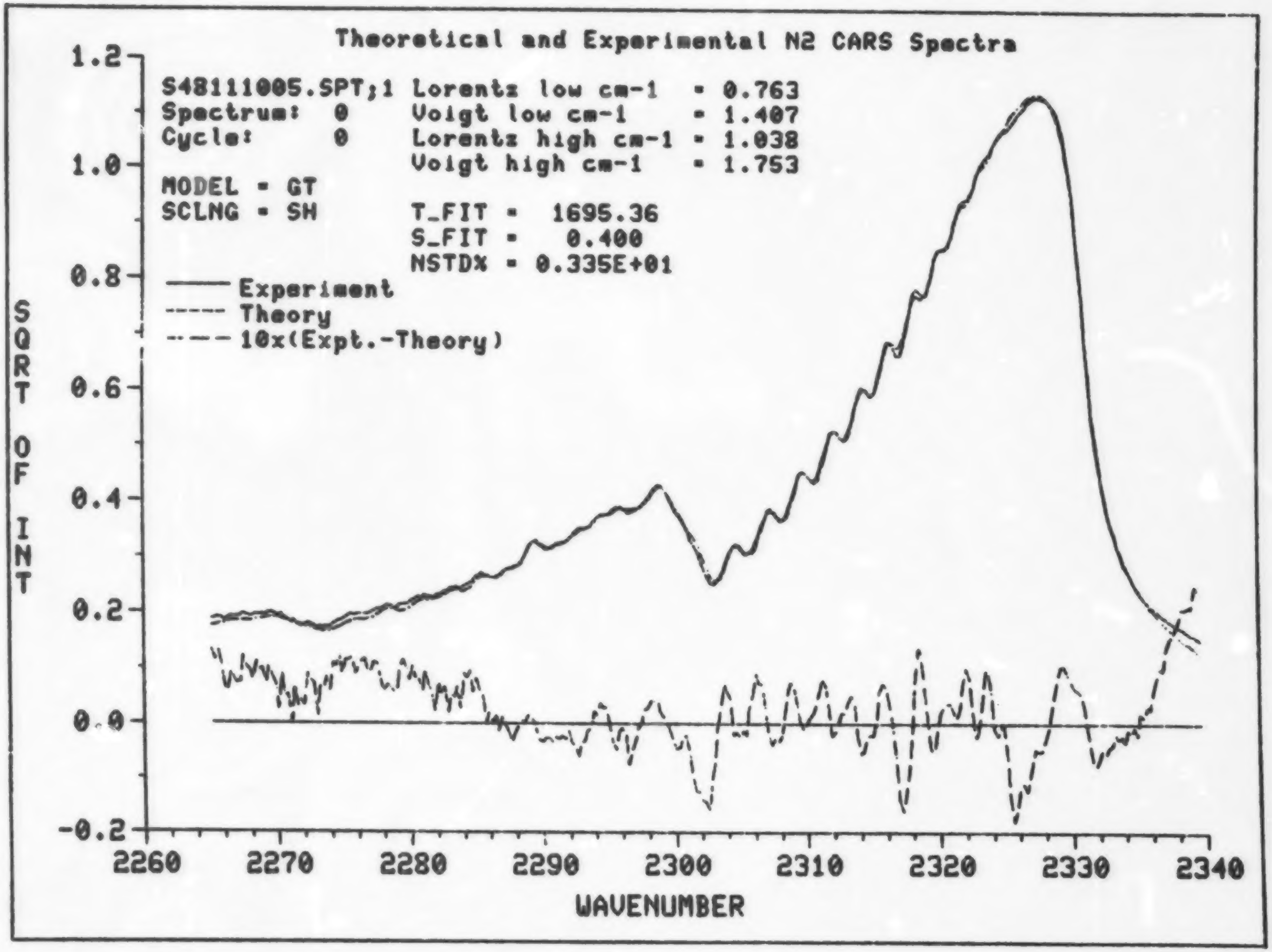

APPENDIX A.
DESCRIPTION OF THE CARS SPECTRA GENERATING PROGRAM ENTITLED GENERATE

CONTENTS

		Page
A1.0	INTRODUCTION	A3
A2.0	ENVIRONMENT	A3
A3.0	DESCRIPTION	A3
A4.0	SUBROUTINES USED IN ALPHABETICAL ORDER	A5
A5.0	FILES NEEDED	A6
A6.0	DEFINITION OF OTHER IMPORTANT VARIABLES	A7
A7.0	REFERENCES	A9

APPENDIX A.
DESCRIPTION OF THE CARS SPECTRA GENERATING PROGRAM ENTITLED GENERATE

A1.0 INTRODUCTION

This program generates one or more theoretical coherent anti-Stokes Raman spectra (CARS) for diatomic molecules. The calculation can take into account collisional narrowing owing to line overlap and the cross-coherence terms if necessary. The estimation of collisional narrowing effects is based on the Gordon McGinnis algorithm (McGinnis 1968). Cross coherence evaluation is based on the Greenhalgh-Hall algorithm (Greenhalgh and Hall 1986). Option is also provided to compute all the CARS integrals using closed form expressions of complex error functions. The elements of the relaxation rate matrix may be obtained from an exponential gap law model or a modified exponential scaling law (Rahn and Palmer 1986).

The convolutions assume a Gaussian spectral profile for the pump laser.

A2.0 ENVIRONMENT

This program was written in Fortran for a DEC_VAX_11 (730) computer.

A3.0 DESCRIPTION

In brief, GENERATE works as follows.

a. The program reads input data from a user supplied input file. The data should be entered in a name list format. An existing file can be edited to provide new data.

b. It sets up necessary frequency arrays for CARS generation within the specified range and at the specified sampling interval.

c. It calculates frequency independent variables, such as number density and nonresonant susceptibility, at the relevant temperature and pressure.

d. It computes vibrational rotational energy levels of the molecule.

e. SUBROUTINE TRAN_FREQ computes Raman transition frequencies for Q, O, and S branches of the molecule.

f. SUBROUTINE POPLN_FACTR generates the population factors.

g. The off-diagonal matrix elements of the relaxation matrix and the Raman line widths are calculated. This can be done with the Polanyi Woodall exponential gap law using SUBROUTINE PW_EXP_GAP_LAW or modified exponential gap law with the SUBROUTINE SANDIA_EXP_GAP_LAW.

The latter subroutine based on most recent inverse Raman data from Sandia, is the one recommended for use in CARS spectra generation.

h. SUBROUTINE TRAN_LINCD is called to calculate the population factors, cross sections, and centrifugal distortion corrections and yield the line strength factors.

i. The program selects the overlap model for CARS generation. Choice is provided for using isolated line or full G-matrix models. If the latter is chosen, the complex G-matrix is set up and diagonalized with the set of programs in the software package CGMOD. Diagonalization may be done for one or all the vibrational bands. For more accurate (but slower) results all the bands are separately diagonalized.

   The SUBROUTINE INVRT_CMPLX_MATRX is then called to invert the transformation matrix obtained from the eigenvectors. From the transformation matrix and the transition amplitudes, the complex weight factors are calculated for the G-matrix model. For the isolated line model, the products of d^2, $\Delta\rho$, and number density give the weight factors.

j. The program selects the procedure used for pump convolution. Choice is provided to use Yuratich convolution or partially numeric Kataoka Teets convolution with either the isolated line or full G-matrix models. The completely analytic convolution option is provided with full G-matrix only.

k. With Yuratich convolution the monochromatic CARS spectrum is convolved with the Gaussian pump, laser profile specified. This convolution is based on a Simpson's rule algorithm of numerical integration.

   With the partially analytic K-T option the above convolution is still performed, but the purely resonant term is reduced by half. Then the cross coherence (Teets term) is calculated by calling the FUNCTION ERF to evaluate the complex error functions and added to the previously convolved spectrum.

   If completely analytic convolution is selected, all the CARS integrals are calculated by means of the closed form complex error function representation. In any case, the pump convolved CARS spectrum is calculated and saved in an output file.

l. The program checks for the next temperature in the input file and loops back to generate the corresponding spectrum. CARS spectra for all temperatures in an input file are generated within the same frequency range, at the same frequency intervals.

A4.0 SUBROUTINES USED IN ALPHABETICAL ORDER

The following subroutines are part of the Fortran source file.

AMPTST	Finds transition of maximum amplitude in the specified frequency range.
ERF	Computes the complex error function.
INVRT_CMPLX_MATRX	Inverts a complex matrix.
LIB$INIT_TIMER	VAX-11 routine to initialize time.
LIB$STAT_TIMER	VAX-11 routine to compute cpu time expired.
POPLN_FACTR	Generates the population factors.
PW_EXP_GAP_LAW	Uses Polanyi Woodall exponential gap law for computing off diagonal matrix elements.
ROTNL_PARTN_FUNC	Yields rotational partition functions.
SANDIA_EXP_GAP_LAW	Uses modified exponential gap law from Sandia for off diagonal matrix elements.
TRAN_FREQ	Determines Raman transition frequencies and classifies them according to type (Q,O,S) and quantum numbers.
TRAN_LIN_CD	Calculates the weight coeffecients (line strength) that contain the scattering cross section, centrifugal distortion correction, and population differences.
VIBRNL_PARTN_FUNC	Yields vibrational partition functions.
WRITE_GMAT	Writes the elements of the relaxation matrix in terminal output.
WRITE_SPEC	Writes CARS spectra at every 20th point in terminal output.
ZERO	Clears a matrix.

The following is an include file.

SPT_RECORD_INC	Defines the variables in record one of the output file that contains the CARS spectra as binary digits.
SPT_ENTER_FILE_NAME	Accepts an input file name from the user. To use this subroutine the library SPTMLIB must be linked to the main program.

CGMOD	Diagonalizing software package for complex matrices; this subroutine must be linked.

A5.0 FILES NEEDED

a. The executable file obtained by compiling GENERATE.FOR and linking with the object module of CGMOD and the library SPTMLIB (a set of in-house utility routines developed on the VAX computer at NRC).

b. A data file containing the relevant input parameters. The data should be entered in the NAMELIST format. The variables therein are defined below.

Definitions of the name list variables in the input file are as follows.

PRESSURE	Pressure
MOLAR_CONC	Concentration (mole fraction or xmole) of the probed species
NON_RESN_SUSCEP	Sum of the effective nonresonant susceptibilities of all the species at NTP.
START_TEMP	Starting temperature for CARS spectrum generation.
FINISH_TEMP	Ending temperature for CARS spectrum generation.
TEMP_STEP	Temperature step for above spectra.
WE, XWE, YWE, ZWE	Molecular constants ω_e, $x\omega_e$, $y\omega_e$, and $z\omega_e$, respectively.
BE, DE, B1, B2, D1	Molecular constants B_e, D_e, α_e, γ_e, and β_e, respectively.
MODEL	Controls the model used for overlap of Raman lines and the type of convolution

= 'IY' Isolated line (neglects overlap) with Yuratich convolution
= 'IT' Isolated line with K-T convolution
= 'GY' Full G matrix inversion with Yuratich convolution
= 'GT' Full G matrix inversion with K-T convolution; K-T implies Kataoka-Teets convolution which includes the cross coherence terms.
= 'GTAN' Full G matrix inversion with K-T convolution and all CARS integrals evaluated with the error function approach.

GDIAG	Selects number of G-matrix diagonalizations and inversions;

= 'ONE' Diagonalizes the G matrix and inverts the eigenvector matrix for the 0 -1 band only.
= 'ALL' Does above diagonalization and inversion for all the vibrational bands.

SCLNG	Specifies the scaling law for getting the elements of the G matrix for the GT, and GY models and the line widths for the other models.

= 'PW'	Polanyi-Woodall exponential gap law.
= 'SN'	Modified exponential gap law from Sandia (N_2-N_2 broadening)
= 'SH'	Modified exponential gap law from Sandia with relaxation matrix corrected for H_2O broadening
TRY_ALPHA_FIT	Trial value of fitting parameter for PW exponential gap law.
H2O_BRD_CORR	Factor for augmenting the G matrix elements for water broadening.
PUMP_CENTR_FREQ	Centre frequency of pump laser.
PUMP_WID	Band width FWHM of pump laser.
STNUC(2)	Statistical weight factors.
CHISQFRQSTP	Frequency step used for $\|\chi\|^2$ calculation.
PUMP_CONV_STP	Frequency step after pump convolution.
STRT_FREQ	Starting frequency for CARS spectra.
FIN_FREQ	Finishing frequency for CARS spectra.
CONST	Constant multiplying term in CARS susceptibility.
ALPHA, GAMMA	Polarizability derivatives.
FILE_TYPE	Chooses output file type.
= 'DAT'	Sets .DAT file ; default = 'SPT'; .DAT is a text file; .SPT is a binary file.
CWRITE	Controls output on line or log file.
= 'DETAILED'	Gives lengthy output with eigen values and off-diagonal matrix elements of the G-matrix, in addition to the partial output.
= 'PARTIAL'	Gives partial output with transition frequency population, line width, type, peak amplitude, eigenvalues, weighting coefficients, and the components of CARS intensities at every 20th point. default = limited output.
FIRST_WN_FIT, LAST_WN_FIT ,FIRST_WN_SLIT, LAST_WN_SLIT	These are the default fitting range and slit convolution range to be used by the fitting and convolution programs.
CONST1,CONST2	Constants used set up a vibrational temperature different from the rotational temperature; normally CONST1 = 1.; CONST2 = 0.

A6.0 DEFINITION OF OTHER IMPORTANT VARIABLES

NUM_ROTNL_LVLS	Number of rotational levels.
NUM_CHISQ_PTS	Number of frequency points before pump convolution.
NUM_PUMP_CONV_PTS	Number of frequency points after pump convolution.

NUM_DENSY	Number density
EFF_NON_RESN_SUSCEP	Effective nonresonant susceptibility at the specified temperature and pressure.
INPUT_FILE_NAME	Name of input file.
OUTPUT_FILE_NAME	Name of output file.
MOLECULE_NAME	Must be one of N_2,CO,or O_2
SPEC_TYPE	Selects susceptibility square or pump convolved spectrum; must be CHI_SQRE or PUMP_CONV.
TRAN_TYPE	Contains the type (Q,O,S) of the transitions.
ERF	Complex error function.
ZH	Complex argument (in double precision) of ERF.

The G-matrix referred to in this program is the frequency independent part of the full G matrix.

G_REAL	Elements of real part of relaxation rate matrix.
G_IMAG	Elements of imaginary part above matrix.
G_COPY	Copy of G_IMAG.
EIGENR	Real part of eigenvalues of G-matrix.
EIGENI	Imaginary part of eigenvalue of G-matrix.
EIGEN_VAL_REAL	Real part of eigenvalues as two-dimensional (vib. no., rot. no.) array.
EIGEN_VAL_IMAG	Imaginary part of above array.
EIGEN_VEC_REAL	Real part of eigenvector matrix.
EIGEN_VEC_IMAG	Imaginary part of eigenvector matrix.
EIGEN_INV	Inverse of complex eigenvector matrix.
CWEIGHT1	Complex matrix product of TOT_COEF and EIGEN_INV.
CWEIGHT2	Complex matrix product of (EIGEN_VEC_REAL,EIGEN_VEC IMAG) and constant column.matrix.
CWEIGHT	Matrix of complex weight factors = the matrix product of CWEIGHT1 and CWEIGHT2.
U(300)	An intermdiate complex array used in the GTAN analytic integration model.
RZ,CIMAGZ	Double precision arguments for the error function.
RMN_FREQ	Raman transition frequencies.
FV1,FV2,FV3	Working arrays for CGMOD.
EVIB	Vibrational band centre positions.
EMOL	Molecular energy levels.
B	Intermediate array used by POPLN_FACTR.
POPLN	Population factor for vibrational rotational levels.
TOT_COEFI	Line strength factors for isolated line model that contain population factor, centrifugal distortion correction, and scattering cross section.
TOT_COEFG	Square root of TOT_COEF without the population; used for Q branch in full G-matrix models only.
FREQ	CARS frequency vector before pump convolution.
OMEGA3	CARS frequency vector after pump convolution.
RESON_MOD	Term with modulus of resonant susceptibility.
RESON_REAL	Interference term with real part of resonant susceptibility.
PUMP_CONVD_CARS	Pump convolved CARS intensities.
SUMNR	Nonresonant part of PUMP_CONVD_CARS.

SUMRR	Purely resonant part of PUMP_CONVD_CARS.
SUMRNR	Interference term in PUMP_CONVD_CARS.
CRSCOH	Cross-coherence term in PUMP_CONVD_CARS.
EXP1	Array of stored pump exponents.
E_OFFSET	Frequency offset energy levels to increase the precision of the Raman shifts.
QUANTUM_NO	The vibrational quantum numbers and the rotational quantum numbers for the upper and lower levels
NUM_TRANS	Number of transitions.
Q_FREQ	Q branch Raman frequencies stored as two dimensional array.
RE	Inter nuclear distance in Bohr radii. Bohr radius = 0.52918E-8 cm.
GAMM	Anisotropic component of polarizability in units of cm**3/Bohr radius**3.

A7.0 REFERENCES

GREENHALGH, D.A., and R.J. Hall. 1986. A Closed Form Solution for the CARS Intensity Confolution. Optics Communications, **57**: 125.

GORDON, R.G., and R.P. McGinnis. 1968. Line Shapes in Molecular Spectra. Journal of Chemical Ph;ysics, **49**: 2455.

RAHN, L.A., and R.A. Palmer. 1986. Studies of Nitrogen Self Broadening at High Temperature with Inverse Raman Spectroscopy. Journal of the Optics Society of America, b3: 1164.

APPENDIX B.

COMPARISON OF CARS SPECTRA CALCULATED WITH NRC AND SANDIA CARS GENERATING PROGRAMS

CONTENTS

		Page
B1.0	INTRODUCTION	B3
B2.0	IMPROVEMENTS IMPLEMENTED IN GEN	B3
	B2.1 O and S Branches: Intensity Corrections	B3
	B2.2 Sampling Grid	B4
B3.0	ISOLATED LINE MODEL	B4
B4.0	THE GT MODEL WITH COLLISIONAL NARROWING AND CROSS COHERENCE	B5
B5.0	COMPARISON AT HIGH PRESSURE	B6
B6.0	CARS SPECTRA WITH LARGER PUMP WIDTHS	B6
B7.0	FITTING THE SANDIA SPECTRA AGAINST A LIBRARY OF NRC SPECTRA	B6
B8.0	REFERENCES	B6

LIST OF ILLUSTRATIONS

Figure		Page
B1	Comparison of NRC and Sandia codes (isolated line model, 1550 K	B8
B2	Raman line position difference between NRC and Sandia code for Q, O, and S branch N_2 transitions	B9
B3	Comparison of NRC and Sandia codes (isolated line model, 1550 K) with NRC spectrum shifted by +0.004 cm^{-1}	B10
B4a	Comparison of NRC and Sandia codes with collisional narrowing and cross coherence for 1000 K N_2 CARS spectra from 2260 to 2300 cm^{-1}	B11
B4b	Comparison of NRC and Sandia codes with collisional narrowing and cross coherence from 1000 K N_2 CARS spectra from 300 to 2340 cm^{-1}	B12
B5a	Comparison of NRC and Sandia codes with collisional narrowing and cross coherence from 1550 K N_2 CARS spectra from 2260 to 2300 cm^{-1}	B13
B5b	Comparison of NRC and Sandia codes with collisional narrowing and cross coherence from 1550 K N_2 CARS spectra from 2300 to 2340 cm^{-1}	B14
B6a	Comparison of NRC and Sandia codes with collisional narrowing and cross coherence for 2000 K N_2 CARS spectra from 2260 to 2300 cm^{-1}	B15
B6b	Comparison of NRC and Sandia codes with collisional narrowing and cross coherence for 2000 K N_2 CARS spectra from 2300 to 2340 cm^{-1}	B16
B7	Comparison of NRC and Sandia codes at the high pressure $P = 20$ atm and $T = 1550$ K	B17
B8	Comparison of NRC and Sandia codes at the high pressure $P = 20$ atm and $T = 2000$ K	B18

LIST OF ILLUSTRATIONS (Cont'd)

Figure **Page**

B9a Comparison of NRC and Sandia codes with 0.7 cm^{-1} pump width at T = 1550 K; lower plot shows the difference A - B B19

B9b Comparison of NRC and Sandia codes with 0.7 cm^{-1} pump width at T = 1550 K; lower plot shows the ratio A/B

LIST OF TABLES

Table **Page**

B1 Q, O, and S branch nitrogen branch line positions ordered by wave numbers B21

B2 Fit of SAND spectrum against a GEN library B25

APPENDIX B.

COMPARISON OF CARS SPECTRA CALCULATED WITH NRC AND SANDIA CARS GENERATING PROGRAMS

B1.0 INTRODUCTION

During the latter part of 1987, a copy of a computer program that generates theoretical CARS spectra was kindly given to us by Dr. Richard Palmer of Sandia National Laboratories, Livermore, California. This program is similar to the CARS computer program developed at the National Research Council, in that it contains the recent improvements such as collisional narrowing and K-T convolution. In the rest of this section the Sandia program will be referred to as SAND and the NRC program as GEN. The software package SAND has additional capabilities of using Voigt and Galatry (Galatry 1961) line shape functions. Further it can fit experimental spectra (both broadband and scanning CARS) with calculated spectra, which makes it very versatile. Comparing the theoretical spectra from both the codes provides a means of validating the results obtained. While the basic susceptibility calculation in both codes is similar, different algorithms are used for convolution with the pump laser profile. SAND employs fast Fourier transform routines, while GEN uses numerical integration procedures based on Simpson's rule. The CARS integrals in SAND are evaluated by convolving χ and $|\chi|^2$ separately and taking their mean (Farrow and Rahn 1985). GEN, on the other hand, uses closed form expressions for all the above integrals in the analytic approach and for just the cross coherence term in the partially numeric approach. These similarities and differences between the two codes prompted the comparative study of the spectra produced under varying conditions of temperature, pressure, and pump band width.

Both codes can handle the isolated line model and the full G matrix model with Yuratich convolution (IY, GY) and with K-T convolution (IT, GT). The molecular constants and line strength parameters for N_2 used for the comparison are given as part of the input file in Appendix C.

B2.0 IMPROVEMENTS IMPLEMENTED IN GEN

One of the first steps taken was to look for any refinements included in SAND and implement them in GEN, to make the two programs equivalent and justify the comparison. These improvements to GEN are discussed below.

B2.1 O and S Branches; Intensity Corrections

The older version of GEN performed only a Q branch calculation. Anharmonicity and centrifugal distortion corrections were based on rotation vibration matrix elements calculated for infrared spectra (Bounaich and Brodbeck 1975, 1976).

The largest contribution to the intensity of the N_2 CARS spectrum originates from the Q branch transitions. On examination it was found that SAND also includes the O, S, and pure rotational branches in the calculations. In this code, centrifugal distortion corrections to the Raman polarizability matrix element for all the above branches (James and Klemperer 1959; Buckingham and Szabo 1978) are also incorporated. The Sandia approach to intensity corrections seems to be more appropriate because it is based on Raman spectra. Thus one of the first modifications done to GEN was to implement the O and S branch transitions, along with intensity corrections using the formalism followed by SAND.

B2.2 Sampling Grid

In our earlier work (Snelling et al. 1985), the CARS susceptibility was calculated at interval of 0.01 cm^{-1} and the pump convolved CARS spectrum was at intervals of 0.1 cm^{-1}. Although a χ grid spacing of 0.01 cm^{-1} is reasonable when the Raman line width is around 0.1 cm^{-1} or more, errors can arise at flame temperatures with Raman line widths less than or equal to 0.03 cm^{-1}. The SAND program uses 0.2 times the narrowest Raman line width for the grid spacing. This number can approach a value as low as 0.0002 cm^{-1} for lines with a large rotational quantum number (J). Therefore, an upper limit of 65,768 points is also imposed to make the calculation time more manageable. For N_2 CARS in the 80 cm^{-1} region, this amounts to using a grid of 0.00125 cm^{-1}. In the NRC calculations, a grid of 0.00125 cm^{-1} is used, which provides 16 points for a Raman line with a width of 0.02 cm^{-1}. Since the very high J lines are generally very weak, this value will adequately describe all the significant Raman lines (see Section 4.2).

In the NRC calculations the pump convolved CARS spectrum is generated every 0.02 cm^{-1} for a 0.2 cm^{-1} pump and at 0.04 cm^{-1} for pump widths greater than or equal to 0.67 cm^{-1}. These grid parameters are part of the input data file and can be changed as needed. The SAND program originally designed to get the pump convolved spectrum at 1000 points or less was modified to accommodate up to 4000 points.

B3.0 ISOLATED LINE MODEL

The initial comparisons were done with a pump of 0.2 cm^{-1}, which retains most of the high resolution of the $|\chi|^2$ spectrum. A flame temperature of 1550 K and pressure of 1 atm were chosen for this purpose. The spectra were generated using the isolated line model with Yuratich convolution.

During this process it was found that SAND excludes O and S branch transitions that are less than a certain percentage of the strongest transition. This cutoff scheme was added to GEN and the cutoff limit was set to be 0.001 in both programs. When the spectra were compared, it was noticed that a systematic difference of the order of a few percent in the shape of the curves was present. To understand this, the line positions, widths, and population factors output by the two codes were compared. Indeed, the population factors were slightly different. This is related to the fact that SAND uses the ground state rotational partition function (Qrot) for all the bands, while GEN calculates Qrot for each band. Since the NRC method is more accurate, SAND was modified accordingly.

CARS spectra generated after the above changes to the code are presented on Fig. B1. Square roots of the CARS intensities are plotted to enable one to see the finer details of the spectra. There is close agreement between the two spectra; the superimposed plots cannot be distinguished. The difference spectra in the lower plots reveal small disagreement that arise owing to differences in the line positions in the two spectra [Table B1] of the order 0.0005 cm^{-1}. The uncertainties in the spectroscopic constants that are used to calculate the line positions are of the order ≈0.001 cm^{-1}. Thus shifts less than 0.001 cm^{-1} are not significant. However, these small spectral shifts show up in the difference spectrum, especially in regions where there are many closely spaced lines.

The relative shifts between SAND and GEN are plotted as a function of frequency in Fig. B2. On examination Fig. B2 shows that the SAND line positions are shifted by 0.0004 cm^{-1} (0.4 m Kayser) from the GEN values in the region of 2305 to 2325 cm^{-1}. That the major differences in Fig. B1 are due to the different line positions can be demonstrated by repeating the comparison as shown in Fig. B3, where the GEN spectrum is shifted by 0.0004 cm^{-1}. It is seen that the difference spectrum is greatly reduced and that the exceptions can be correlated with lines that are shifted by other than 0.0004 cm^{-1} in Fig. B2. The difference spectrum in Fig. B1 is largely made up of "dispersion-like" features characteristic of shifted spectra, but the features at 2289 and 2294 cm^{-1} are stronger in the SAND spectrum. Studying Fig. B2 and the line position in Table B1, it is clear that in these two regions there are abrupt changes in the line positions of adjacent lines, whose spacing falls within the Raman line width at 1550 K. Thus the SAND code predicts that the overlapped lines are closer together, producing a net increase in the CARS intensity because of its dependence on $|\chi|^2$.

B4.0 THE GT MODEL WITH COLLISIONAL NARROWING AND CROSS COHERENCE

Having checked the factors that contribute to the transition matrix elements by means of the simple IY model the next step was to check the more accurate GT model with corrections for high pressure and degeneracy of the two pump photons. Holding the pressure at 1 atm, spectra are compared at 1000, 1550, and 2000 K in Figs. B4-B6. Spectra from both codes were generated with separate matrix diagonalization and inversion for each vibrational band. As before, the agreement between the spectra from SAND (curve A) and GEN (curve B) is very good. The structure seen in the difference plots is again partly due to small shifts in line positions. Peak excursions in the difference plot are <1% and systematic differences are quite small.

B5.0 COMPARISON AT HIGH PRESSURE

A better check of the GT model is to compare the spectra at higher pressures where the G-matrix formalism plays a significant role. Spectra obtained at 20 atm and temperatures of 1550 and 2000 K, from SAND and GEN are compared in Figs. B7 and B8, respectively. Once again the spectra from GEN (curve A) and SAND (curve B) are extremely close. Line position shifts become less important here, because of line broadening with pressure.

B6.0 CARS SPECTRA WITH LARGER PUMP WIDTHS

In practice, multimode pump lasers widths (FWHM) are often greater than 0.2 cm^{-1}. Typical width for a multimode laser is about 0.7 to 1.0 cm^{-1}. With this in mind, SAND and GEN spectra produced at 1550 K for a pump width of 0.7 cm^{-1} are compared in Fig. B9. The difference spectrum in Fig. B9a and the ratio spectrum in Fig. B9b show discrepancies between the SAND and GEN plots to be less than 0.2%.

B7.0 FITTING THE SANDIA SPECTRUM AGAINST A LIBRARY OF NRC SPECTRA

As a final test at 1550 K , 1 atm. spectrum with a pump width of 0.67 cm^{-1}, generated by SAND, was fitted against a library of pump convolved spectra generated by GEN. The fitting process gave a best fit of 1549.3 K as shown in Table B2, i.e., a value within a fraction of a degree of the true value. The least mean square fit converged very quickly inspite of a distant initial guess temperature of 1800 K.

B8.0 REFERENCES

BOUNAICH, J.P., and C. BRODBECK. 1975. Vibrational matrix Elements for Diatomic Molecules. Journal of Quantitative Spectroscopy and Radiative Transfer, **15**: 873.

BOUNAICH, J.P., and C. BRODBECK. 1976. Vibration Rotation Matrix Elements for Diatomic Molecules. Journal of Quantitative Spectroscopy and Radiative Transfer, **16**: 153.

BUCKINGHAM, A.D., and A. AZABO. 1978. Determination of Derivatives of the Polarizability Anisotropy in Diatomic Molecule from Relative Raman Intensities. Journal of Raman Spectroscopy, **7**: 46-48.

FARROW, R.L., and L.A. RAHN. 1985. Interpreting Coherent Anti-Stokes Raman Spectra Measured with Multimode Nd:Yag Pump Lasers. Journal of the Optical Society of America, **2**: 903-906.

GALATRY, L. 1961. Simultaneous Effect of Doppler and Foreign Gas Broadening on Spectral Lines. Physical Review, **122**: 1218.

JAMES, T.C. and W. KLEMPERER. 1959. Line Intensities in the Raman Effect of $^1\Sigma$ Diatomic Molecules. Journal of Chemical Physics, **31**: 130-134.

SNELLLNG, D.R., R.A. SAWCHUK, and R.E. MUELLER. 1985. Single Pulse CARS Noise: A Comparison Between Singlemode and Multimode Pump Lasers. Applied Optics, **24**: 2771.

Fig. B1. Comparison of NRC and Sandia codes (isolated line model, 1550 K)

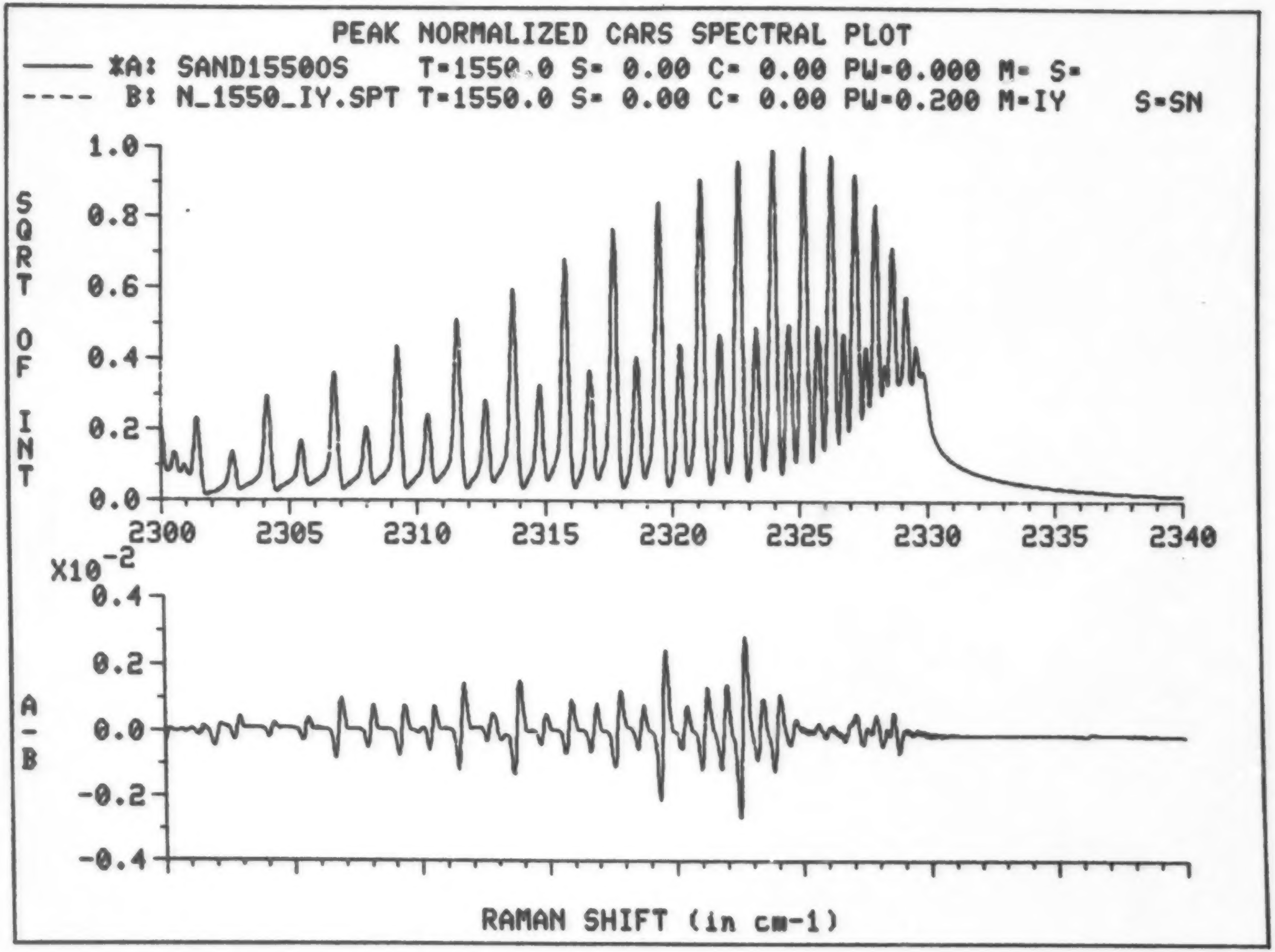

Fig. B2. Raman line position difference between NRC and Sandia code for Q, O, and S branch N_2 transitions

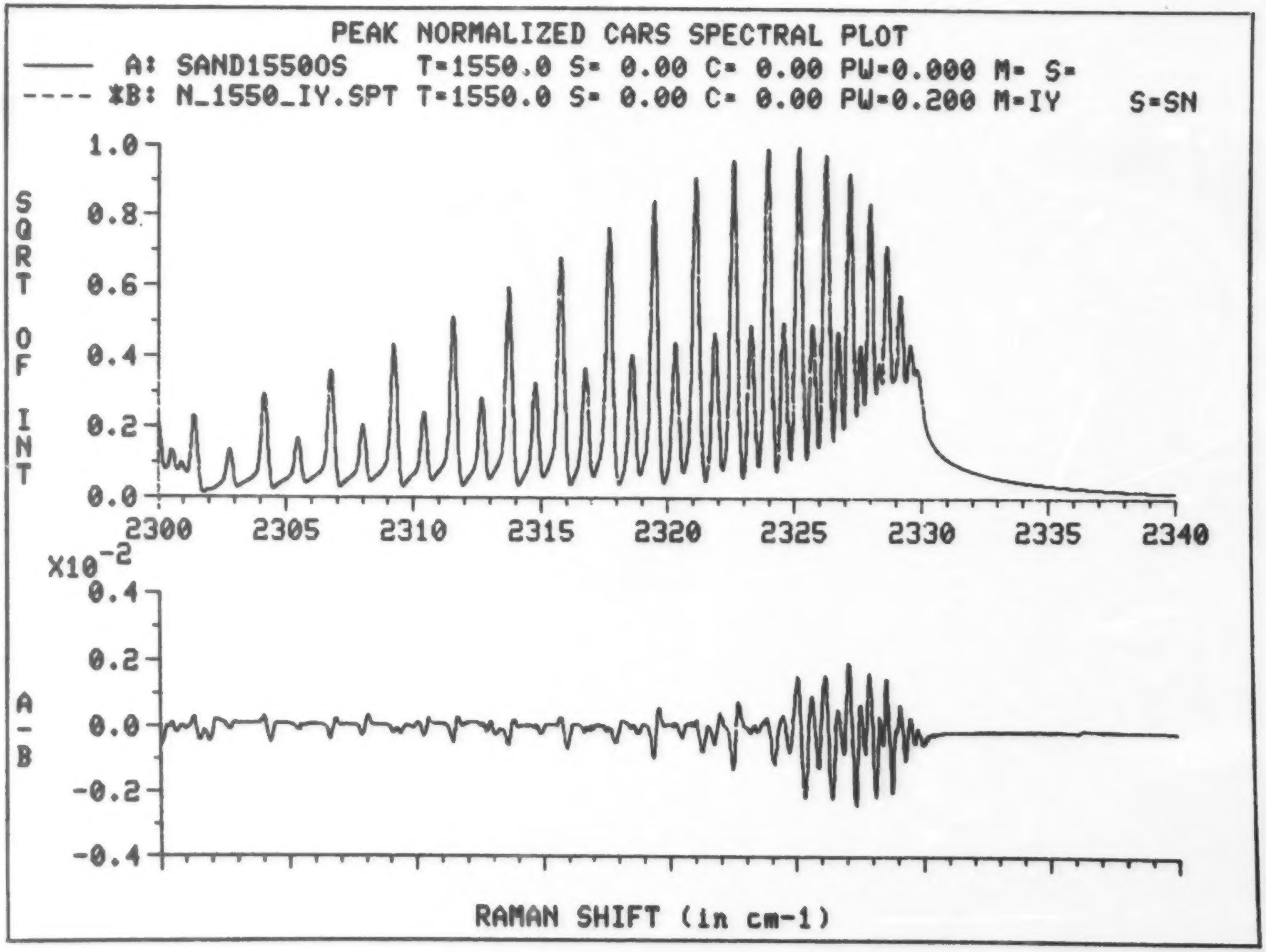

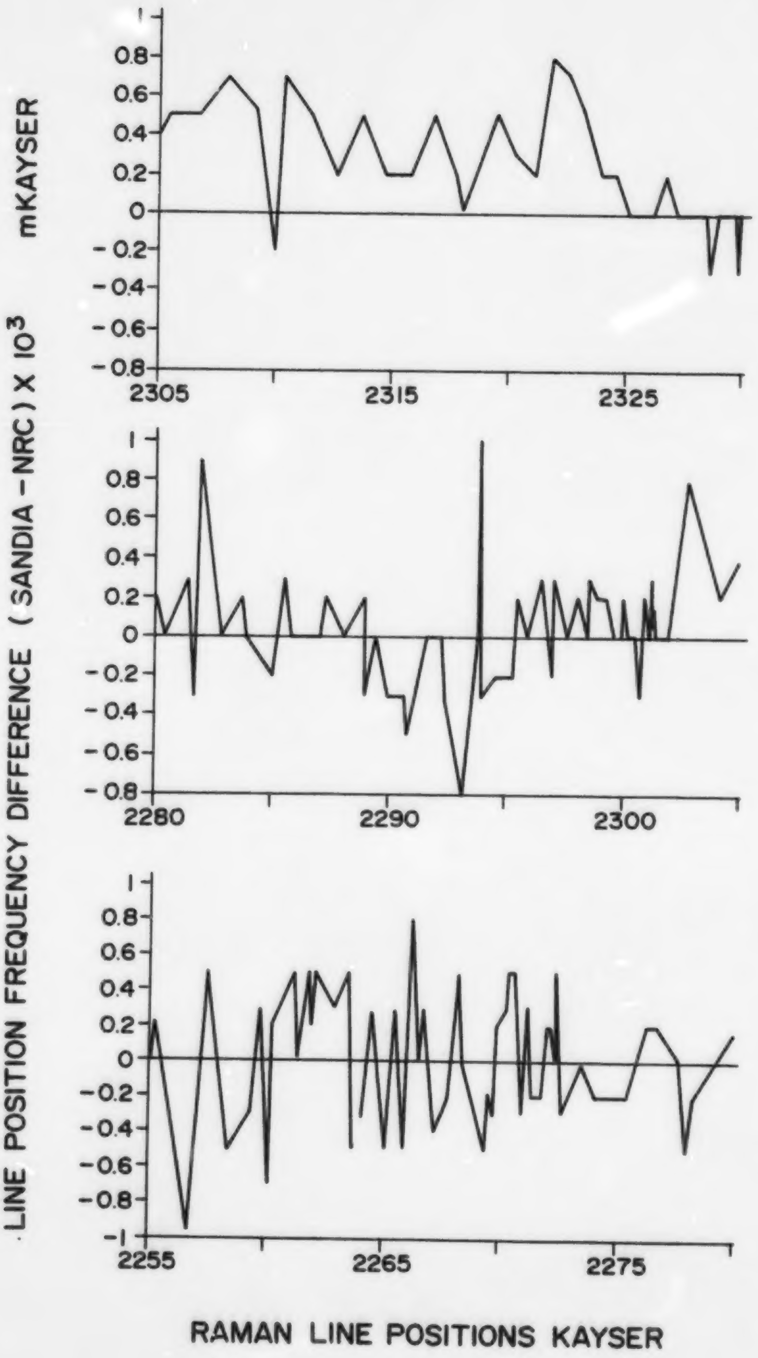

Fig. B3. Comparison of NRC and Sandia codes (isolated line model, 1550 K), with NRC spectrum shifted by +0.0004 cm^{-1}

Fig. B4a. Comparison of NRC and Sandia codes with collisional narrowing and cross-coherence for 1000 K N_2 CARS spectra from 2260 to 2300 cm^{-1}

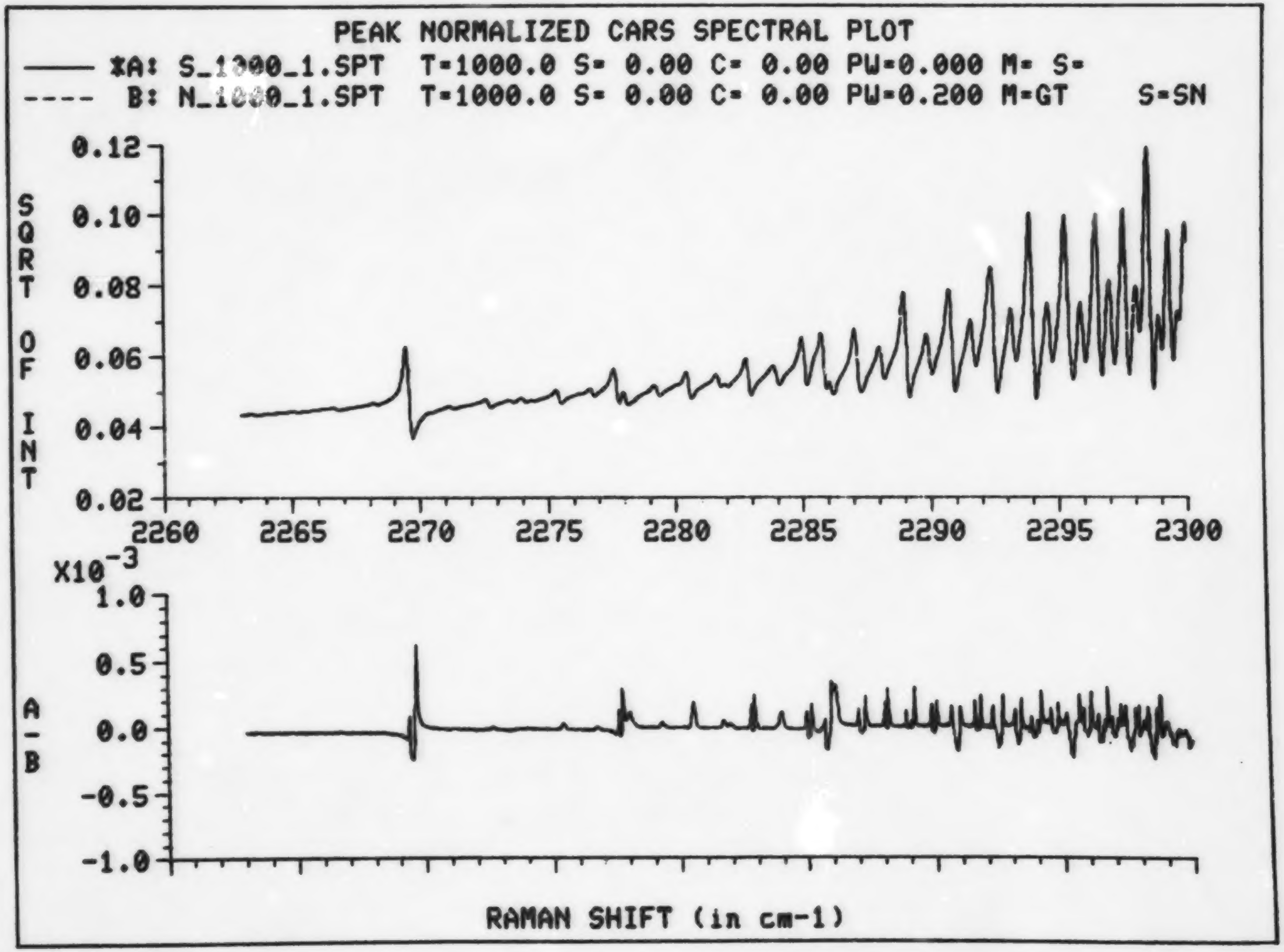

Fig. B4b. Comparison of NRC and Sandia codes with collisional narrowing and cross coherence for 1000 K N_2 CARS spectra from 2300 to 2340 cm^{-1}

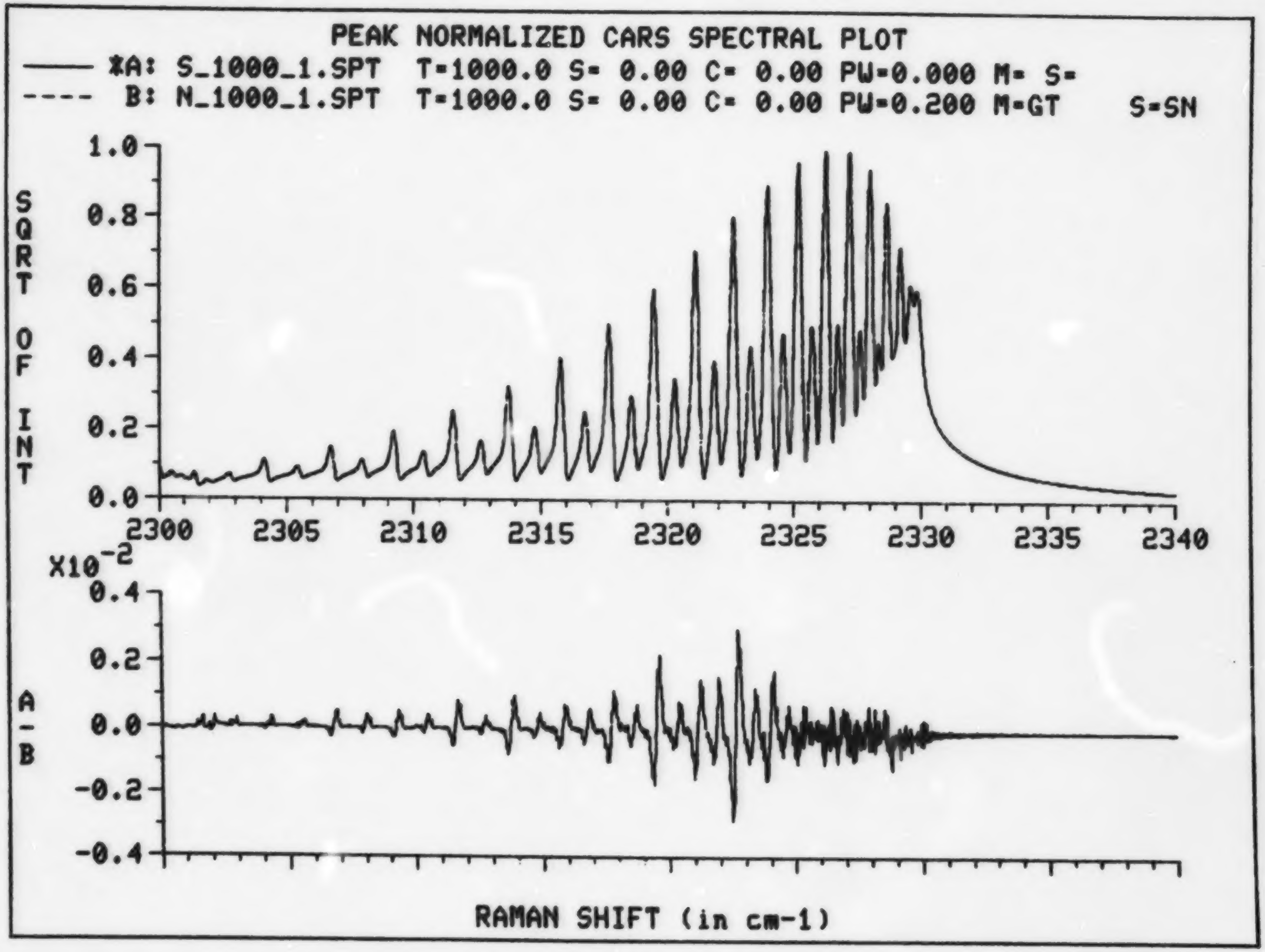

Fig. B5a. Comparison of NRC and Sandia codes with collisional narrowing and cross coherence for 1550 K N_2 CARS spectra from 2260 to 2300 cm^{-1}

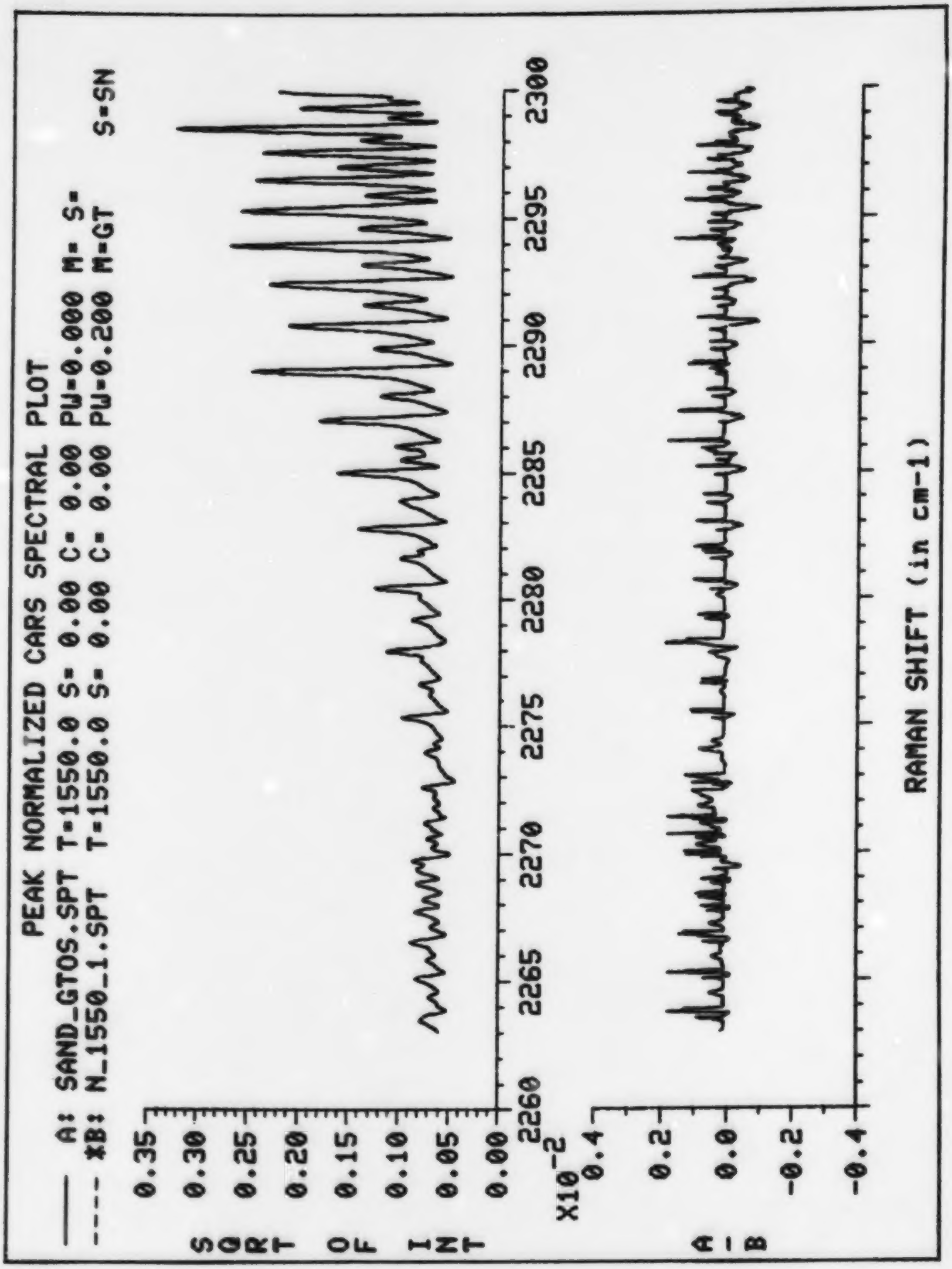

Fig. B5b. Comparison of NRC and Sandia codes with collisional narrowing and cross coherence for 1550 K N_2 CARS spectra from 2300 to 2340 cm^{-1}

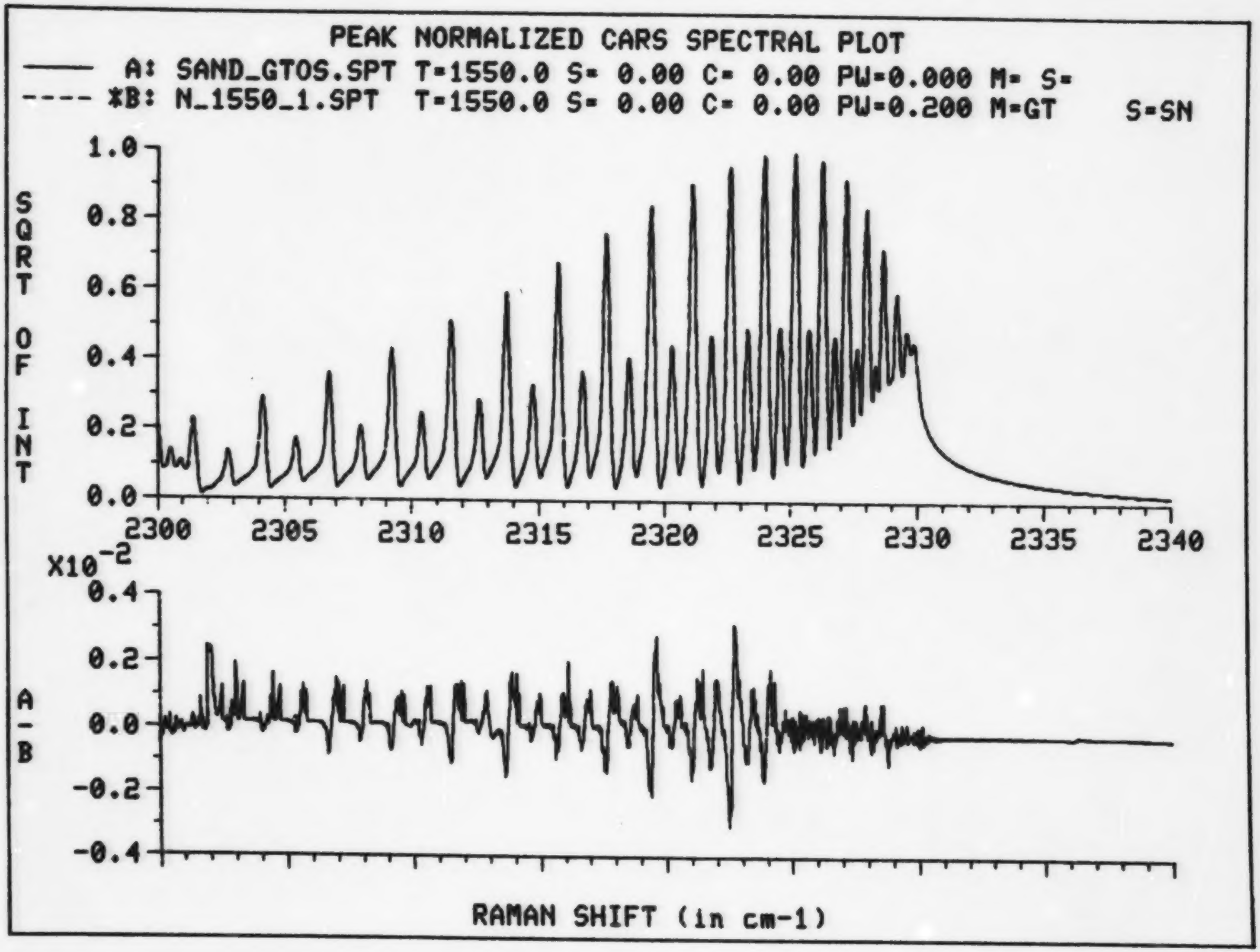

Fig. B6a. Comparison of NRC and Sandia codes with collisional narrowing and cross coherence for 2000 K N_2 CARS spectra from 2260 to 2300 cm^{-1}

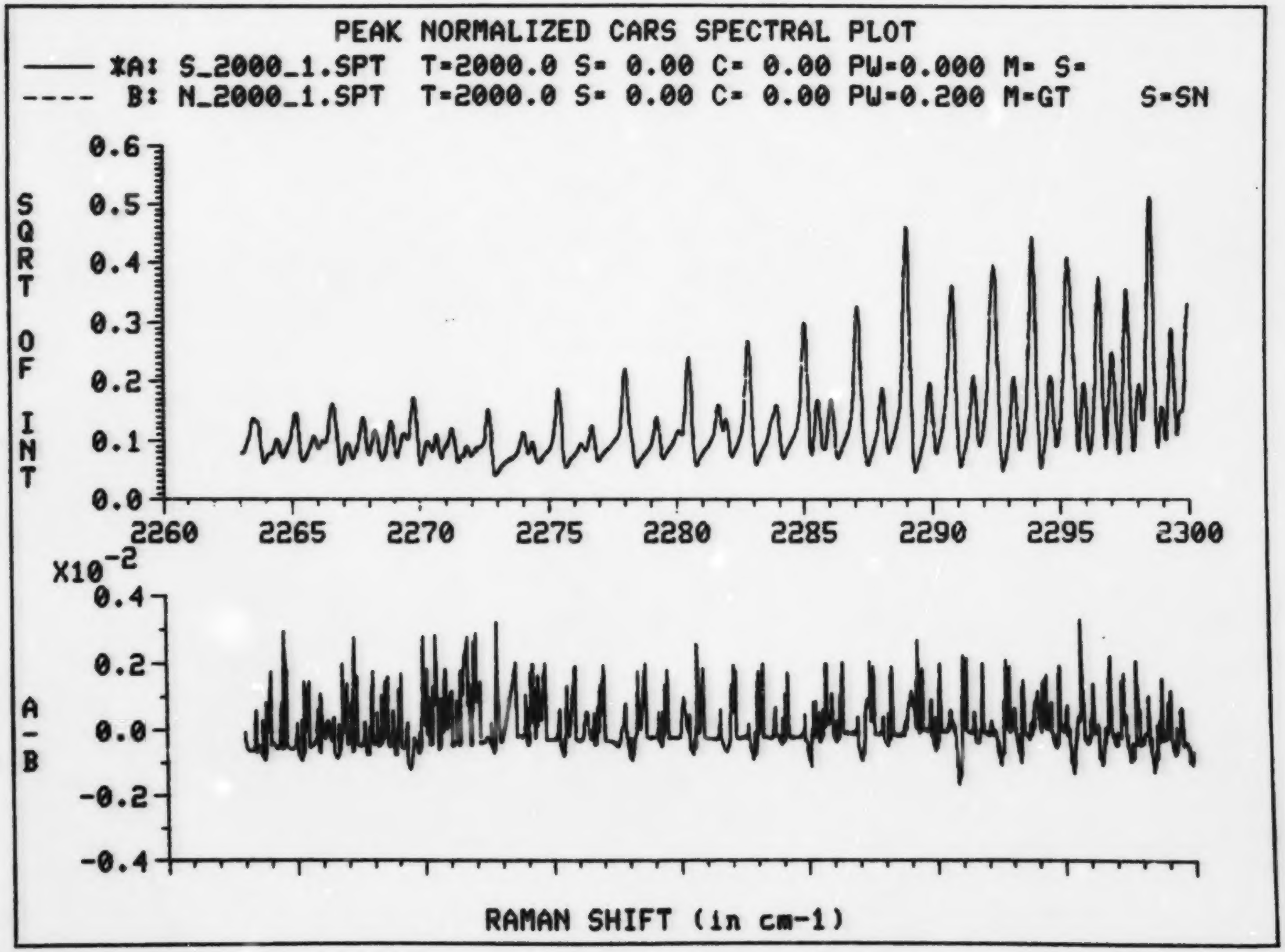

Fig. B6b. Comparison of NRC and Sandia codes with collisional narrowing and cross coherence for 2000 K N_2 CARS spectra from 2300 to 2340 cm^{-1}

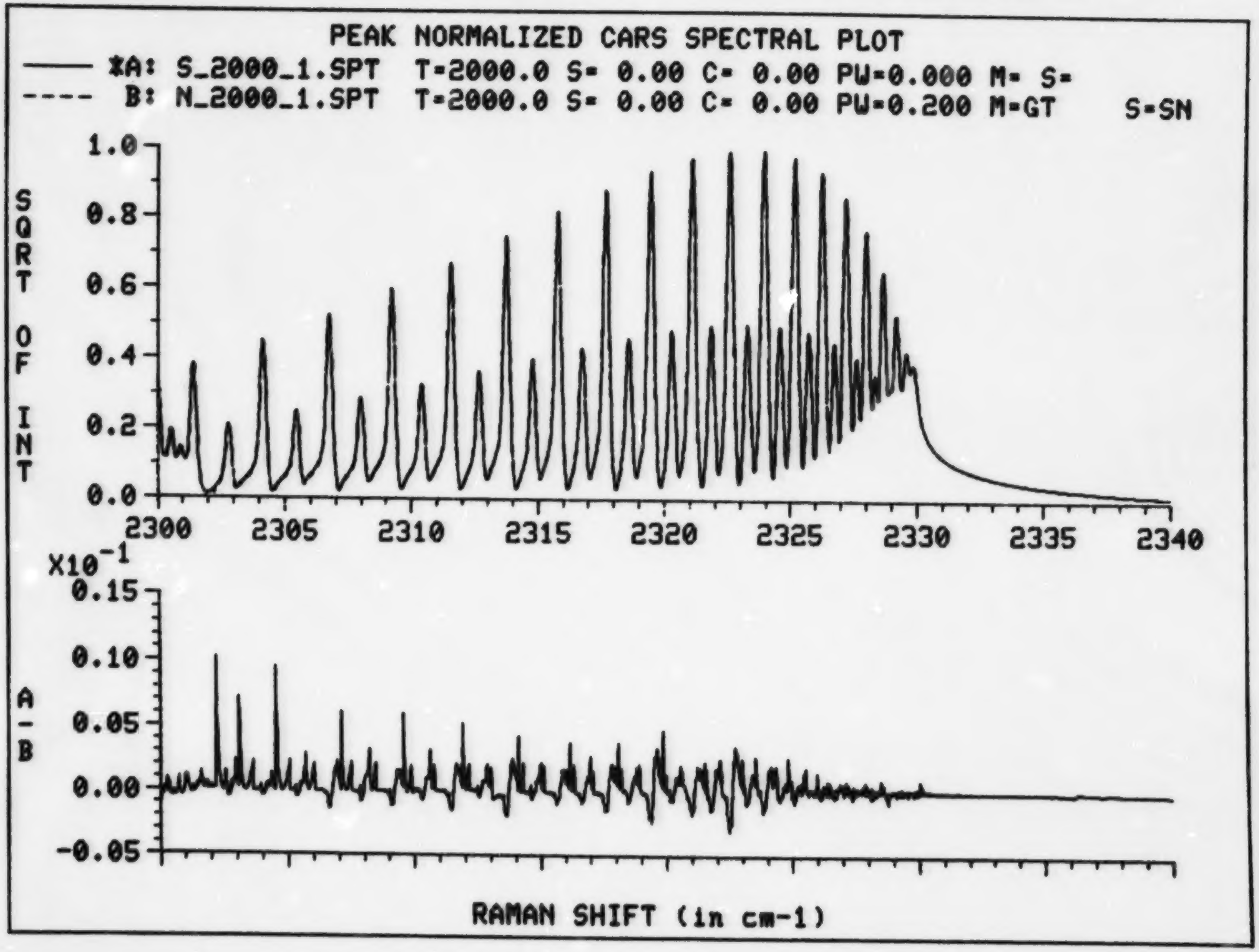

Fig. B7. Comparison of NRC and Sandia codes at the high pressure P = 20 atm and T = 1550 K

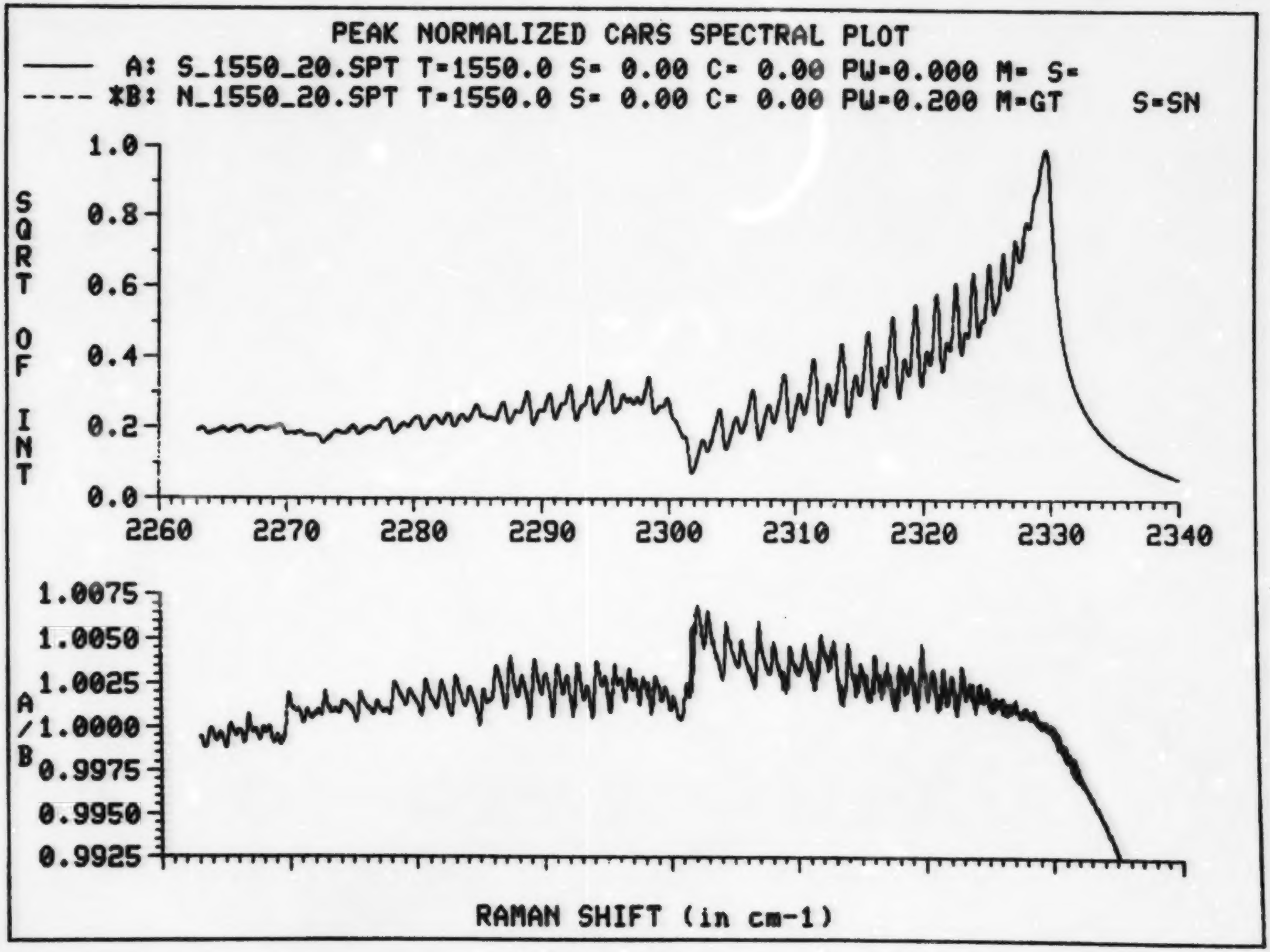

Fig. B8. Comparison of NRC and Sandia codes at the high pressure P = 20 atm and T = 2000 K

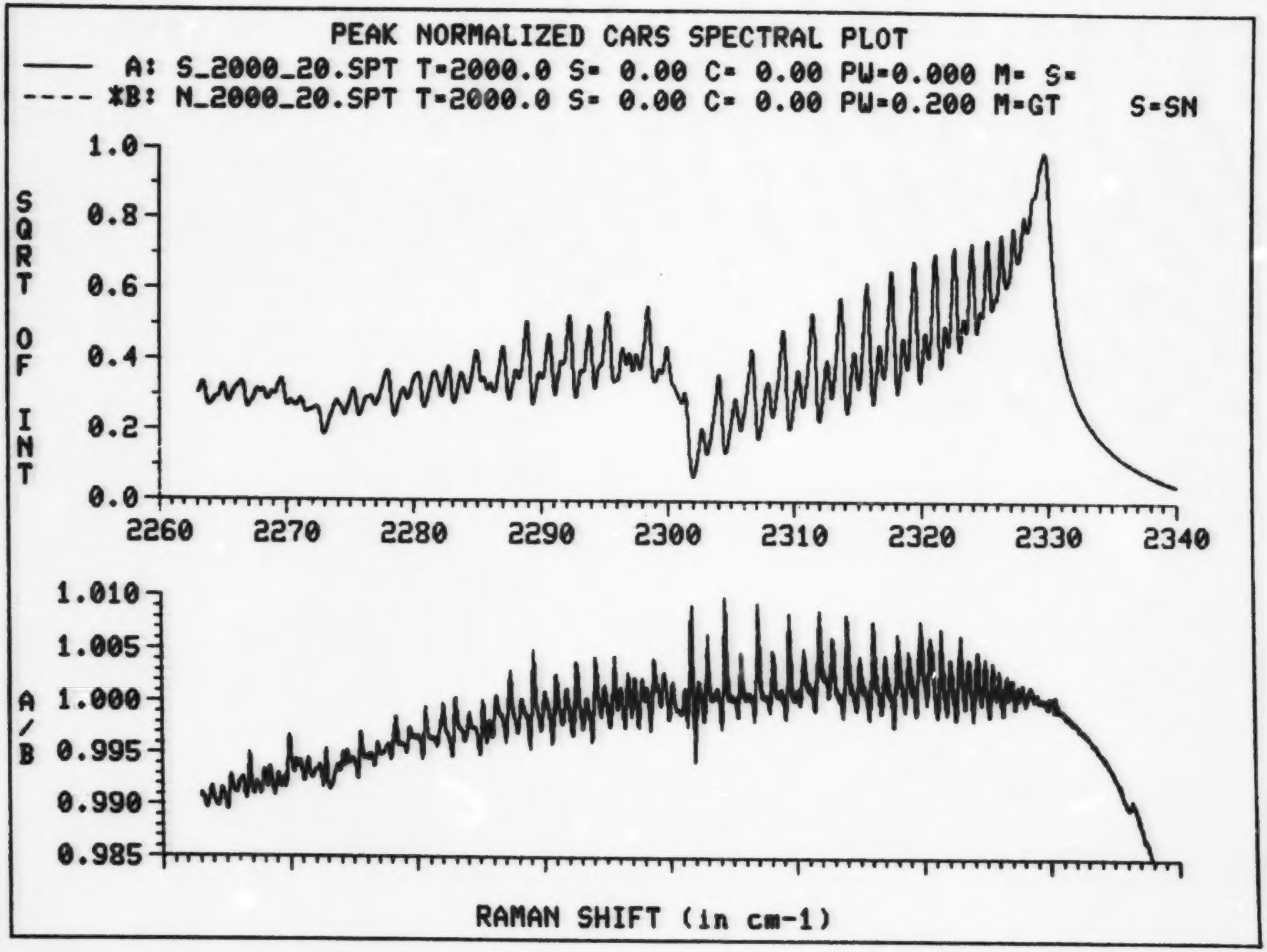

Fig. B9a. Comparison of NRC and Sandia codes with 0.7 cm^{-1} pump width at T = 1550 K; lower plot shows the difference A - B

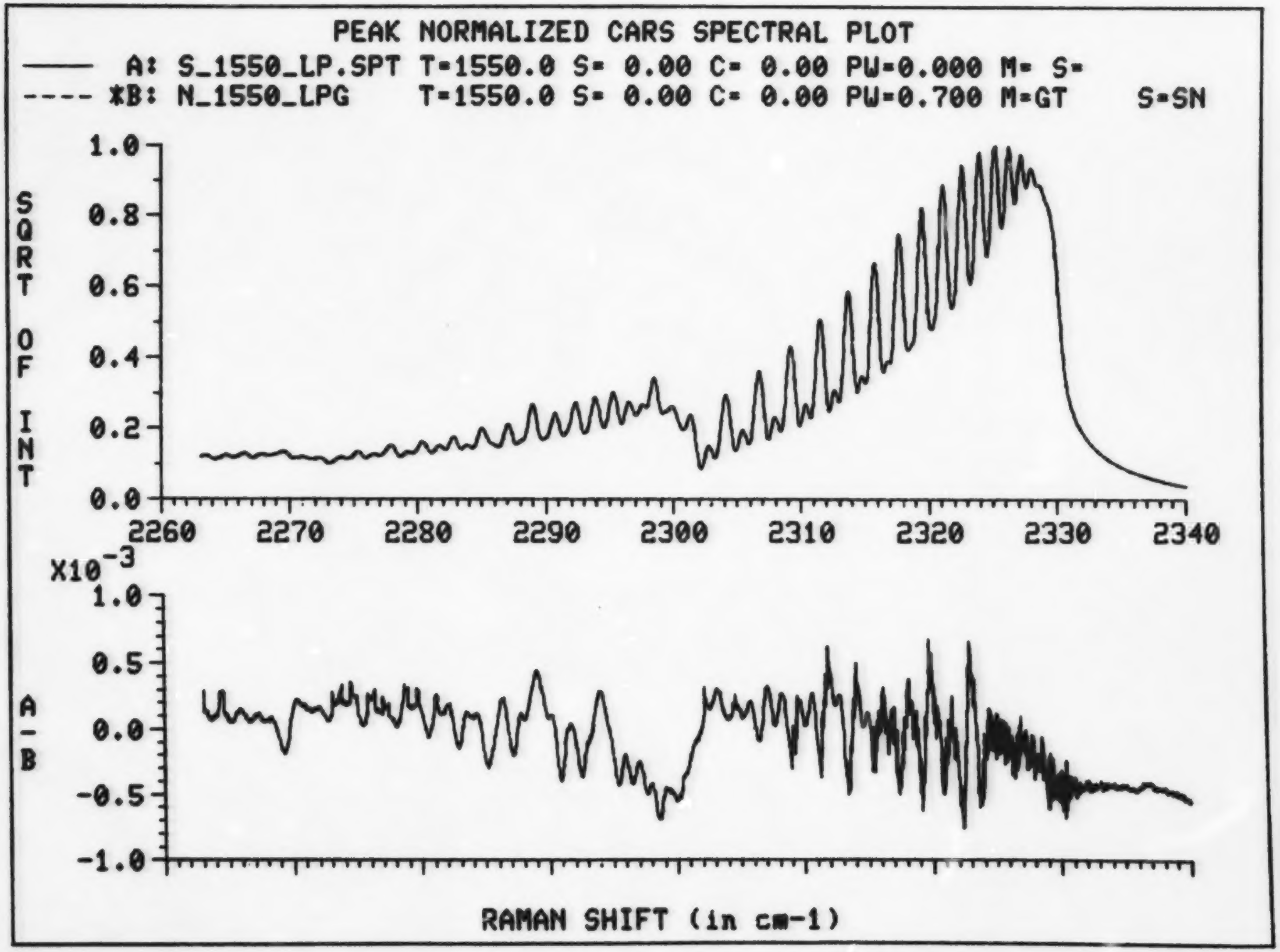

Fig. B9b. Comparison of NRC and Sandia codes with 0.7 cm^{-1} pump width at T = 1550 K; lower plot shows the ratio A/B

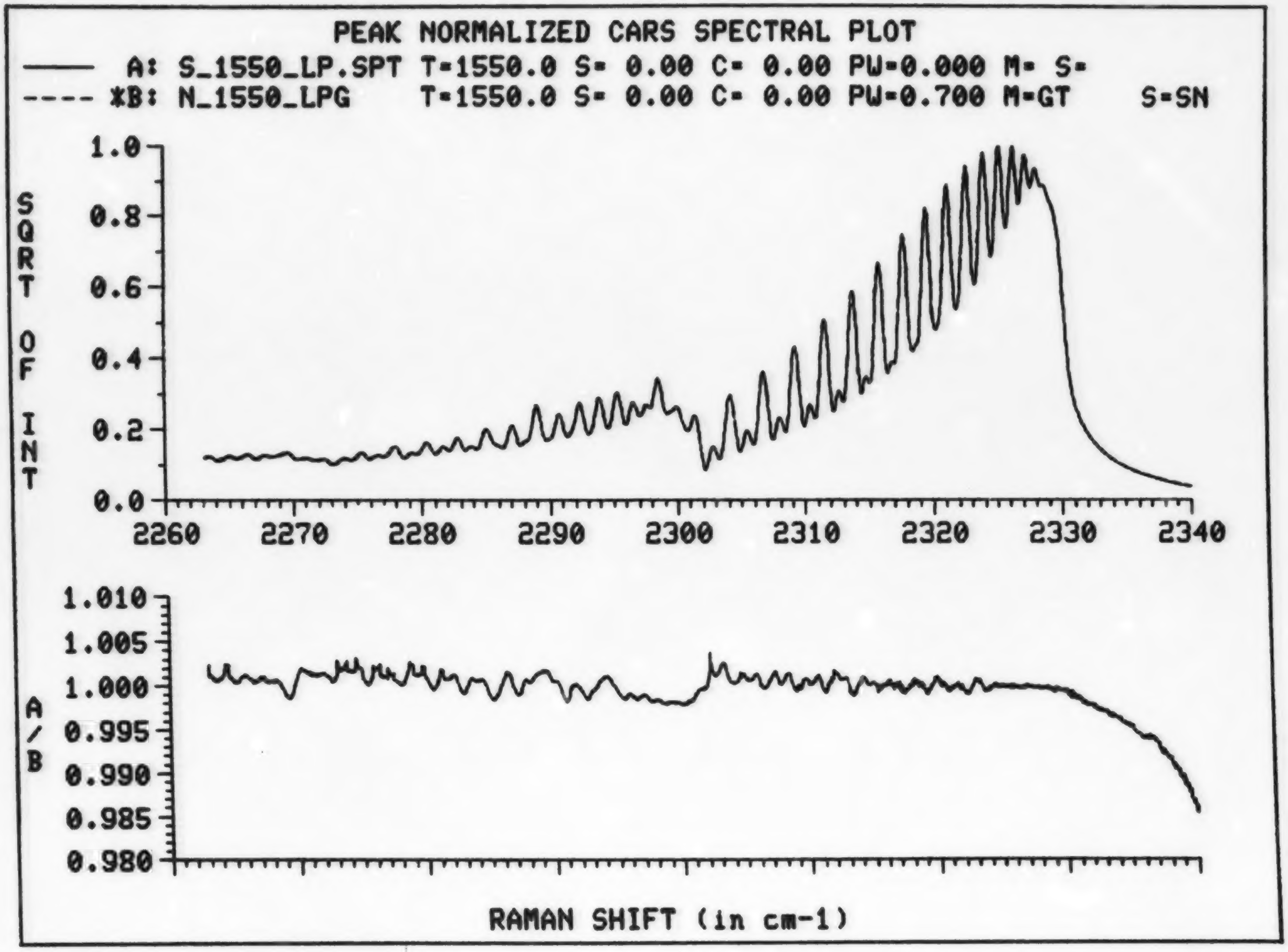

TABLE B-1

Q, O, and S Branch nitrogen branch line positions ordered by wave numbers

VL	VU	JL	JU	SANDIA	NRC	SANDIA-NRC
1	2	5	7	2351.5522	2351.5522	0.0000
0	1	1	3	2349.5974	2349.5974	0.0000
2	3	8	10	2344.8872	2344.8867	0.0005
1	2	3	5	2343.9124	2343.9124	0.0000
0	1	0	2	2341.7439	2341.7439	0.0000
1	2	3	5	2336.2361	2336.2361	0.0000
2	3	6	8	2329.9336	2329.9336	0.0000
0	1	0	0	2329.9106	2329.9106	0.0000
0	1	1	1	2329.8757	2329.8760	-0.0003
0	1	2	2	2329.8064	2329.8064	0.0000
0	1	3	3	2329.7021	2329.7021	0.0000
0	1	4	4	2329.5632	2329.5632	0.0000
0	1	5	5	2329.3896	2329.3896	0.0000
0	1	6	6	2329.1812	2329.1812	0.0000
0	1	7	7	2328.9380	2328.9380	0.0000
0	1	8	8	2328.6599	2328.6602	-0.0003
1	2	2	4	2328.5239	2328.5239	0.0000
0	1	9	9	2328.3474	2328.3474	0.0000
0	1	10	10	2328.0000	2328.0000	0.0000
0	1	11	11	2327.6179	2327.6179	0.0000
0	1	12	12	2327.2009	2327.2009	0.0000
0	1	13	13	2326.7495	2326.7493	0.0002
0	1	14	14	2326.2629	2326.2629	0.0000
0	1	15	15	2325.7417	2325.7417	0.0000
0	1	16	16	2325.1858	2325.1858	0.0000
0	1	17	17	2324.5952	2324.5950	0.0002
0	1	18	18	2323.9697	2323.9695	0.0002
0	1	19	19	2323.3096	2323.3091	0.0005
0	1	20	20	2322.6147	2322.6140	0.0007
0	1	21	21	2321.8848	2321.8840	0.0008
0	1	22	22	2321.1196	2321.1194	0.0002
0	1	23	23	2320.3201	2320.3198	0.0003
0	1	24	24	2319.4861	2319.4856	0.0005
0	1	25	25	2318.6167	2318.6165	0.0002
0	1	2	0	2317.9731	2317.9731	0.0000
0	1	26	26	2317.7126	2317.7124	0.0002
0	1	27	27	2316.7739	2316.7734	0.0005
0	1	28	28	2315.8000	2315.7998	0.0002
0	1	29	29	2314.7915	2314.7913	0.0002
0	1	30	30	2313.7483	2313.7478	0.0005
0	1	31	31	2312.6699	2312.6697	0.0002
0	1	32	32	2311.5569	2311.5564	0.0005
0	1	33	33	2310.4089	2310.4082	0.0007
0	1	3	1	2309.9805	2309.9807	-0.0002
0	1	34	34	2309.2261	2309.2256	0.0005
0	1	35	35	2308.0083	2308.0076	0.0007
0	1	36	36	2306.7556	2306.7551	0.0005

Table B1 (Cont'd)

VL	VU	JL	JU	SANDIA	NRC	SANDIA-NRC
0	1	37	37	2305.4680	2305.4675	0.0005
0	1	38	38	2304.1455	2304.1453	0.0002
0	1	39	39	2302.7886	2302.7878	0.0008
0	1	4	2	2301.9541	2301.9541	0.0000
0	1	40	40	2301.3960	2301.3960	0.0000
1	2	0	0	2301.2634	2301.2632	0.0002
1	2	1	1	2301.2288	2301.2285	0.0003
1	2	2	2	2301.1587	2301.1587	0.0000
1	2	3	3	2301.0544	2301.0542	0.0002
1	2	4	4	2300.9148	2300.9146	0.0002
1	2	5	5	2300.7402	2300.7405	-0.0003
1	2	6	6	2300.5313	2300.5313	0.0000
1	2	7	7	2300.2871	2300.2871	0.0000
1	2	8	8	2300.0085	2300.0083	0.0002
0	1	41	41	2299.9688	2299.9688	0.0000
1	2	9	9	2299.6946	2299.6946	0.0000
1	2	10	10	2299.3459	2299.3457	0.0002
1	2	11	11	2298.9626	2298.9624	0.0002
1	2	12	12	2298.5442	2298.5439	0.0003
0	1	42	42	2298.5068	2298.5068	0.0000
1	2	13	13	2298.0908	2298.0906	0.0002
1	2	14	14	2297.6023	2297.6023	0.0000
1	2	15	15	2297.0796	2297.0793	0.0003
0	1	43	43	2297.0098	2297.0100	-0.0002
1	2	16	16	2296.5215	2296.5212	0.0003
1	2	17	17	2295.9282	2295.9282	0.0000
0	1	44	44	2295.4780	2295.4778	0.0002
1	2	18	18	2295.3003	2295.3005	-0.0002
1	2	19	19	2294.6377	2294.6379	-0.0002
1	2	20	20	2293.9399	2293.9402	-0.0003
0	1	45	45	2293.9121	2293.9111	0.0010
0	1	5	3	2293.8938	2293.8938	0.0000
1	2	21	21	2293.2070	2293.2078	-0.0008
1	2	22	22	2292.4399	2292.4402	-0.0003
0	1	46	46	2292.3101	2292.3101	0.0000
1	2	23	23	2291.6377	2291.6377	0.0000
1	2	24	24	2290.7998	2290.8003	-0.0005
0	1	47	47	2290.6733	2290.6736	-0.0003
1	2	25	25	2289.9277	2289.9280	-0.0003
1	2	2	0	2289.4302	2289.4302	0.0000
1	2	26	26	2289.0205	2289.0208	-0.0003
0	1	48	48	2289.0024	2289.0022	0.0002
1	2	27	27	2288.0781	2288.0781	0.0000
0	1	49	49	2287.2959	2287.2957	0.0002
1	2	28	28	2287.1011	2287.1011	0.0000
1	2	29	29	2286.0889	2286.0889	0.0000
0	1	6	4	2285.8000	2285.8000	0.0000
0	1	50	50	2285.5552	2285.5549	0.0003
1	2	30	30	2285.0415	2285.0417	-0.0002
1	2	31	31	2283.9595	2283.9595	0.0000
0	1	51	51	2283.7793	2283.7791	0.0002
1	2	32	32	2282.8423	2282.8423	0.0000

Table B1 (Cont'd)

VL	VU	JL	JU	SANDIA	NRC	SANDIA-NRC
0	1	52	52	2281.9692	2281.9683	0.0009
1	2	33	33	2281.6899	2281.6902	-0.0003
1	2	3	1	2281.5071	2281.5068	0.0003
1	2	34	34	2280.5029	2280.5029	0.0000
0	1	53	53	2280.1230	2280.1228	0.0002
1	2	35	35	2279.2808	2279.2808	0.0000
0	1	54	54	2278.2422	2278.2424	-0.0002
1	2	36	36	2278.0229	2278.0234	-0.0005
0	1	7	5	2277.6729	2277.6729	0.0000
1	2	37	37	2276.7314	2276.7312	0.0002
0	1	55	55	2276.3276	2276.3274	0.0002
1	2	38	38	2275.4043	2275.4045	-0.0002
0	1	56	56	2274.3770	2274.3772	-0.0002
1	2	39	39	2274.0420	2274.0422	-0.0002
1	2	4	2	2273.5496	2273.5496	0.0000
1	2	40	40	2272.6445	2272.6448	-0.0003
2	3	0	0	2272.5688	2272.5688	0.0000
2	3	1	1	2272.5342	2272.5339	0.0003
2	3	2	2	2272.4644	2272.4639	0.0005
0	1	57	57	2272.3931	2272.3926	0.0005
2	3	3	3	2272.3589	2272.3589	0.0000
2	3	4	4	2272.2192	2272.2190	0.0002
2	3	5	5	2272.0444	2272.0442	0.0002
2	3	6	6	2271.8340	2271.8342	-0.0002
2	3	7	7	2271.5889	2271.5891	-0.0002
2	3	8	8	2271.3091	2271.3093	-0.0002
1	2	41	41	2271.2129	2271.2126	0.0003
2	3	9	9	2270.9941	2270.9944	-0.0003
2	3	10	10	2270.6450	2270.6445	0.0005
0	1	58	58	2270.3735	2270.3730	0.0005
2	3	11	11	2270.2598	2270.2595	0.0003
2	3	12	12	2269.8398	2269.8396	0.0002
1	2	42	42	2269.7451	2269.7454	-0.0003
0	1	8	6	2269.5127	2269.5129	-0.0002
2	3	13	13	2269.3843	2269.3848	-0.0005
2	3	14	14	2268.8945	2268.8948	-0.0003
2	3	15	15	2268.3696	2268.3696	0.0000
0	1	59	59	2268.3193	2268.3191	0.0002
1	2	43	43	2268.2432	2268.2427	0.0005
2	3	16	16	2267.8096	2267.8098	-0.0002
2	3	17	17	2267.2144	2267.2148	-0.0004
1	2	44	44	2266.7061	2266.7058	0.0003
2	3	18	18	2266.5845	2266.5845	0.0000
0	1	60	60	2266.2305	2266.2297	0.0008
2	3	19	19	2265.9189	2265.9194	-0.0005
1	2	5	3	2265.5586	2265.5583	0.0003
2	3	20	20	2265.2192	2265.2192	0.0000
1	2	45	45	2265.1328	2265.1333	-0.0005
2	3	21	21	2264.4844	2264.4841	0.0003
0	1	61	61	2264.1064	2264.1067	-0.0003
2	3	22	22	2263.7134	2263.7139	-0.0005
1	2	46	46	2263.5264	2263.5259	0.0005

Table B1 (Cont'd)

VL	VU	JL	JU	SANDIA	NRC	SANDIA-NRC
2	3	23	23	2262.9087	2262.9084	0.0003
2	3	24	24	2262.0684	2262.0679	0.0005
0	1	62	62	2261.9482	2261.9480	0.0002
1	2	47	47	2261.8838	2261.8833	0.0005
0	1	9	7	2261.3203	2261.3203	0.0000
2	3	25	25	2261.1929	2261.1924	0.0005
2	3	26	26	2260.2822	2260.2820	0.0002
1	2	48	48	2260.2056	2260.2063	-0.0007
0	1	63	63	2259.7549	2259.7546	0.0003
2	3	27	27	2259.3359	2259.3362	-0.0003
1	2	49	49	2258.4941	2258.4946	-0.0005
2	3	28	28	2258.3550	2258.3555	-0.0005
1	2	6	4	2257.5337	2257.5334	0.0003
0	1	64	64	2257.5283	2257.5278	0.0005
2	3	29	29	2257.3394	2257.3396	-0.0002
1	2	50	50	2256.7461	2256.7471	-0.0010
2	3	30	30	2256.2881	2256.2886	-0.0005
0	1	65	65	2255.2656	2255.2654	0.0002
2	3	31	31	2255.2026	2255.2024	0.0002
1	2	51	51	2254.9639	2254.9641	-0.0002
0	1	10	8	2253.0952	2253.0952	0.0000

MEAN= 0.000070

ST. DEV.= 0.00033

Note: VL, VU refer to the vibrational quantum numbers of the lower and upper levels of the Raman transition. Similarly JL, JU refer to the corresponding rotational quantum numbers.

TABLE B2 Fit of SAND Spectrum against a GEN library

Cycle	Temperature	Frequency shift	% SD
0	1800.0	0.000	23.585
2	1550.4	0.004	0.763
1	1549.0	0.001	0.172
4	1549.3	0.000	0.169

APPENDIX C.

TYPICAL INPUT DATA FILE FOR N_2 CARS SPECTRUM

```
$INPUT1
PRESSURE            =  1.0000     ,
MOLAR_CONC          =  .70000000     ,
NON_RESN_SUSCEP     =  10.40000E-18,
START_TEMP          =  1200.0000E+00,
FINISH_TEMP         =  2000.000E+00,
TEMP_STEP           =  50.000E+00
$END
$INPUT2
WE       =   2358.5180    ,
XWE      =    14.2935    ,
YWE      =  -5.9294901E-03,
ZWE      =  -2.4E-04
$END
$INPUT3
BE       =    1.99826    ,
DE       =  5.774E-06,
B1       =  1.73035E-02,
B2       = -3.1536099E-05,
D1       =  1.55E-08
$END
$INPUT4
MODEL =  'GT'     ,
GDIAG =  'ALL'     ,
SCLNG  =  'SN'      ,
H2O_BRD_CORR  = 0.,
FILE_TYPE     ='SPT'
CWRITE        = ''
$END
$INPUT5
PUMP_CENTR_FREQ  =   18797.00    ,
PUMP_WID         =  0.2
$END
$INPUT7
STNUC          =   6.000000    ,    3.000000    ,
CHISQFRQSTP    =  0.00125,
PUMP_CONV_STP  =  0.02 ,
STRT_FREQ      =   21060.00,
FIN_FREQ       =   21140.00
$END
$INPUT9
CONST   =  1.958538E+08
ALPHA   =  1.772E-16,
GAMMA   =  2.066E-16
$END
$INPUT11
FIRST_WN_FIT  = 21070.
LAST_WN_FIT   = 21140.
FIRST_WN_SLIT = 21050.
LAST_WN_SLIT  = 21150.
CONST1        = 1.
CONST2        = 0.
$END
```

APPENDIX D.

TYPICAL RUN OF THE THEORETICAL CARS SPECTRUM GENERATING PROGRAM

```
$RUN GEN.EXE.39

Select a molecular species
Enter N2  or , CO  or , O2
N2
Enter the parameter filename
 (default="N2DATA"):
N2DATA_SANDIA.DAT.80
Enter SPEC_TYPE ; choose PUMP_CONV or CHI_SQRE
PUMP_CONV


Input data are read from the file N2DATA.DAT;80

They are given below :
$INPUT1
PRESSURE        =   1.000000    ,
MOLAR_CONC      =  0.7000000    ,
NON_RESN_SUSCEP =  1.0400000E-17,
START_TEMP      =   1550.000    ,
FINISH_TEMP     =   1550.000    ,
TEMP_STEP       =   50.00000
$END
$INPUT2
WE       =   2358.518    ,
XWE      =   14.29350    ,
YWE      = -5.9294901E-03,
ZWE      = -2.3999999E-04
$END
$INPUT3
BE       =   1.998260    ,
DE       =  5.7739999E-06,
B1       =  1.7303500E-02,
B2       = -3.1536099E-05,
D1       =  1.5500000E-08
$END
$INPUT4
MODEL    = 'GT   ',
GDIAG    = 'ALL  ',
SCLNG    = 'SN ',
TRY_ALPHA_FIT   =  0.0000000E+00,
H2O_BRD_CORR    =  0.0000000E+00,
FILE_TYPE       = 'SPT',
CWRITE  = '                   '
$END
$INPUT5
PUMP_CENTR_FREQ =   18797.00    ,
PUMP_WID        =  0.7000000
$END
```

```
$INPUT7
STNUC  =   6.000000     ,    3.000000     ,
CHISQFRQSTP     =  1.2500000E-03,
PUMP_CONV_STP   =  3.9999999E-02,
STRT_FREQ       =   21060.00     ,
FIN_FREQ        =   21140.00
$END
$INPUT9
CONST   =  1.9585381E+08,
ALPHA   =  1.7719999E-16,
GAMMA   =  2.0660000E-16
$END
$INPUT11
FIRST_WN_FIT    =   21060.00     ,
LAST_WN_FIT     =   21140.00     ,
FIRST_WN_SLIT   =   21050.00     ,
LAST_WN_SLIT    =   21150.00     ,
CONST1   =    1.000000     ,
CONST2  =  0.0000000E+00
$END

PUMP_CONV
$OUTPUT1
NUM_CHISQ_PTS   =        69602,
NUM_PUMP_CONV_PTS        =          2001
$END
```

```
Temperature is    1550.00

Some useful computed variables are :
$OUTPUT2
NUM_DENSY       =  4.7341425E+18,
EFF_NON_RESN_SUSCEP      =  1.8327483E-18,
NUM_VIBR_LVLS   =            3,
NUM_ROTNL_LVLS  =           70
$END
Number of transitions for N2 =   283


Matrix diagonalization entered
Vibrational band centres are:
 0.0000000E+00  -28.64733      -57.34173
The real part of the eigen values are:
 -220.4924       -211.0997       -201.9805       -225.2924       -193.1405
 -215.7622       -184.5769       -206.5053       -176.2902       -197.5271
 -168.2820       -188.8232       -160.5515       -180.3979       -153.0998
 -172.2511       -145.9263       -164.3814       -139.0321       -156.7909
 -132.4163       -149.4781       -126.0806       -142.4448       -120.0225
 -135.6889       -114.2444       -129.2139       -108.7455       -123.0159
 -103.5261       -117.0987       -98.58485       -111.4604       -93.92352
 -101.0212       -106.1012       -89.54066       -96.21958       -85.43662
 -91.69708       -81.61157       -87.45386       -78.06518       -83.48918
 -74.79751       -79.80347       -71.80795       -76.39666       -73.26787
 -69.09724       -70.41786       -66.66456       -64.51025       -57.21500
 -62.63408       -61.03595       -57.42337       -59.71590       -58.67381
 -57.90964       -57.28445       -57.63173       -58.25698       -59.16009
 -60.34119       -67.84605       -61.80024       -63.53736       -65.55262
The imaginary part of the eigenvalues are :
-9.2638107E-03 -1.1207397E-02 -1.2317250E-02 -9.1130389E-03 -1.3103500E-02
-1.0992735E-02 -1.3753978E-02 -1.2127181E-02 -1.4370249E-02 -1.2877830E-02
-1.4983902E-02 -1.3504464E-02 -1.5609620E-02 -1.4077768E-02 -1.6262215E-02
-1.4688404E-02 -1.6943790E-02 -1.5295409E-02 -1.7655702E-02 -1.5941268E-02
-1.8390831E-02 -1.6605537E-02 -1.9148294E-02 -1.7297946E-02 -1.9920316E-02
-1.8025395E-02 -2.0709207E-02 -1.8767854E-02 -2.1501070E-02 -1.9527627E-02
-2.2284605E-02 -2.0316958E-02 -2.3056453E-02 -2.1092653E-02 -2.3806298E-02
-2.2671938E-02 -2.1886691E-02 -2.4518725E-02 -2.3431582E-02 -2.5185654E-02
-2.4162222E-02 -2.5799965E-02 -2.4862155E-02 -2.6358033E-02 -2.5502989E-02
-2.6849283E-02 -2.6086997E-02 -2.7282676E-02 -2.6609572E-02 -2.7070833E-02
-2.7667297E-02 -2.7478509E-02 -2.8019615E-02 -2.8363898E-02 -3.7198935E-02
-2.8746266E-02 -2.9213207E-02 -3.3590138E-02 -2.9838450E-02 -3.0688053E-02
-3.1882603E-02 -3.4806959E-02 -3.2653943E-02 -3.1231355E-02 -3.0228302E-02
-2.9500358E-02 -2.7844949E-02 -2.8967569E-02 -2.8547844E-02 -2.8197356E-02
Inverting the eigen-vector matrix...
Cpu time for matrix manipulation is       7.73 min
Matrix diagonalization entered
The real part of the eigen values are:
 -278.3809       -268.9531       -283.1985       -259.8028       -250.9293
 -273.6313       -242.3335       -264.3430       -234.0175       -255.3305
 -225.9799       -246.5972       -218.2211       -210.7421       -238.1409
 -229.9646       -203.5423       -222.0658       -196.6236       -214.4469
 -189.9844       -207.1079       -183.6248       -200.0472       -177.5457
 -193.2697       -171.7466       -186.7699       -166.2272       -180.5509
 -160.9893       -174.6112       -156.0304       -168.9519       -151.3515
 -158.4745       -163.5737       -146.9527       -153.6559       -142.8341
 -149.1172       -138.9949       -144.8586       -135.4356       -140.8798
 -132.1559       -137.1802       -133.7609       -129.1558       -126.4349
 -130.6209       -123.9936       -127.7604       -125.1796       -121.8314
 -114.5096       -114.7188       -115.2068       -114.5793       -115.9738
 -117.0197       -119.9484       -118.3445       -114.9279       -115.5555
 -116.4618       -117.6472       -119.1116       -122.8776       -120.8550
The imaginary part of the eigenvalues are :
-9.2718014E-03 -1.1199918E-02 -9.1119474E-03 -1.2314761E-02 -1.3103248E-02
-1.1017313E-02 -1.3759395E-02 -1.2111666E-02 -1.4371121E-02 -1.2846255E-02
-1.4982312E-02 -1.3506879E-02 -1.5606184E-02 -1.6256377E-02 -1.4095505E-02
-1.4663133E-02 -1.6941309E-02 -1.5308498E-02 -1.7655307E-02 -1.5928417E-02
-1.8389186E-02 -1.6606268E-02 -1.9146880E-02 -1.7298300E-02 -1.9922234E-02
-1.8019555E-02 -2.0708816E-02 -1.8763835E-02 -2.1496993E-02 -1.9533422E-02
-2.2283111E-02 -2.0318273E-02 -2.3056384E-02 -2.1103797E-02 -2.3800489E-02
-2.2673219E-02 -2.1894731E-02 -2.4519196E-02 -2.3428593E-02 -2.5183523E-02
-2.4155157E-02 -2.5799032E-02 -2.4849225E-02 -2.6355825E-02 -2.5487568E-02
-2.6854042E-02 -2.6094602E-02 -2.6611017E-02 -2.7281947E-02 -2.7665341E-02
-2.7072385E-02 -2.8019683E-02 -2.7484206E-02 -2.7844202E-02 -2.8365854E-02
-3.7198994E-02 -3.3590373E-02 -3.1878792E-02 -3.4809429E-02 -3.0686209E-02
```

```
-2.9833812E-02 -2.8744940E-02 -2.9210761E-02 -3.2657191E-02 -3.1229408E-02
-3.0218592E-02 -2.9513264E-02 -2.8960602E-02 -2.8185468E-02 -2.8553147E-02
Inverting the eigen-vector matrix...
Cpu time for matrix manipulation is       7.68 min
Matrix diagonalization entered
The real part of the eigen values are:
 -336.3615      -326.8984      -317.7160      -341.1965      -308.8112
 -331.5963      -300.1842      -322.2748      -291.8379      -313.2282
 -283.7711      -304.4625      -275.9849      -295.9759      -268.4785
 -287.7693      -261.2542      -279.8433      -254.3092      -272.1961
 -247.6457      -264.8316      -241.2636      -257.7464      -235.1625
 -250.9418      -229.3425      -244.4189      -223.8035      -238.1780
 -218.5455      -232.2172      -213.5691      -226.5379      -208.8734
 -216.0220      -221.1398      -204.4590      -211.1858      -200.3251
 -206.6313      -196.4723      -202.3568      -192.9003      -198.3636
 -189.6087      -194.6513      -186.5976      -191.2193      -183.8670
 -188.0682      -185.1973      -181.4166      -182.6068      -179.2467
 -171.8985      -177.3569      -175.7472      -172.1083      -171.9686
 -172.5981      -174.4176      -173.3678      -172.3183      -172.9481
 -173.8578      -175.0474      -180.2968      -176.5171      -178.2668
The imaginary part of the eigenvalues are :
-9.2673786E-03 -1.1192649E-02 -1.2320844E-02 -9.1277082E-03 -1.3106603E-02
-1.1012309E-02 -1.3754674E-02 -1.2114685E-02 -1.4368398E-02 -1.2881131E-02
-1.4975731E-02 -1.3500374E-02 -1.5611266E-02 -1.4096287E-02 -1.6266542E-02
-1.4652093E-02 -1.6943851E-02 -1.5292239E-02 -1.7657775E-02 -1.5941381E-02
-1.8395752E-02 -1.6601693E-02 -1.9152885E-02 -1.7305847E-02 -1.9924480E-02
-1.8019101E-02 -2.0715071E-02 -1.8756423E-02 -2.1500902E-02 -1.9528616E-02
-2.2284172E-02 -2.0320548E-02 -2.3056719E-02 -2.1098807E-02 -2.3805302E-02
-2.2683419E-02 -2.1866446E-02 -2.4513206E-02 -2.3437161E-02 -2.5188437E-02
-2.4160434E-02 -2.5806846E-02 -2.4855668E-02 -2.6352992E-02 -2.5497010E-02
-2.6846312E-02 -2.6080467E-02 -2.7282584E-02 -2.6610395E-02 -2.7667847E-02
-2.7072020E-02 -2.7481411E-02 -2.8020373E-02 -2.7840741E-02 -2.8365236E-02
-3.7198953E-02 -2.8743818E-02 -2.9217031E-02 -3.3591341E-02 -3.4809027E-02
-3.1883776E-02 -2.9832589E-02 -3.0689541E-02 -3.2656010E-02 -3.1236667E-02
-3.0239454E-02 -2.9509973E-02 -2.8201804E-02 -2.8976519E-02 -2.8537573E-02
Inverting the eigen-vector matrix...
Cpu time for matrix manipulation is       7.68 min

Transitions included in the calculation are:

TYPE  VL VU JL JU    FREQ      RMN_WID   POP(V1,J1)  POP(V2,J2)   PEAKAMP

0      0  1  2  0  2317.9731   0.0336  0.1077E-01  0.2484E-03  0.1180E-17
0      0  1  3  1  2309.9807   0.0327  0.7456E-02  0.3713E-03  0.1055E-17
0      0  1  4  2  2301.9541   0.0319  0.1889E-01  0.1229E-02  0.3006E-17
0      0  1  5  3  2293.8938   0.0312  0.1133E-01  0.8507E-03  0.1939E-17
0      0  1  6  4  2285.8000   0.0307  0.2620E-01  0.2156E-02  0.4721E-17
0      0  1  7  5  2277.6729   0.0302  0.1473E-01  0.1293E-02  0.2762E-17
0      0  1  8  6  2269.5129   0.0298  0.3242E-01  0.2991E-02  0.6274E-17
0      0  1  9  7  2261.3203   0.0295  0.1752E-01  0.1682E-02  0.3482E-17
0      0  1 10  8  2253.0952   0.0292  0.3733E-01  0.3702E-02  0.7584E-17
0      1  2  2  0  2289.4302   0.0336  0.1229E-02  0.2910E-04  0.2690E-18
0      1  2  3  1  2281.5068   0.0327  0.8507E-03  0.4349E-04  0.2404E-18
0      1  2  4  2  2273.5496   0.0319  0.2156E-02  0.1439E-03  0.6847E-18
```

O	1	2	5	3	2265.5583	0.0312	0.1293E-02	0.9966E-04	0.4417E-18
O	1	2	6	4	2257.5334	0.0307	0.2991E-02	0.2526E-03	0.1075E-17
Q	0	1	0	0	2329.9106	0.0372	0.2178E-02	0.2484E-03	0.8033E-17
Q	0	1	1	1	2329.8760	0.0348	0.3255E-02	0.3713E-03	0.1345E-16
Q	0	1	2	2	2329.8064	0.0336	0.1077E-01	0.1229E-02	0.4550E-16
Q	0	1	3	3	2329.7021	0.0327	0.7456E-02	0.8507E-03	0.3233E-16
Q	0	1	4	4	2329.5632	0.0319	0.1889E-01	0.2156E-02	0.8383E-16
Q	0	1	5	5	2329.3896	0.0312	0.1133E-01	0.1293E-02	0.5131E-16
Q	0	1	6	6	2329.1812	0.0307	0.2620E-01	0.2991E-02	0.1207E-15
Q	0	1	7	7	2328.9380	0.0302	0.1473E-01	0.1682E-02	0.6888E-16
Q	0	1	8	8	2328.6602	0.0298	0.3242E-01	0.3702E-02	0.1536E-15
Q	0	1	9	9	2328.3474	0.0295	0.1752E-01	0.2002E-02	0.8393E-16
Q	0	1	10	10	2328.0000	0.0292	0.3733E-01	0.4266E-02	0.1805E-15
Q	0	1	11	11	2327.6179	0.0290	0.1963E-01	0.2244E-02	0.9573E-16
Q	0	1	12	12	2327.2009	0.0287	0.4083E-01	0.4669E-02	0.2006E-15
Q	0	1	13	13	2326.7493	0.0285	0.2101E-01	0.2404E-02	0.1039E-15
Q	0	1	14	14	2326.2629	0.0284	0.4287E-01	0.4907E-02	0.2134E-15
Q	0	1	15	15	2325.7417	0.0282	0.2168E-01	0.2483E-02	0.1085E-15
Q	0	1	16	16	2325.1858	0.0280	0.4351E-01	0.4986E-02	0.2191E-15
Q	0	1	17	17	2324.5950	0.0278	0.2167E-01	0.2485E-02	0.1098E-15
Q	0	1	18	18	2323.9695	0.0277	0.4288E-01	0.4919E-02	0.2186E-15
Q	0	1	19	19	2323.3091	0.0275	0.2107E-01	0.2419E-02	0.1081E-15
Q	0	1	20	20	2322.6140	0.0273	0.4116E-01	0.4727E-02	0.2127E-15
Q	0	1	21	21	2321.8840	0.0271	0.1998E-01	0.2296E-02	0.1040E-15
Q	0	1	22	22	2321.1194	0.0268	0.3856E-01	0.4434E-02	0.2023E-15
Q	0	1	23	23	2320.3198	0.0266	0.1850E-01	0.2129E-02	0.9793E-16
Q	0	1	24	24	2319.4856	0.0264	0.3532E-01	0.4068E-02	0.1887E-15
Q	0	1	25	25	2318.6165	0.0261	0.1676E-01	0.1932E-02	0.9046E-16
Q	0	1	26	26	2317.7124	0.0258	0.3166E-01	0.3653E-02	0.1727E-15
Q	0	1	27	27	2316.7734	0.0255	0.1488E-01	0.1718E-02	0.8207E-16
Q	0	1	28	28	2315.7998	0.0252	0.2782E-01	0.3215E-02	0.1553E-15
Q	0	1	29	29	2314.7913	0.0249	0.1294E-01	0.1497E-02	0.7319E-16
Q	0	1	30	30	2313.7478	0.0245	0.2397E-01	0.2776E-02	0.1374E-15
Q	0	1	31	31	2312.6697	0.0242	0.1105E-01	0.1280E-02	0.6420E-16
Q	0	1	32	32	2311.5564	0.0238	0.2027E-01	0.2352E-02	0.1195E-15
Q	0	1	33	33	2310.4082	0.0234	0.9254E-02	0.1075E-02	0.5542E-16
Q	0	1	34	34	2309.2256	0.0231	0.1683E-01	0.1957E-02	0.1024E-15
Q	0	1	35	35	2308.0076	0.0227	0.7614E-02	0.8864E-03	0.4709E-16
Q	0	1	36	36	2306.7551	0.0223	0.1372E-01	0.1599E-02	0.8629E-16
Q	0	1	37	37	2305.4675	0.0219	0.6156E-02	0.7183E-03	0.3938E-16
Q	0	1	38	38	2304.1453	0.0215	0.1100E-01	0.1285E-02	0.7162E-16
Q	0	1	39	39	2302.7878	0.0211	0.4891E-02	0.5722E-03	0.3243E-16
Q	0	1	40	40	2301.3960	0.0207	0.8665E-02	0.1015E-02	0.5852E-16
Q	0	1	41	41	2299.9688	0.0203	0.3821E-02	0.4482E-03	0.2629E-16
Q	0	1	42	42	2298.5068	0.0199	0.6713E-02	0.7884E-03	0.4707E-16
Q	0	1	43	43	2297.0100	0.0195	0.2936E-02	0.3453E-03	0.2099E-16
Q	0	1	44	44	2295.4778	0.0191	0.5115E-02	0.6025E-03	0.3728E-16
Q	0	1	45	45	2293.9111	0.0188	0.2219E-02	0.2617E-03	0.1649E-16
Q	0	1	46	46	2292.3101	0.0184	0.3835E-02	0.4530E-03	0.2907E-16
Q	0	1	47	47	2290.6736	0.0180	0.1650E-02	0.1952E-03	0.1276E-16
Q	0	1	48	48	2289.0022	0.0177	0.2830E-02	0.3353E-03	0.2231E-16
Q	0	1	49	49	2287.2957	0.0173	0.1208E-02	0.1434E-03	0.9715E-17
Q	0	1	50	50	2285.5549	0.0169	0.2055E-02	0.2442E-03	0.1686E-16
Q	0	1	51	51	2283.7791	0.0166	0.8703E-03	0.1036E-03	0.7283E-17

Q	0	1	52	52	2281.9683	0.0163	0.1469E-02	0.1752E-03	0.1254E-16
Q	0	1	53	53	2280.1228	0.0159	0.6173E-03	0.7375E-04	0.5375E-17
Q	0	1	54	54	2278.2424	0.0156	0.1034E-02	0.1237E-03	0.9183E-17
Q	0	1	55	55	2276.3274	0.0153	0.4312E-03	0.5170E-04	0.3905E-17
Q	0	1	56	56	2274.3772	0.0150	0.7166E-03	0.8607E-04	0.6623E-17
Q	0	1	57	57	2272.3926	0.0147	0.2966E-03	0.3569E-04	0.2794E-17
Q	0	1	58	58	2270.3730	0.0144	0.4892E-03	0.5898E-04	0.4707E-17
Q	0	1	59	59	2268.3191	0.0141	0.2010E-03	0.2427E-04	0.1970E-17
Q	0	1	60	60	2266.2297	0.0138	0.3290E-03	0.3981E-04	0.3301E-17
Q	0	1	61	61	2264.1067	0.0135	0.1341E-03	0.1626E-04	0.1371E-17
Q	0	1	62	62	2261.9480	0.0131	0.2179E-03	0.2648E-04	0.2293E-17
Q	0	1	63	63	2259.7546	0.0129	0.8821E-04	0.1074E-04	0.9441E-18
Q	0	1	64	64	2257.5278	0.0123	0.1423E-03	0.1736E-04	0.1589E-17
Q	0	1	65	65	2255.2654	0.0121	0.5716E-04	0.6988E-05	0.6490E-18
Q	0	1	66	66	2252.9683	0.0112	0.9152E-04	0.1121E-04	0.1122E-17
Q	0	1	67	67	2250.6370	0.0110	0.3650E-04	0.4482E-05	0.4547E-18
Q	0	1	68	68	2248.2720	0.0093	0.5802E-04	0.7139E-05	0.8585E-18
Q	0	1	69	69	2245.8718	0.0091	0.2297E-04	0.2833E-05	0.3454E-18
Q	1	2	0	0	2301.2632	0.0372	0.2484E-03	0.2910E-04	0.1826E-17
Q	1	2	1	1	2301.2285	0.0348	0.3713E-03	0.4349E-04	0.3058E-17
Q	1	2	2	2	2301.1587	0.0336	0.1229E-02	0.1439E-03	0.1035E-16
Q	1	2	3	3	2301.0542	0.0327	0.8507E-03	0.9966E-04	0.7352E-17
Q	1	2	4	4	2300.9146	0.0319	0.2156E-02	0.2526E-03	0.1907E-16
Q	1	2	5	5	2300.7405	0.0312	0.1293E-02	0.1516E-03	0.1167E-16
Q	1	2	6	6	2300.5313	0.0307	0.2991E-02	0.3506E-03	0.2746E-16
Q	1	2	7	7	2300.2871	0.0302	0.1682E-02	0.1972E-03	0.1568E-16
Q	1	2	8	8	2300.0083	0.0298	0.3702E-02	0.4342E-03	0.3495E-16
Q	1	2	9	9	2299.6946	0.0295	0.2002E-02	0.2348E-03	0.1911E-16
Q	1	2	10	10	2299.3457	0.0292	0.4266E-02	0.5006E-03	0.4112E-16
Q	1	2	11	11	2298.9624	0.0290	0.2244E-02	0.2634E-03	0.2181E-16
Q	1	2	12	12	2298.5439	0.0287	0.4669E-02	0.5483E-03	0.4572E-16
Q	1	2	13	13	2298.0906	0.0285	0.2404E-02	0.2824E-03	0.2370E-16
Q	1	2	14	14	2297.6023	0.0284	0.4907E-02	0.5767E-03	0.4867E-16
Q	1	2	15	15	2297.0793	0.0282	0.2483E-02	0.2919E-03	0.2477E-16
Q	1	2	16	16	2296.5212	0.0280	0.4986E-02	0.5865E-03	0.5004E-16
Q	1	2	17	17	2295.9282	0.0278	0.2485E-02	0.2925E-03	0.2509E-16
Q	1	2	18	18	2295.3005	0.0277	0.4919E-02	0.5794E-03	0.4998E-16
Q	1	2	19	19	2294.6379	0.0275	0.2419E-02	0.2850E-03	0.2473E-16
Q	1	2	20	20	2293.9402	0.0273	0.4727E-02	0.5575E-03	0.4868E-16
Q	1	2	21	21	2293.2078	0.0271	0.2296E-02	0.2709E-03	0.2382E-16
Q	1	2	22	22	2292.4402	0.0268	0.4434E-02	0.5237E-03	0.4638E-16
Q	1	2	23	23	2291.6377	0.0266	0.2129E-02	0.2517E-03	0.2246E-16
Q	1	2	24	24	2290.8003	0.0264	0.4068E-02	0.4811E-03	0.4331E-16
Q	1	2	25	25	2289.9280	0.0261	0.1932E-02	0.2287E-03	0.2078E-16
Q	1	2	26	26	2289.0208	0.0258	0.3653E-02	0.4328E-03	0.3971E-16
Q	1	2	27	27	2288.0781	0.0255	0.1718E-02	0.2037E-03	0.1889E-16
Q	1	2	28	28	2287.1011	0.0252	0.3215E-02	0.3816E-03	0.3578E-16
Q	1	2	29	29	2286.0889	0.0249	0.1497E-02	0.1779E-03	0.1687E-16
Q	1	2	30	30	2285.0417	0.0245	0.2776E-02	0.3300E-03	0.3170E-16
Q	1	2	31	31	2283.9595	0.0242	0.1280E-02	0.1524E-03	0.1483E-16
Q	1	2	32	32	2282.8423	0.0238	0.2352E-02	0.2802E-03	0.2764E-16
Q	1	2	33	33	2281.6902	0.0234	0.1075E-02	0.1282E-03	0.1283E-16
Q	1	2	34	34	2280.5029	0.0231	0.1957E-02	0.2336E-03	0.2372E-16
Q	1	2	35	35	2279.2808	0.0227	0.8864E-03	0.1060E-03	0.1092E-16

Q	1	2	36	36	2278.0234	0.0223	0.1599E-02	0.1914E-03	0.2004E-16
Q	1	2	37	37	2276.7312	0.0219	0.7183E-03	0.8607E-04	0.9159E-17
Q	1	2	38	38	2275.4045	0.0215	0.1285E-02	0.1542E-03	0.1667E-16
Q	1	2	39	39	2274.0422	0.0211	0.5722E-03	0.6873E-04	0.7561E-17
Q	1	2	40	40	2272.6448	0.0207	0.1015E-02	0.1221E-03	0.1366E-16
Q	1	2	41	41	2271.2126	0.0203	0.4482E-03	0.5398E-04	0.6146E-17
Q	1	2	42	42	2269.7454	0.0199	0.7884E-03	0.9509E-04	0.1102E-16
Q	1	2	43	43	2268.2427	0.0195	0.3453E-03	0.4170E-04	0.4919E-17
Q	1	2	44	44	2266.7058	0.0191	0.6025E-03	0.7287E-04	0.8750E-17
Q	1	2	45	45	2265.1333	0.0188	0.2617E-03	0.3170E-04	0.3876E-17
Q	1	2	46	46	2263.5259	0.0184	0.4530E-03	0.5496E-04	0.6843E-17
Q	1	2	47	47	2261.8833	0.0180	0.1952E-03	0.2372E-04	0.3008E-17
Q	1	2	48	48	2260.2063	0.0177	0.3353E-03	0.4080E-04	0.5268E-17
Q	1	2	49	49	2258.4946	0.0173	0.1434E-03	0.1747E-04	0.2298E-17
Q	1	2	50	50	2256.7471	0.0169	0.2442E-03	0.2981E-04	0.3993E-17
Q	1	2	51	51	2254.9641	0.0166	0.1036E-03	0.1267E-04	0.1728E-17
Q	1	2	52	52	2253.1470	0.0163	0.1752E-03	0.2146E-04	0.2980E-17
Q	1	2	53	53	2251.2947	0.0159	0.7375E-04	0.9049E-05	0.1279E-17
Q	1	2	54	54	2249.4077	0.0156	0.1237E-03	0.1521E-04	0.2190E-17
Q	1	2	55	55	2247.4854	0.0153	0.5170E-04	0.6365E-05	0.9328E-18
Q	1	2	56	56	2245.5281	0.0150	0.8607E-04	0.1062E-04	0.1585E-17
Q	1	2	57	57	2243.5359	0.0147	0.3569E-04	0.4410E-05	0.6699E-18
Q	1	2	58	58	2241.5093	0.0144	0.5898E-04	0.7302E-05	0.1131E-17
Q	1	2	59	59	2239.4478	0.0141	0.2427E-04	0.3011E-05	0.4741E-18
Q	1	2	60	60	2237.3513	0.0138	0.3981E-04	0.4948E-05	0.7961E-18
Q	1	2	61	61	2235.2195	0.0135	0.1626E-04	0.2026E-05	0.3311E-18
Q	1	2	62	62	2233.0535	0.0131	0.2648E-04	0.3304E-05	0.5550E-18
Q	1	2	63	63	2230.8528	0.0129	0.1074E-04	0.1343E-05	0.2290E-18
Q	1	2	64	64	2228.6167	0.0123	0.1736E-04	0.2175E-05	0.3863E-18
Q	1	2	65	65	2226.3467	0.0121	0.6988E-05	0.8774E-06	0.1581E-18
Q	1	2	66	66	2224.0415	0.0112	0.1121E-04	0.1411E-05	0.2740E-18
Q	1	2	67	67	2221.7026	0.0110	0.4482E-05	0.5652E-06	0.1112E-18
Q	1	2	68	68	2219.3276	0.0093	0.7139E-05	0.9023E-06	0.2105E-18
Q	1	2	69	69	2216.9189	0.0091	0.2833E-05	0.3589E-06	0.8487E-19
Q	2	3	0	0	2272.5688	0.0372	0.2910E-04	0.3500E-05	0.3197E-18
Q	2	3	1	1	2272.5339	0.0348	0.4349E-04	0.5232E-05	0.5354E-18
Q	2	3	2	2	2272.4639	0.0336	0.1439E-03	0.1731E-04	0.1812E-17
Q	2	3	3	3	2272.3589	0.0327	0.9966E-04	0.1199E-04	0.1287E-17
Q	2	3	4	4	2272.2190	0.0319	0.2526E-03	0.3039E-04	0.3339E-17
Q	2	3	5	5	2272.0442	0.0312	0.1516E-03	0.1824E-04	0.2044E-17
Q	2	3	6	6	2271.8342	0.0307	0.3506E-03	0.4219E-04	0.4811E-17
Q	2	3	7	7	2271.5891	0.0302	0.1972E-03	0.2374E-04	0.2747E-17
Q	2	3	8	8	2271.3093	0.0298	0.4342E-03	0.5228E-04	0.6126E-17
Q	2	3	9	9	2270.9944	0.0295	0.2348E-03	0.2829E-04	0.3351E-17
Q	2	3	10	10	2270.6445	0.0292	0.5006E-03	0.6032E-04	0.7212E-17
Q	2	3	11	11	2270.2595	0.0290	0.2634E-03	0.3175E-04	0.3827E-17
Q	2	3	12	12	2269.8396	0.0287	0.5483E-03	0.6611E-04	0.8024E-17
Q	2	3	13	13	2269.3848	0.0285	0.2824E-03	0.3407E-04	0.4161E-17
Q	2	3	14	14	2268.8948	0.0284	0.5767E-03	0.6960E-04	0.8550E-17
Q	2	3	15	15	2268.3696	0.0282	0.2919E-03	0.3525E-04	0.4354E-17
Q	2	3	16	16	2267.8098	0.0280	0.5865E-03	0.7086E-04	0.8800E-17
Q	2	3	17	17	2267.2148	0.0278	0.2925E-03	0.3535E-04	0.4414E-17
Q	2	3	18	18	2266.5845	0.0277	0.5794E-03	0.7007E-04	0.8798E-17
Q	2	3	19	19	2265.9194	0.0275	0.2850E-03	0.3450E-04	0.4357E-17

Q	2	3	20	20	2265.2192	0.0273	0.5575E-03	0.6751E-04	0.8580E-17
Q	2	3	21	21	2264.4841	0.0271	0.2709E-03	0.3283E-04	0.4201E-17
Q	2	3	22	22	2263.7139	0.0268	0.5237E-03	0.6351E-04	0.8186E-17
Q	2	3	23	23	2262.9084	0.0266	0.2517E-03	0.3054E-04	0.3968E-17
Q	2	3	24	24	2262.0679	0.0264	0.4811E-03	0.5843E-04	0.7656E-17
Q	2	3	25	25	2261.1924	0.0261	0.2287E-03	0.2780E-04	0.3677E-17
Q	2	3	26	26	2260.2820	0.0258	0.4328E-03	0.5265E-04	0.7031E-17
Q	2	3	27	27	2259.3362	0.0255	0.2037E-03	0.2480E-04	0.3347E-17
Q	2	3	28	28	2258.3555	0.0252	0.3816E-03	0.4651E-04	0.6346E-17
Q	2	3	29	29	2257.3396	0.0249	0.1779E-03	0.2170E-04	0.2996E-17
Q	2	3	30	30	2256.2886	0.0245	0.3300E-03	0.4030E-04	0.5634E-17
Q	2	3	31	31	2255.2024	0.0242	0.1524E-03	0.1863E-04	0.2638E-17
Q	2	3	32	32	2254.0813	0.0238	0.2802E-03	0.3429E-04	0.4922E-17
Q	2	3	33	33	2252.9253	0.0234	0.1282E-03	0.1571E-04	0.2287E-17
Q	2	3	34	34	2251.7336	0.0231	0.2336E-03	0.2865E-04	0.4234E-17
Q	2	3	35	35	2250.5071	0.0227	0.1060E-03	0.1301E-04	0.1952E-17
Q	2	3	36	36	2249.2454	0.0223	0.1914E-03	0.2353E-04	0.3585E-17
Q	2	3	37	37	2247.9482	0.0219	0.8607E-04	0.1059E-04	0.1640E-17
Q	2	3	38	38	2246.6165	0.0215	0.1542E-03	0.1899E-04	0.2990E-17
Q	2	3	39	39	2245.2493	0.0211	0.6873E-04	0.8480E-05	0.1357E-17
Q	2	3	40	40	2243.8469	0.0207	0.1221E-03	0.1508E-04	0.2455E-17
Q	2	3	41	41	2242.4094	0.0203	0.5398E-04	0.6677E-05	0.1106E-17
Q	2	3	42	42	2240.9368	0.0199	0.9509E-04	0.1178E-04	0.1986E-17
Q	2	3	43	43	2239.4292	0.0195	0.4170E-04	0.5173E-05	0.8878E-18
Q	2	3	44	44	2237.8862	0.0191	0.7287E-04	0.9051E-05	0.1582E-17
Q	2	3	45	45	2236.3086	0.0188	0.3170E-04	0.3944E-05	0.7017E-18
Q	2	3	46	46	2234.6953	0.0184	0.5496E-04	0.6846E-05	0.1240E-17
Q	2	3	47	47	2233.0474	0.0180	0.2372E-04	0.2960E-05	0.5461E-18
Q	2	3	48	48	2231.3635	0.0177	0.4080E-04	0.5098E-05	0.9579E-18
Q	2	3	49	49	2229.6448	0.0173	0.1747E-04	0.2187E-05	0.4184E-18
Q	2	3	50	50	2227.8911	0.0169	0.2981E-04	0.3738E-05	0.7284E-18
Q	2	3	51	51	2226.1023	0.0166	0.1267E-04	0.1591E-05	0.3157E-18
Q	2	3	52	52	2224.2788	0.0163	0.2146E-04	0.2699E-05	0.5454E-18
Q	2	3	53	53	2222.4202	0.0159	0.9049E-05	0.1140E-05	0.2346E-18
Q	2	3	54	54	2220.5256	0.0156	0.1521E-04	0.1920E-05	0.4022E-18
Q	2	3	55	55	2218.5964	0.0153	0.6365E-05	0.8049E-06	0.1716E-18
Q	2	3	56	56	2216.6326	0.0150	0.1062E-04	0.1345E-05	0.2922E-18
Q	2	3	57	57	2214.6335	0.0147	0.4410E-05	0.5598E-06	0.1237E-18
Q	2	3	58	58	2212.5991	0.0144	0.7302E-05	0.9285E-06	0.2092E-18
Q	2	3	59	59	2210.5303	0.0141	0.3011E-05	0.3836E-06	0.8787E-19
Q	2	3	60	60	2208.4260	0.0138	0.4948E-05	0.6317E-06	0.1478E-18
Q	2	3	61	61	2206.2869	0.0135	0.2026E-05	0.2591E-06	0.6162E-19
Q	2	3	62	62	2204.1125	0.0131	0.3304E-05	0.4235E-06	0.1035E-18
Q	2	3	63	63	2201.9041	0.0129	0.1343E-05	0.1725E-06	0.4279E-19
Q	2	3	64	64	2199.6602	0.0123	0.2175E-05	0.2799E-06	0.7232E-19
Q	2	3	65	65	2197.3809	0.0121	0.8774E-06	0.1132E-06	0.2966E-19
Q	2	3	66	66	2195.0688	0.0112	0.1411E-05	0.1824E-06	0.5151E-19
Q	2	3	67	67	2192.7202	0.0110	0.5652E-06	0.7321E-07	0.2096E-19
Q	2	3	68	68	2190.3374	0.0093	0.9023E-06	0.1171E-06	0.3975E-19
Q	2	3	69	69	2187.9199	0.0091	0.3589E-06	0.4669E-07	0.1606E-19
S	0	1	0	2	2341.7439	0.0372	0.2178E-02	0.1229E-02	0.4745E-18
S	0	1	1	3	2349.5974	0.0348	0.3255E-02	0.8507E-03	0.7674E-18
S	1	2	2	4	2328.5239	0.0336	0.1229E-02	0.2526E-03	0.5510E-18
S	1	2	3	5	2336.2361	0.0327	0.8507E-03	0.1516E-03	0.3743E-18

```
S     1  2  4  6  234[illegible].9124   0.0319  0.2156E-02  0.3506E-03  0.9409E-18
S     1  2  5  7  2351.5522   0.0312  0.1293E-02  0.1972E-03  0.5629E-18
S     2  3  6  8  2329.[illegible]36   0.0307  0.3506E-03  0.5228E-04  0.2277E-18
S     2  3  8 10  [illegible]44.38[illegible]7   0.0298  0.4342E-03  0.6032E-04  0.2823E-18

Non-resonant [illegible] =     0.[illegible]E+00

      FREQ          RES_NRES       RES_RES        CRS_COH      PUMP_CONVD_CARS

0.2106076E+05 0.4[illegible]215E+00 [illegible] 0.8522508E-01 0.1058453E+01
0.2106156E+05 0.4864270E+00 [illegible] 0.9181529E-01 0.1051742E+01
0.2106236E+05 0.46[illegible]5602E+00 [illegible]584E+00 0.9125584E-01 0.1081576E+01
0.2106316E+05 0.5575679E+00 [illegible] 0.[illegible]29334E+00 0.1208293E+01
0.2106396E+05 0.4327183E+00 [illegible] [illegible]078796E-01 0.1035642E+01
0.2106476E+05 0.5365735E+00 [illegible]126E+00 [illegible]277400E+00 0.1214548E+01
0.2106556E+05 0.5181030E+00 [illegible] [illegible]738E+00 0.1159645E+01
0.2106636E+05 0.5882646E+00 [illegible]365E+00 0.15[illegible]294E+00 0.1382642E+01
0.2106716E+05 0.3880974E+00 0.[illegible]5155E+00 0.7844577E-01 0.1007611E+01
0.2106796E+05 0.4500214E+00 0.1867981E+00 0.9521604E-01 0.1067848E+01
0.2106876E+05 0.4107168E+00 0.2378849E+00 0.79[illegible]23E-01 0.9639459E+00
0.2106956E+05 0.3255878E+00 0.2436744E+00 [illegible]152E-01 0.9712756E+00
0.2107036E+05 0.3868379E+00 0.7457[illegible]E-01 0.[illegible]568231E-01 0.8529109E+00
0.2107116E+05 0.4574296E+00 0.1564[illegible] 0.8334886E-01 0.1033025E+01
0.2107196E+05 0.5482287E+00 0.216167[illegible]E+00 0.1120375E+00 0.1212245E+01
0.2107276E+05 0.4344486E+00 0.2186504E+00 0.7413666E-01 0.1063048E+01
0.2107356E+05 0.5583072E+00 0.2004196E+00 0.1209734E+00 0.1215512E+01
0.2107436E+05 0.6359313E+00 0.2071160E+00 0.1505291E+00 0.1329388E+01
0.2107516E+05 0.4954824E+00 0.5496371E+00 0.1245437E+00 0.1505475E+01
0.2107596E+05 0.5929731E+00 0.2145655E+00 0.1310543E+00 0.1274405E+01
0.2107676E+05 0.6436939E+00 0.2338394E+00 0.1542998E+00 0.1367645E+01
0.2107756E+05 0.5740684E+00 0.7590045E+00 0.1559671E+00 0.1824852E+01
0.2107836E+05 0.7179092E+00 0.3223289E+00 0.1965561E+00 0.1572606E+01
0.2107916E+05 0.6499159E+00 0.3817995E+00 0.1675823E+00 0.1535110E+01
0.2107996E+05 0.5966115E+00 0.9660712E+00 0.1716720E+00 0.2070167E+01
0.2108076E+05 0.7418274E+00 0.4613647E+00 0.2233427E+00 0.1762347E+01
0.2108156E+05 0.8609985E+00 0.6507494E+00 0.2844409E+00 0.2132001E+01
0.2108236E+05 0.6779886E+00 0.1064694E+01 0.2303543E+00 0.2308849E+01
0.2108316E+05 0.6363878E+00 0.5389141E+00 0.1801307E+00 0.1691245E+01
0.2108396E+05 0.9057872E+00 0.1761962E+01 0.3904593E+00 0.3394021E+01
0.2108476E+05 0.7240970E+00 0.6189468E+00 0.2135831E+00 0.1892439E+01
0.2108556E+05 0.1028975E+01 0.1611058E+01 0.4317802E+00 0.3407625E+01
0.2108636E+05 0.5205427E+00 0.1971748E+01 0.1756166E+00 0.3003720E+01
0.2108716E+05 0.8862957E+00 0.9875104E+00 0.3288658E+00 0.2538484E+01
0.2108796E+05 0.6417221E+00 0.2390600E+01 0.3001286E+00 0.3668263E+01
0.2108876E+05 0.9859959E+00 0.1334437E+01 0.4238721E+00 0.3080117E+01
0.2108956E+05 0.6007880E+00 0.3340427E+01 0.4006337E+00 0.4677661E+01
0.2109036E+05 0.9502769E+00 0.1680103E+01 0.4160730E+00 0.3382265E+01
0.2109116E+05 0.6113712E+00 0.3498278E+01 0.3687440E+00 0.4814205E+01
0.2109196E+05 0.1126644E+01 0.2961926E+01 0.6497371E+00 0.5074120E+01
0.2109276E+05 0.5302809E+00 0.2759751E+01 0.3608629E+00 0.3986707E+01
0.2109356E+05 0.8148162E+00 0.4015257E+01 0.5755402E+00 0.5741426E+01
0.2109436E+05 0.7616404E+00 0.3400696E+01 0.5326024E+00 0.5030750E+01
0.2109516E+05 0.9417349E+00 0.4606089E+01 0.7541686E+00 0.6637805E+01
0.2109596E+05 0.3161147E+00 0.3925040E+01 0.4699632E+00 0.5046930E+01
```

```
0.2109676E+05 0.4803291E+00 0.3650303E+01 0.6658879E+00 0.5132332E+01
0.2109756E+05 0.6654667E-01 0.2225415E+01 0.5122645E+00 0.3140038E+01
0.2109836E+05-0.4667496E+00 0.3871953E+01 0.5232856E+00 0.4264301E+01
0.2109916E+05-0.7372818E-01 0.3071955E+00 0.5016076E-02 0.5742953E+00
0.2109996E+05 0.1353021E+00 0.9371076E+00 0.4265743E-01 0.1450879E+01
0.2110076E+05 0.7458995E+00 0.2586171E+01 0.2564563E+00 0.3924339E+01
0.2110156E+05 0.8323012E-01 0.2105676E+01 0.3919958E-01 0.2563917E+01
0.2110236E+05 0.6156169E+00 0.1714364E+01 0.2101071E+00 0.2875900E+01
0.2110316E+05 0.8667122E+00 0.1556830E+01 0.2927138E+00 0.3052068E+01
0.2110396E+05 0.2577816E+00 0.6523098E+01 0.2666934E+00 0.7383385E+01
0.2110476E+05 0.8527446E+00 0.2062161E+01 0.3337837E+00 0.3584502E+01
0.2110556E+05 0.9310181E+00 0.1827400E+01 0.3422795E+00 0.3436509E+01
0.2110636E+05 0.4584143E+00 0.1091069E+02 0.5563387E+00 0.1226126E+02
0.2110716E+05 0.9769822E+00 0.2963373E+01 0.4566232E+00 0.4732790E+01
0.2110796E+05 0.1161126E+01 0.3515964E+01 0.5506400E+00 0.5563541E+01
0.2110876E+05 0.3658273E+00 0.1340864E+02 0.5924369E+00 0.1470272E+02
0.2110956E+05 0.1051174E+01 0.5051846E+01 0.6386506E+00 0.7077482E+01
0.2111036E+05 0.1644517E+01 0.1117777E+02 0.1272378E+01 0.1443048E+02
0.2111116E+05 0.3942247E+00 0.9613264E+01 0.3080243E+00 0.1065133E+02
0.2111196E+05 0.9690194E+00 0.6526950E+01 0.6362898E+00 0.8468072E+01
0.2111276E+05 0.1204217E+01 0.3033216E+02 0.2109820E+01 0.3398201E+02
0.2111356E+05 0.1112890E+01 0.8222441E+01 0.8096653E+00 0.1048081E+02
0.2111436E+05 0.1843568E+01 0.2137336E+02 0.1963434E+01 0.2551618E+02
0.2111516E+05 0.5046510E+00 0.1575897E+02 0.6462425E+00 0.1724567E+02
0.2111596E+05 0.1454591E+01 0.1610658E+02 0.1373343E+01 0.1927033E+02
0.2111676E+05 0.2747883E+00 0.3234981E+02 0.1513005E+01 0.3447341E+02
0.2111756E+05 0.1323241E+01 0.1913498E+02 0.1545861E+01 0.2233990E+02
0.2111836E+05 0.2376070E+00 0.4195963E+02 0.2230190E+01 0.4476324E+02
0.2111916E+05 0.1401890E+01 0.2913111E+02 0.2224720E+01 0.3309352E+02
0.2111996E+05 0.1527444E+00 0.3884449E+02 0.2206398E+01 0.4153944E+02
0.2112076E+05 0.1284374E+01 0.5610603E+02 0.4138053E+01 0.6186427E+02
0.2112156E+05 0.4564456E+00 0.3243822E+02 0.2401579E+01 0.3563205E+02
0.2112236E+05-0.1512440E+00 0.6297252E+02 0.4828602E+01 0.6798569E+02
0.2112316E+05 0.2572757E+00 0.6672798E+02 0.5740442E+01 0.7306152E+02
0.2112396E+05-0.1474925E+00 0.5609672E+02 0.5527963E+01 0.6181300E+02
0.2112476E+05-0.9077362E+00 0.5471254E+02 0.6769699E+01 0.6091032E+02
0.2112556E+05-0.1920233E+01 0.5216817E+02 0.9393628E+01 0.5997737E+02
0.2112636E+05-0.4005438E+01 0.4047270E+02 0.1478268E+02 0.5158575E+02
0.2112716E+05-0.5699200E+01 0.1656373E+02 0.1254499E+02 0.2374533E+02
0.2112796E+05-0.3479639E+01 0.4589842E+01 0.4506350E+01 0.5952365E+01
0.2112876E+05-0.2695593E+01 0.2720292E+01 0.2706838E+01 0.3067349E+01
0.2112956E+05-0.2266425E+01 0.1918106E+01 0.1912916E+01 0.1900410E+01
0.2113036E+05-0.1979426E+01 0.1461487E+01 0.1459708E+01 0.1277581E+01
0.2113116E+05-0.1768842E+01 0.1166382E+01 0.1165375E+01 0.8987265E+00
0.2113196E+05-0.1605189E+01 0.9602084E+00 0.9595500E+00 0.6503815E+00
0.2113276E+05-0.1471394E+01 0.8067031E+00 0.8064751E+00 0.4775961E+00
0.2113356E+05-0.1370029E+01 0.6992724E+00 0.6990877E+00 0.3641431E+00
0.2113436E+05-0.1275729E+01 0.6061897E+00 0.6062915E+00 0.2725640E+00
0.2113516E+05-0.1195670E+01 0.5324389E+00 0.5325218E+00 0.2051026E+00
0.2113596E+05-0.1125942E+01 0.4721171E+00 0.4721815E+00 0.1541683E+00
0.2113676E+05-0.1064032E+01 0.4216065E+00 0.4217676E+00 0.1151538E+00
0.2113756E+05-0.1007798E+01 0.3782134E+00 0.3783491E+00 0.8457613E-01
0.2113836E+05-0.9537132E+00 0.3388647E+00 0.3389122E+00 0.5987576E-01
0.2113916E+05-0.9169440E+00 0.3132356E+00 0.3133158E+00 0.4541928E-01
0.2113996E+05-0.8646567E+00 0.2784542E+00 0.2787411E+00 0.2835047E-01
```

```
  Section        CPU Time (Min)      % CPU Time
 CHISQRE          171.14766       70.81992


 Pump convln        70.51833       29.18008


Cpu time for this spectrum is        241.66600 MIN


PUMP_CONVD_CARS spectra for all temp. are in the file
    N2PC.SPT;140
FORTRAN STOP
Charged CPU time:     0 04:01:59.72   Elapsed time:     0 05:26:30.44
```

APPENDIX E.

DESCRIPTION OF THE FIT PROGRAMS

CONTENTS

	Page
E1.0 PROGRAM FIT	E3
E1.1 Functional Description	E3
E2.0 PROGRAM FIT_FLAME	E4
E2.1 Functional Description	E4
E3.0 REFERENCES	E4

APPENDIX E

DESCRIPTION OF THE FIT PROGRAMS

E1.0 PROGRAM FIT

This program convolves a theoretical CARS spectrum with a Voigt slit function and fits it to an experimental spectrum. The program finds the best fitting shift and Voigt slit parameters and, optionally, the best fitting temperature.

E1.1 Functional Desciption

1. FIT reads an experimental CARS spectrum. As a rule a certain percentage of noise is always associated with a CARS signal. The total noise associated with a given diode count C may be expressed as a variance σ_T^2 given by (Snelling et al. 1987)

$$\sigma_T^2 = \sigma_o^2 + kC + mC^2 \qquad \text{(E1)}$$

   where σ_o^2 is the dark noise, kC is the shot noise component, and mC^2 represents the component due to shot to shot variation in the CARS signal. Because of this noise, it is necessary to assign appropriate weights to diode counts of varying magnitude. FIT uses the above equation to calculate the weights associated with each diode count as

$$Wi = 1/\sigma_i^2 \qquad \text{(E2)}$$

2. Another problem affecting CARS spectra is detector nonlinearity. For all of the intensified diode array detectors examined so far (Snelling 1988), the detector sensitivity has been found to fall off logarithmically with detector output, in counts down to a threshold value where it remains constant. The experimentally measured slope of the logarithmic falloff and the threshold (in counts) are used to construct a "lookup" table of corrected counts versus uncorrected counts, which is used by all the fitting programs to perform the nonlinear correction to the experimental data before fitting it to theory.

3. The experimental spectrum is then corrected for background signal and linearly interpolated to the wave number scale used by the theoretical spectrum.

4. FIT reads the theoretical spectra from a library of pump convolved theoretical spectra. One or two theoretical CARS spectra are linearly interpolated to get a spectrum at the initially guessed temperature. It is then shifted (via linear interpolation) by a trial amount and convolved with a Voigt slit function of trial parameters.

5. A nonlinear least mean square fit is performed between theory and experiment by means of the subroutines FITFIVE or FITSIX. If a room temperature spectrum is fitted, subroutine FITFIVE is called and best fit values of the four Voigt parameters and shift are output. If a hot N_2 spectrum is being fitted, FITSIX is called and temperature is included as an additional sixth parameter.

6. The program also outputs a normalized standard deviation between theory and experiment (as a measure of convergence), and optionally provides plots of experimental and theoretical spectra at the end of each cycle of iteration.

E2.0 PROGRAM FIT_FLAME

FIT_FLAME is a fast analysis program used to find the temperature and frequency shift of a theoretical CARS spectrum with the closest fit to a given experimental flame spectrum.

F2.1 Functional Description

FIT_FLAME is a special version of the FIT program in Appendix E-1. Background subtraction and detector nonlinearity corrections are incorporated in both programs. The fitting scheme in both codes employ weighted experimental data. FIT_FLAME differs from FIT in that it fits only the two parameters temperature and shift. It is thus designed to work with a slit convolved theoretical spectral library. The least mean square fit is done by the subroutine TEMP_FIT, which is similar to FIT FIVE but fits only two parameters. Further FIT FLAME has no plot options. This enables the user to submit analysis of several hundred spectra in the batch mode. The resulting temperatures and shifts are written in suitably named output files. Once the slit parameters are determined, the FIT_FLAME program is ideally suited for routine analysis of averaged and single shot spectra.

E3.0 REFERENCES

SNELLING, D.R. 1988. Unpublished results. Gas Dynamics Laboratory, Division of Mechanical Engineering, National Research Council Canada, Ottawa, Ont.

SNELLING, D.R., G.J. SMALLWOOD, R.A. SAWCHUK, and T. PARAMESWARAN. 1987. Precision of Multiplex CARS Temperatures Using Both Singlemode and Multimode Pump Lasers. Applied Optics, 26: 99.

REPORT DOCUMENTATION PAGE/PAGE DE DOCUMENTATION DE RAPPORT

REPORT/RAPPORT TR-GD-013 1a	**REPORT/RAPPORT** NRC NO. 29810 1b
SECURITY CLASSIFICATION/ CLASSIFICATION DE SÉCURITÉ UNCLASSIFIED 2	**DISTRIBUTION/DIFFUSION** ☐ Controlled/Contrôlé ☒ Unlimited/Illimité 3

TITLE/SUBTITLE/TITRE/SOUS-TITRE

The Calculation of Theoretical Coherent Anti-Stokes Raman Spectra

4

AUTHOR(S)/AUTEUR(S)

Thangam Parameswaran and D.R. Snelling

5

SERIES/SÉRIE

Unlimited/Unclassified Technical Report

6

CORPORATE AUTHOR/PERFORMING AGENCY/AUTEUR D'ENTREPRISE/AGENCE D'EXÉCUTION

National Research Council of Canada
Division of Mechanical Engineering
Gas Dynamics Laboratory

7

SPONSORING AGENCY/AGENCE DE SUBVENTION

8

DATE 1988/10 9	**FILE/DOSSIER** 10	**LAB. ORDER COMMANDE DU LAB.** 11	**PAGES** 12a	**DIAGS** 12b	**REFS** 12c

NOTES

13

DESCRIPTORS(KEY WORDS)/MOTS-CLÉS

CARS spectral generation, Raman Spectroscopy, CARS computer program, nitrogen thermometry

14

SUMMARY/SOMMAIRE

The theoretical principles underlying coherent anti-Stokes Raman spectroscopy (CARS), and the implementation of a computer code to calculate broadband nitrogen CARS spectra are described. The validation of this code and its use to fit experimental CARS spectra using precalculated theoretical spectral libraries are presented.

15

ADDRESS/ADRESSE

Dr. R.G. Williamson, Head
Gas Dynamics Laboratory
Division of Mechanical Engineering
Montreal Road, Building M-10
Ottawa, Ontario KIA OR6
TEL: (613) 993-2442

16